Space Science Reviews manuscript No.
(will be inserted by the editor)

Solar fine-scale structures. I. Spicules and other small-scale, jet-like events at the chromospheric level: observations and physical parameters

G. Tsiropoula[1], K. Tziotziou[1], I. Kontogiannis[1], M. S. Madjarska[2*], J.G. Doyle[2], Y. Suematsu[3]

Received: date / Accepted: date

Abstract Over the last two decades the uninterrupted, high resolution observations of the Sun, from the excellent range of telescopes aboard many spacecraft complemented with observations from sophisticated ground-based telescopes have opened up a new world producing significantly more complete information on the physical conditions of the solar atmosphere than before. The interface between the lower solar atmosphere where energy is generated by subsurface convection and the corona comprises the chromosphere, which is dominated by jet-like, dynamic structures, called mottles when found in quiet regions, fibrils when found in active regions and spicules when observed at the solar limb. Recently, space observations with Hinode have led to the suggestion that there should exist two different types of spicules called Type I and Type II which have different properties. Ground-based observations in the Ca II H and K filtergrams reveal the existence of long, thin emission features called straws in observations close to the limb, and a class of short-lived events called rapid blue-shifted excursions characterized by large Doppler shifts that appear only in the blue wing of the Ca II infrared line. It has been suggested that the key to understanding how the solar plasma is accelerated and heated may well be found in the studies of these jet-like, dynamic events. However, while these structures are observed and studied for more than 130 years in the visible, but also in the UV and EUV emission lines and continua, there are still many questions to be answered. Thus, despite their importance and a multitude of observations performed and theoretical models proposed, questions regarding their origin, how they are formed, their physical parameters, their association with the underlying photospheric magnetic field, how they appear in the different spectral lines, and the interrelationship between structures observed in

[1]Institute for Space Applications and Remote Sensing, National Observatory of Athens, Lofos Koufos, 15236 P. Penteli, Greece
[2]Armagh Observatory, College Hill, Armagh BT61 9DG, UK
[3]Hinode Science Center, National Observatory of Japan, 2-21-1 Osawa, Mitaka, Tokyo 181-8588, Japan
*now at: UCL-Mullard Space Science Laboratory, Holmbury St Mary, Dorking, Surrey, RH5 6NT, UK
Corresponding author: G. Tsiropoula (e-mail: georgia@noa.gr)

quiet and active regions on the disk and at the limb, as well as their role in global processes has not yet received definitive answers. In addition, how they affect the coronal heating and solar wind need to be further explored. In this review we present observations and physical properties of small-scale jet-like chromospheric events observed in active and quiet regions, on the disk and at the limb and discuss their interrelationship.

Keywords Sun · chromosphere · spicules · jet-like structures · small-scale events · physical parameters

1 Introduction

During the last 2 – 3 decades, observations from space combined with ground-based data, as well as state-of-the-art, post-processing reconstruction techniques combined with progress in numerical modelling and theory have increased our understanding of the physical processes occurring in the solar atmosphere. Apart from demonstrating that the solar atmosphere is highly dynamic and inhomogeneous these studies have also provided a deep insight into all phenomena occurring in its different parts. They have revealed a number of different types of structures that exist in the different atmospheric layers for which a range of formation mechanisms have to be investigated. They have also provided important information about the physical conditions of the emitting plasma, as well as hints about the physical nature of related dynamic phenomena which continuously occur on the Sun over a large range of spatial and temporal scales.

The solar chromosphere is an intricately structured and dynamic layer of the Sun. It is traditionally defined as the layer, about 2 000 km thick, lying between the photosphere and the transition region and has long been known not to be in hydrostatic equilibrium. Therefore, its nature is that of dynamic fine-scale structures which uniquely characterize this part of the solar atmosphere. These appear to be structured by the magnetic fields that extend from network boundaries and plages and be directly related to its evolution. The appearance of the underlying atmosphere is, mainly, due to processes involving the emergence, buffeting and re-arrangement of the magnetic flux generated by interior dynamo action. The resulting spatial inhomogeneity produces a fruitful environment for the emerging fluxes to undergo quite complex changes as they dynamically evolve and interact with the pre-existing magnetic fields in the ambient medium. Complex and concentrated, mainly unipolar, strong magnetic fields produce the so-called active regions, which are the locations of some jet-like structures, such as the (traditional) fibrils and dynamic fibrils (DFs). Outside active regions, what is generally known as the quiet solar chromosphere, is not really quiet. It is continually subject to a variety of small-scale events, such as mottles, straws and the, recently reported, rapid blue excursions, occurring at the boundaries of cellular patterns that constitute the magnetic network. The magnetic network is believed to be sustained by magnetic bipoles, which emerge in the interiors of supergranules, move apart and are fragmented by granular buffeting. Eventually, the fragments are driven to the supergarnular boundaries where they interact with the existing magnetic flux (Wang et al., 1996; Schrijver et al., 1997). Opposite polarity fluxes cancel and submerge, whereas like-polarity flux merges to form larger flux concentrations.

When observing the chromosphere at different wavelengths, from the EUV to the radio domain its very large range of inhomogeneity and structuring is revealed. Chromospheric structures can be seen against the solar disk, by means of monochromatic or narrow-band filters or spectrometers operating in strong spectral lines, such as Hα, Ca II H & K, and the Ca II infrared triplet (IR). In particular, filtergrams recorded in the wings and line center of Hα reveal a wealth of fine-scale structures. The most prominent small-scale features residing at the network boundaries are certainly mottles. Mottles are thin jet-like features, better observed in Hα. Rutten (2007) identified in Ca II H images taken close to the solar limb as very thin and short-lived bright structures which occur in "hedge rows". He called them "straws". Recently, Langangen et al. (2008c) and Rouppe van der Voort et al. (2009) found sudden, large line shift changes in both Hα and Ca II IR lines on their blue side. The authors interpreted these events, which occur at the edges of rosettes (cluster of mottles expanding radially around a common center), as chromospheric up-flows and called them "rapid blue-shifted excursions" (RBEs). In active regions, a subset of dark structures called fibrils includes relatively short, thin, jet-like structures called dynamic fibrils (DFs). They are found in the central area of plages where the magnetic field is more dense, and more vertically oriented. Another large subset includes very inclined, almost horizontal, long fibrils which are clearly more stable than the DFs. The relationship between all these on-disk structures, as well as their relationship to spicules, thin, elongated, jet-like structures observed at the solar limb, is under strong debate. Spicules are the most obvious component of the chromospheric limb. Although they were discovered almost 130 years ago, they still remain one of the mysterious phenomena in the solar atmosphere because, at least until recently, remained very close to the resolution limits of current solar observations. As a result, several of their properties have not been well defined and this has led to a plethora of theoretical models for their interpretation (for a review see Sterling (2000)). Recently, with its high resolution and high cadence, as well as an uninterrupted view of the Sun, the Hinode space mission provided a new picture of spicules. De Pontieu et al. (2007b), based on time series observations of the solar limb taken with Solar Optical Telescope (SOT) aboard Hinode in the Ca II H broad filter, suggested that spicules can be grouped in two categories, called Type I and Type II, which seem to have different properties and formation mechanisms. The origin of short duration/high velocity spicules (Type II) has been attributed to magnetic field reconnection. On the other hand, the origin of Type I, classic spicules (long duration/low velocities) seems to be associated with the leakage of p-modes into the upper atmosphere and subsequent development of shocks that follow the magnetic field lines.

While spicules are ubiquitous at the limb, there is still a debate on the issue of their counterparts are on the solar disk. Grossmann-Doerth and Schmidt (1992) concluded from the different velocity distributions of mottles and spicules, that mottles are not the disk counterparts of (classical) spicules. Tsiropoula and Schmieder (1997), on the other hand, based on the similarity of their physical parameters, argued for a close relationship between them. Type I spicules appear to rise up from the limb and fall back again. They show a similar dynamical behaviour as active region DFs (De Pontieu et al., 2007a), as well as a subset of mottles. Type II spicules, on the other hand, seem to exhibit an upward motion followed by rapid fading from the Hinode Ca II H passband, although more recent work by Zhang et al. (2012), were unable to locate any Type II spicules. Rouppe van der Voort et al. (2009)

suggested that the disk counterpart of Type II spicules are RBEs based on the similarities of their properties.

When observed in the line center of Hα, the chromospheric plasma is clearly seen to be organized along fine-scale magnetic structures which have different inclinations. Recently, Kontogiannis et al. (2010a) and Kontogiannis et al. (2010b) using high-resolution Hα observations together with magnetograms obtained with the spectropolarimeter on Hinode, revealed through a potential magnetic field extrapolation another very important aspect of these structures when observed on the disk. They showed that magnetic flux tubes following the local inclination of the magnetic field lines, define the layer of the magnetic canopy, i.e. the plasma-$\beta \sim 1$ layer, where the plasma-β is the ratio of gas pressure to magnetic pressure. It is at this layer, where acoustic waves generated by the convective motions, undergo mode conversion, refraction, reflection and transmission with important effects to the upper solar atmosphere and thus these structures play a very important role in wave propagation.

The fact that the solar corona has a temperature more than 1 million degrees is still a puzzling problem of solar physics, despite the considerable theoretical and experimental efforts. Since the energy release in the largest explosive events (flares and microflares) does not supply enough power to heat the corona, the behaviour of smaller-scale and less energetic, but much more frequent events is an essential constituent of the problem (Doyle and Butler, 1985; Parker, 1988). Both magnetic reconnection and waves related to spicules are powerful mechanisms for energy release and transfer and have been considered as heating agents of the solar corona. Tsiropoula et al. (1994) and Tziotziou et al. (2003) examining the temporal evolution of the line-of-sight velocity of mottles found bi-directional flows and proposed a model according to which spicules are due to magnetic reconnection. Tsiropoula and Tziotziou (2004) showed that if magnetic reconnection is considered as the driving mechanism of mottles, the material they supply to the solar corona is in excess of that needed to compensate for coronal mass losses in the solar wind, while the amount of energy released to heat the corona depends on several parameters, among which are the number of the events, their axial velocity and magnetic field, etc., and can be negligible or substantial. De Pontieu et al. (2007b), on the other hand, showed that the energy flux provided by the Alfvén waves identified in spicules is large enough to supply the energy necessary to heat the quiet solar corona and drive the solar wind. Thus the question arises of how these small-scale features participate and contribute into the larger scale observable phenomena, and how a more accurate determination of the physical parameters, which are related to the physical processes, can be extracted from observations.

This review is the first part of a series of four reviews. The aim of these reviews is to present an overview of our current understanding (observations, modelling, physical parameters, etc.) of solar small-scale, jet-like structures observed both on the disk and at the limb, in active, as well as in quiet regions. In this review (Part I) we present an overview of the chromospheric fine-scale structures. More specifically, we will present their morphological properties, their derived physical parameters, such as height, width, lifetime, velocities, etc., as well as methods used for the derivation of some of them, their dynamical behaviour, and comment on their interrelationship. In subsequent papers we will discuss transition region

small-scale events (Part II), and the role of the various small-scale events in coronal heating (Part III).

2 The solar photosphere

The solar surface is threaded by a complex network of magnetic fields. Observations of these fields at the photospheric level reveal them to be concentrated into regions of mixed (negative and positive) polarities covering a wide range of values for the (unsigned) magnetic flux and lifetimes. In *quiet areas* the dynamic interplay between the magnetic field concentrations and the plasma has been called the Sun's "magnetic carpet" (Title and Schrijver, 1998). In these areas, photospheric motions are dominated by the flow pattern of large convective cells called supergranules. These cells range in diameter from roughly 10 000 km to 50 000 km, with an average diameter of between 13 000 and 18 000 km (Hagenaar et al., 1997). Their flow pattern takes the form of an up-flow at the cell center, followed by radial outflow of $\sim$0.5 km s^{-1}, and down-flow at the cell boundaries (Simon and Leighton, 1964). Wang and Zirin (1989) derived an upper limit of 0.1 km s^{-1} for the magnitude of the supergranule's vertical velocity (both up-flow and down-flow). The strongest down-flow occurring at points where two or more cells meet, and as a result, the magnetic flux tends to build up along the boundaries of supergranular cells after being swept from the center by the radial outflow. It is now well established from investigations of high resolution magnetograms that new bipolar elements emerge continuously inside the cell interiors and are, subsequently, swept by the supergranular flow at the periphery of supergranular cells where they gather and form the network boundaries with kG field strengths (Wang et al., 1996; Schrijver et al., 1997). This is illustrated well by the SoHO/MDI magnetogram shown in Figure 1. The supergranule cell boundaries are marked in yellow, and it can be seen that the majority of the flux concentrations are located along these lines, and in particular at the intersection of multiple cells. These concentrations called *network concentrations* are typically found at sites of strong down-flow, at the boundaries of supergranular cells (Martin, 1988). Their fluxes are of the order of 10^{18} – 10^{19} Mx and have typical diameters of 1 000 – 10 000 km (Parnell, 2001). They tend to be larger than *ephemeral regions* which are clumps of newly emerged flux of varying strengths with total net flux equal to zero. Ephemeral regions emerge preferentially near supergranular boundaries, without influencing the flow pattern. After emergence, they most often fragment into several concentrations where their flux quickly merges into the pre-existing network. Schrijver et al. (1997) give the average flux of an ephemeral region to be $\sim 1.3\times 10^{19}$ Mx. Martin (1990) determined that the network concentrations are produced from the residuals of other flux concentrations. It is estimated that 90% or more of their flux originates from ephemeral regions, with the remaining 10% being contributed by *intranetwork fields*. *Intranetwork (IN) fields* are the smallest of the three types of small-scale magnetic flux concentrations. They typically last 2 to 4 hours. Their mean diameter is about 2 000 km, while their total flux content ($\sim 10^{16}$ Mx) tends to be close to the detection limit of present instruments. They emerge within supergranule cells due to the emergence of small bipolar pairs. They are then swept towards the cell boundaries by radial flows, where they interact with network fields (Martin, 1988). Recently, Centeno et al. (2007) using observations obtained

with Solar Optical Telescope Spectropolarimeter (SOT/SP) on board the Hinode spacecraft presented clear evidence of an emerging IN magnetic loop showing strong horizontal magnetic signal and traces of vertical opposite polarities on each side of it. The lower parts of the loop were advected into the intergranular lanes, where they aggregate to other magnetic field concentrations resulting in larger flux elements. Lites et al. (2008) based on the high spatial resolution and polarimetric sensitivity of the SOT/SP reported the existence of horizontal magnetic fields in the IN regions whose mean field strength surpasses considerably that of the vertical component. The vertical fields are concentrated in the intergranular lanes, whereas the stronger horizontal fields occur preferentially at the edges of the bright granules or inside them aside from the vertical fields. This kind of spatial relation between the horizontal and the vertical magnetic fields suggests that the IN field consists of small Ω loops having their vertical roots in the intergranular lanes and connected by an horizontal field above granules.

From the previous discussion it becomes clear that the magnetic flux patches within the magnetic carpet, while diffusing along the superganular boundaries due to supergranular flows, interact with one another by the following four main processes: Flux *emergence* which is the appearance in pairs or in clusters of new magnetic flux (with equal amounts of flux in both the positive and negative polarities). *Cancellation* which occurs when concentrations of opposite polarity come into contact and mutually lose flux (Livi et al., 1985; Martin et al., 1985). If two or more concentrations of the same polarity merge together to form a single larger concentration, this is known as *coalescence*. Finally, *fragmentation* which is the splitting of a large concentration of flux into several different smaller concentrations. Using a series of full-disc 96 minute MDI magnetograms, Hagenaar (2001) found that the time taken for all flux within the quiet Sun photosphere to be replaced ("the flux replacement timescale") was around 14 hours. However, later studies determined this value to be an order of magnitude smaller, at just 1 – 2 hours (Hagenaar et al., 2008).

The magnetic network formed by the driving of the magnetic flux to the boundaries of supergranules is made up of clusters of kilogauss flux tubes. By definition the smallest observable structure of the magnetic flux in the photosphere are magnetic elements which have various field strengths and diameters close to or less than the best currently achievable spatial resolution (~ 150 km). Magnetic elements are very important because they not only structure the photosphere but also provide a link to the chromosphere and corona along which energy can be transported from the Sun's interior to the outer layers. They were first observed as "magnetic knots" (Beckers and Schröter, 1968) – small dark structures equivalent to what we now call "micropores" (Topka et al., 1997)– and as "filigree", elongated chains of bright points (Dunn and Zirker, 1973) which have been resolved into strings of adjacent bright points by Mehltretter (1974). When observed at disc center they are usually best seen in the "G-band filtergrams", which are obtained with a wide-band filter centered around 430.5 nm, named G-band by Fraunhofer. The first observations of the network at this wavelength window were carried out by Muller and Roudier (1984). The name "network bright points" (NBPs) was introduced (Stenflo and Harvey, 1985; Muller, 1985) for the bright grains which are visible in filtergrams and are arranged in roughly cellular patterns making up the network boundaries. Since bright points have been presumed to be the visible manifestation of thin magnetic flux tubes and thus related to the magnetic

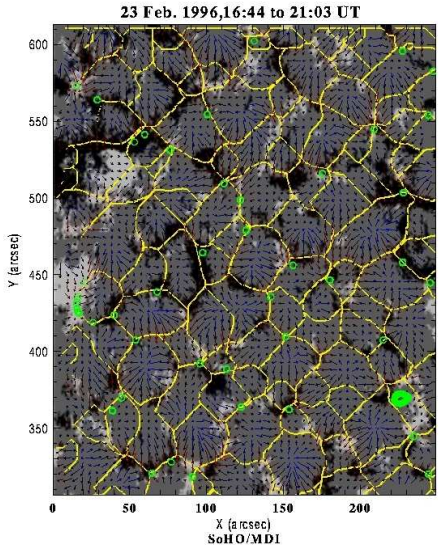

Fig. 1 A SOHO/MDI magnetogram. The boundaries of supergranule cells are marked in yellow, and arrows indicate the supergranular flow pattern (Credits SoHO/MDI).

elements, extensive work has been initiated and it is now well established that NBPs are brightness manifestations of the small, strong field magnetic elements that make up the magnetic network (Muller and Roudier, 1984; Berger and Title, 1996, 2001; Rouppe van der Voort et al., 2005).

In *stronger field areas*, on the other hand, the increased number density of magnetic flux tubes gives rise to large chromospheric areas called plages which consist of many bright elements (sometimes referred to as facular granules) packed together. Granules near network bright points and in plage regions are smaller, display slower temporal evolution and have a lower contrast than those found in quiet areas (Title et al., 1992). The granular pattern in these areas is referred too as "abnormal" (Dunn et al., 1974). Flux concentrations take on structure, behave less passively and seem to affect the granular flow. The larger magnetic filling factor in plage regions gives rise to large amorphous, elongated "ribbons" that contain high net flux. They are characterized by large flux concentrations having a brighter edge and an intensity depression in the center. The majority of them are not resolved into flux tubes, but instead show a substructure which is interpreted as an indication of a range of magnetic field strengths within the structure. Circular manifestations of spread out ribbon structures have been called "flowers". The "flowers" and "ribbons" are small flux concentrations (Berger et al., 2004), while larger flux concentrations are called (micro)-pores and have a distinct dark center. There is a continuous transition between these features evolving from one to another depending on the amount of the magnetic flux that is collected or dispersed. The merging and splitting of "flux sheets", which are concentrations of the magnetic field due to the granular flow, and the transitions between the ribbons, flowers, and micropores are described by Rouppe van der Voort et al. (2005). These authors found also that the plasma is basically at rest in these structures with

small concentrations of weak up-flow sites, while narrow sheets with down-drafts are found right at the edges of the magnetic field concentrations.

Due to the continual motion of mixed polarity concentrations in the magnetic carpet and the different flux evolution processes, the quiet Sun photosphere is highly dynamic. Since magnetic fields from the magnetic carpet extend up into the solar chromosphere and lower corona, it is expected that the quiet Sun chromosphere and corona are also highly dynamic responding to the movement and evolution of the different flux concentrations. Even more, the spatial distribution and rates of the different processes of flux evolution play a major role in determining the distribution of heating events in the upper solar layers. The driving of foot-points of the small-scale magnetic fields on the surface of the Sun plays a fundamental role in sustaining the chromospheric network and leads to the build up of currents and/or the generation of waves, mechanisms considered as potential sources of energy for solving the coronal heating problem. On the other hand, the larger magnetic filling factor in plage regions gives rise to more extended structures. As stated by Rouppe van der Voort et al. (2005), the merging and splitting of flux sheets and the continuous transition between ribbons and micropores, are difficult to reconcile with models that regard these structures as being composed of discrete flux tubes that keep their identity over a long period of time. They also suggested that it should be more appropriate to characterize the temporal behaviour of the magnetic field in these areas as fluid-like, where the "magnetic fluid" is in continuous interaction with the field-free plasma, forming the extended concentrations. Due to the differences between quiet and active regions at the photospheric level described above, differences between the different underlying structures related to them should be expected.

It should be made clear at this point that the aim of this section is not to give an extensive review on the solar photosphere and its magnetic structure, but rather to provide the background for the overlying chromosphere and its structures which is the main topic of this review. The interested reader can be referred to recent, more detailed reviews on the solar photosphere, like e.g. those by de Wijn et al. (2009) and Muller (2011).

3 The solar chromosphere

The photospheric magnetic fields of different forms and strengths extend through the chromosphere into the corona providing the link between the different solar layers. As stated in the previous section in the photospheric layers the supergranular flows carry the magnetic fields to the edges of the supergranular cells resulting in large magnetic flux concentrations. The magnetic flux tubes that constitute the magnetic network expand upwards and appear as bright patches that constitute the chromospheric network. A strong spatial coincidence exists between the photospheric magnetic network concentrations and the overlying network boundaries in the chromosphere. In Ca II H&K images, which sample the low chromosphere, NBPs show up with a larger brightness enhancement over the surrounding area than they do in G-band (cf Fig. 2 of Lites et al. (1999)), but with lower sharpness due to strong resonance scattering and possibly also due to increasing flux tube width with height (Fig. 2, upper row). Also high resolution images taken in the blue wing of Hα were found to display strikingly intense small-scale brightenings

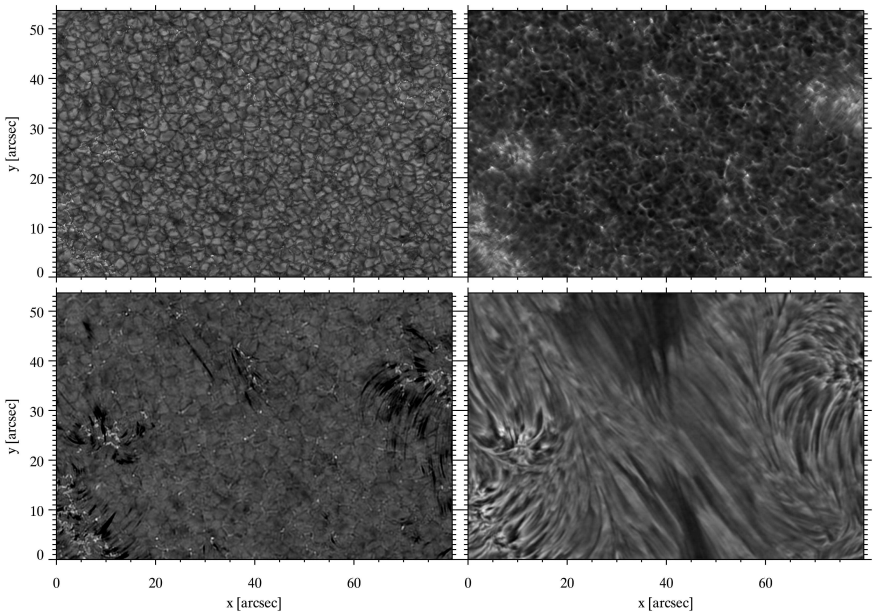

Fig. 2 Images of a quiet-Sun area containing a quiescent filament obtained by the Dutch Open Telescope (DOT) in La Palma (Canary Islands). *Top left*: G-band. *Top right*: Ca II H. *Bottom left*: blue Hα wing at $\Delta\lambda = -0.08$ nm from line center. *Bottom right*: Hα line center. The left-hand one samples quiet network, the right-hand one more enhanced network (figure courtesy of Dr J. Leenaarts, see also Leenaarts et al. (2006))

at the locations where magnetic elements form the NBPs (Fig. 2, lower row, left). Leenaarts et al. (2006) showed the potential of these Hα bright points as proxies of the magnetic elements.

The solar chromosphere being only about 2 500 km thick ($\sim 3''$) actually covers the layer where the solar atmosphere turns from the gas-dominated photosphere/lower chromosphere into the magnetic field dominated upper chromosphere/corona (for recent reviews on the solar chromosphere, as well as to its coupling with the other solar layers the reader can be referred to Rutten (2007), Rutten (2010), Wedemeyer-Böhm et al. (2009)). Chromospheric plasma, especially when seen in the center of the Hα line, is very clearly organized along fine-scale, dark, elongated structures that span out from regions of enhanced magnetic flux. Some of them are connected to neighbouring regions and others fading in between, while covering the IN cells (Fig. 2, lower row, right). Such filamentary structures portray the magnetic field topology and are consistent with the increasing dominance of the magnetic pressure over the gas pressure with increasing heights in the atmosphere. This dominance has as a result the upward expansion of the magnetic fields which fill the space in the chromosphere and affect its dynamics. The relative importance of the pressures is given by the ratio of plasma pressure to magnetic pressure (also referred to as the plasma-β) and is related to the formation of the magnetic canopy zone. This zone, in which $\beta = 1$ and the sound speed equals the Alfvén speed, separates the solar atmosphere into magnetic and non-magnetic regions and plays an important role in the refraction and reflection of

the upward propagating waves, as well as in converting acoustic waves into other modes, such as fast and slow magnetoacoustic waves(see e.g. Rosenthal et al., 2002; Bogdan et al., 2003)). Kontogiannis et al. (2010a) and Kontogiannis et al. (2010b) have shown the important role the dark Hα fine-scale magnetic structures play in the formation of the magnetic canopy (for details see Section 6). As one goes from the Hα line center to the wings, the picture gradually changes (see lower left panel of Fig. 2). It is, usually, suggested that in dark structures observed in the Hα line wings the intensity is coming from lower layers than the core of the line, although it cannot be excluded that it might come from highly Doppler shifted features that are located higher in the atmosphere than the features observed in line center. The dark structures endings in the Hα blue wing image (Fig. 2, lower row, left) – which are part of the elongated mottles seen in Hα line center- are likely to emanate from photospheric bright points which are concentrated into clusters. The relationship between the ends of the dark structures and the photospheric bright points is presented in Section 5.

From the above it becomes clear that the photosphere and chromosphere are coupled via magnetic fields and, furthermore, any description of the solar atmosphere in terms of average properties is incomplete without the consideration of the fine-scale structures and their dynamics.

4 Fine-scale, jet-like chromospheric structures

Mottles, spicules, fibrils and dynamic fibrils, straws, rapid blue excursions (RBEs) are some of the jet-like, fine-scale features that dominate the dynamic and highly-structured chromosphere. Direct, narrow-band or broad-band filtergrams have provided the means for obtaining parameters such as lifetime, size, spatial distribution, inclination, etc., of these structures. On the other hand, spectroscopic observations in different lines are essential to extend our knowledge on the physical conditions, particularly the temperature, density and flows. Determination of the physical conditions in the observed features is also based on the study of the spatial and temporal variation of the observed radiation intensity in different wavelengths, i.e. line intensity or contrast profiles. On the basis of observational findings various theoretical models and numerical simulations have been developed to explain the mechanism responsible for their formation. However, in spite of the remarkable advances made by the high resolution observations and by the development of theories and numerical simulations, their interrelationship, the determination of their physical parameters, the definition of their formation mechanism, as well as their possible role in the heating of the solar corona still remain uncertain. Ambiguities are mainly due to the differences in their appearance when observed in different spectral lines, but also at different wavelengths within the same line, to the different instruments used for their observation (which usually have different spatial and temporal resolution), to the different methods used to infer their physical parameters, especially velocities, to their relatively short duration and rapid changes and, most important, to the different names used by different authors to describe the same structure.

Below we present a description of the appearance and the physical properties of these structures. We follow the traditional terminology, as well as the recent one

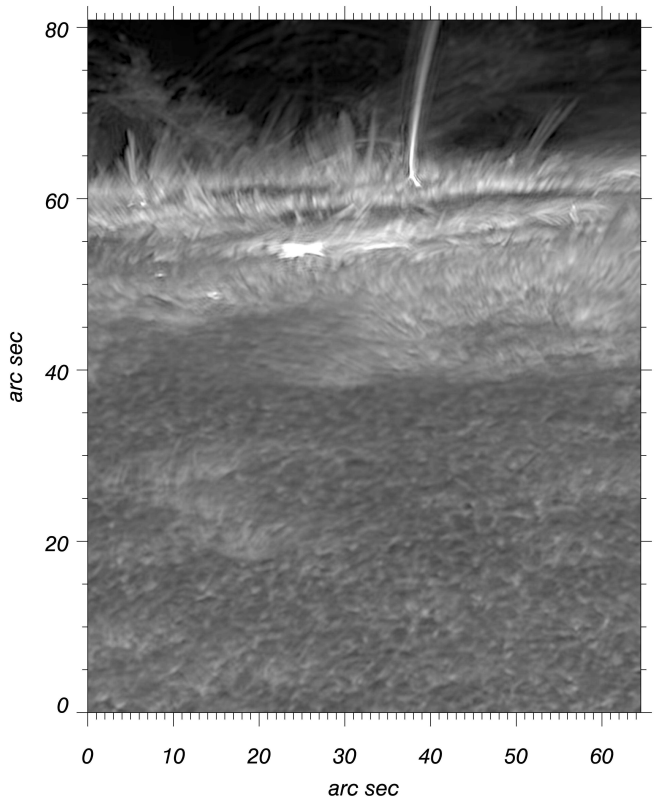

Fig. 3 A sample DOT Ca II H image obtained on November 4, 2003 showing numerous jet–like structures (spicules, active region fibrils, superpenumbral fibrils) clearly visible on the limb in addition to a large surge. The dark elongated structures near the limb are sunspots. At the bottom of the image thin bright structures, called straws, are emanating, from the chromospheric network (which is hardly visible in this image), while around the active regions several dynamic fibrils and penumbral fibrils are visible (from Tziotziou et al. (2005))

which has resulted from high resolution observations of some "new", "spicular-like" structures.

4.1 Off-limb structures

4.1.1 Spicules

The traditional term "spicule" refers to the relatively thin, elongated jet-like structures, seen at the limb of the Sun which appear as bright jet-like features against the dark background of the solar corona. The term was first used by Roberts (1945), to describe jets which dominate the chromosphere seen at the limb shooting up to 10 000 km heights. Spicule-like features, however, were first observed and described by Father Angelo Secchi of the Vatican Observatory in 1877 (Secchi, 1877). As first reported by Lippincott (1957), spicules seem to show a group behavior, the so-called "porcupine" and "wheat" field patterns. In the former, spicules

seem to radiate outward from a common centre forming a 18 Mm wide configuration along the solar limb, whereas in the latter all spicules seem to have the same orientation over a width of 140 Mm. Initially, spicules were associated with quiet Sun regions at the limb, nowadays, however, it is believed that on-disc quiet Sun structures called mottles constitute only a fraction of the observed off-limb spicules and that active region fibrils, as well as superpenubral fibrils are seen as spicules when these regions cross the limb (see Fig. 3). Despite their discovery over 130 years ago, spicules are among the least understood phenomena of the solar chromosphere. Until recently, this was due to the lack of high-resolution observations (their diameters of a few hundred kilometers and lifetimes of a few minutes were close to the observational limits), as well as to the highly simplified and poorly constrained models used for their modelling. Several recent advances not only on the observational side, but also on the modelling side have provided significant progress on the understanding of these structures. However, we still lack definitive answers on several of their physical properties and interrelationships with other limb and on-disk structures, while models still face difficulties in describing them accurately. Beckers (1968, 1972) give comprehensive reviews of early work on mottles and spicules, while a more recent review on the modelling of these structures is given by Sterling (2000).

The morphology and properties of spicules have been under study for the last sixty years although with rather limited interest after the early years of their characterization. Only recently, the interest of the solar physicists on them has been revived by the fact that high resolution instruments are being used. High resolution movies in the Ca II H line obtained with the Broadband Filter Imager (BFI) of SOT on the seeing-free Hinode spacecraft have revealed a remarkably dynamic, spicule-dominated limb. Based on some physical properties derived from SOT/Hinode Ca II H observations, De Pontieu et al. (2007b) suggested that there exist two types of spicules: a) "Type I" spicules, similar to the traditional spicules, which appear to rise up from the limb and then fall back, to be long-lived (3 – 7 min) and to exhibit longitudinal motions of the order of $20\,\mathrm{km\,s^{-1}}$ and b) "Type II" spicules which seem to have much shorter lifetimes (50 – 100 s), higher velocities ($\sim 100\,\mathrm{km\,s^{-1}}$), to be considerably taller and to exhibit only upward motion and then rapidly disappear (Fig. 4).

In that work the authors following the time evolution of the intensity along a fixed cut almost perpendicular to the limb (see Fig. 4), they were able to show at least one clear example of a "Type I" spicule which shows a distinctive different profile than the steep linear streaks caused by "Type II" spicules. However, since spicules are so dynamic and may move in and out of the fixed cut, such intensity profiles that cover the full time series cannot be used to reliably measure the properties of spicules. Thus the authors had to rely on spicules that did not move transversely so that their full life time could be covered by a fixed cut. Quite recently, Zhang et al. (2012) re-analyzing the same data sets adopted by De Pontieu et al. (2007b) identified and traced 105 and 102 spicules in quiet Sun and coronal hole (CH), respectively. They claimed that they could not find a single convincing example of "Type II" spicules. Furthermore, they reported that more than 60% of the identified spicules in each region showed a complete cycle, i.e., the majority are "Type I" spicules. Thirdly, the lifetimes of the spicules in the quiet Sun and CH are 148 s and 112 s, respectively, but there is no fundamental lifetime difference between the spicules in the quiet Sun and CH reported earlier.

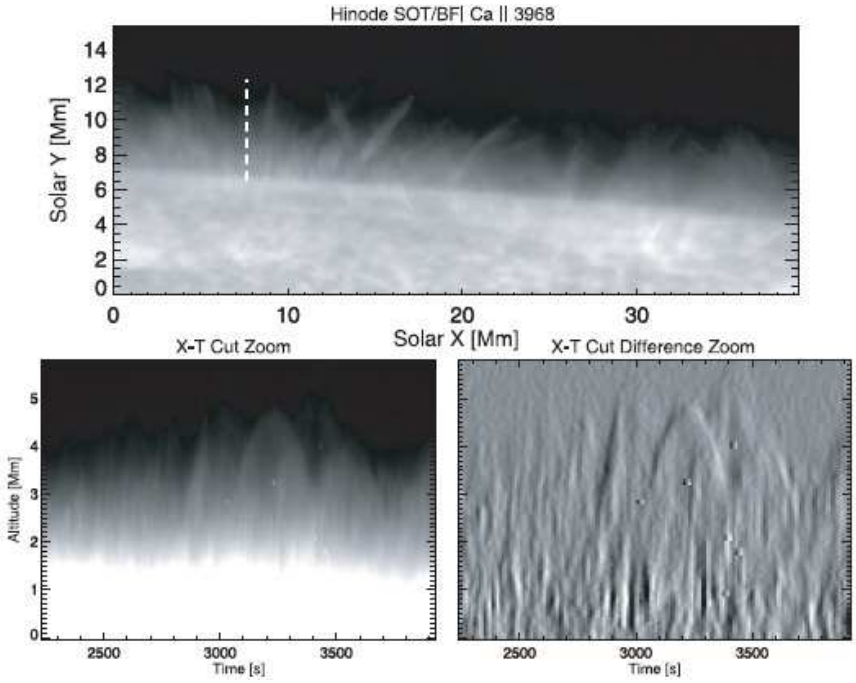

Fig. 4 The top panel shows spicules at the quiet Sun limb obtained with the SOT/Hinode in the Ca II H passband. The bottom panels show space-time (X – T) plots along the location indicated by a dashed line in the top panels, for both the original data and time difference data. The space-time plot is dominated by short-lived vertical stripes (Type II spicules) and longer-lived parabolic paths (Type I spicules) (from De Pontieu et al. (2007b))

In the same paper of De Pontieu et al. (2007b), the authors in order to reveal the two different populations applied two different filters to the time series. The first, low-frequency, filter was a Gaussian centered on 3 mHz with a width of 0.5 mHz and brought out the "Type I" spicules, i.e. the relatively slowly evolving features that typically move up and down during their lifetimes of order 3 – 7 min. The second filter was designed as a combination of a high-pass filter (≥ 15 mHz) with a low-pass filter placed at a frequency which is 2 mHz lower than the Nyquist frequency of the time series studied. This filtering isolates the longer lived Type I spicules from the more dynamic, Type II, spicules which appear and disappear on very short time scales. It has not been checked, however, if there exist spicules having lifetimes in-between the above mentioned timescales.

Tavabi et al. (2011) have recently shown that there exist four types of spicules based on the spicule's diameter, ranging from 0.3″ (220 km), 0.5″ (360 km), 0.75″ (550 km) to 1.15″ (850 km). Unfortunately, detailed comparisons between the "classical" spicules and those called Type I and Type II is not easy to perform for several reasons among which the most important is the lack of spatial and temporal resolution of classical observations. Below we summarize properties of structures seen at the limb.

Spicule abundances In contrast to activity phenomena, spicules are omnipresent at the solar limb. Their abundance has been measured, as a variation of height and solar latitude. A point to emphasize is that the number of counted spicules depends very much on the quality of the observations. Thus their number, in total, is estimated to reach $\sim 10^6$ at zero height, while it is possible that this number is larger (Beckers, 1972). Most of the observational studies reviewed by Beckers (1968) show that the spicule number increases with height reaching a maximum at a height and then decreases again. This is a result of spicules overlapping one another at lower heights and only few of them reaching large heights. An estimation of the variation of spicules' abundance with height gives around 56 000 spicules on the full solar disk, around 5 000 km from the surface. Athay (1976) and Zirin (1988) give 60 000 and 70 000 respectively, for the total number of spicules on the whole Sun at any time. Judge and Carlsson (2010) assuming Type II spicules to be randomly distributed along the boundaries of circular supergranules into 200 small bushes with a common "root", and each bush to have eight spicules, they obtained 1600 spicules per supergranule. With each spicule having a diameter of 0.1 Mm, they obtained an area filling factor of 0.015 and a total of 2×10^7 Type II spicules on the Sun at any time. This value is some 20 times larger than the value given by Beckers (1972), while Type I spicules are not included. Type I classical spicules being shorter are very difficult to count. They obtained this result by comparing Monte Carlo radiative transfer calculations with observations obtained by the SOT/Hinode in the Ca II H line. However, Sekse et al. (2012) questioned this estimate and argue that this number is too high and would imply a much more spicules than observed. Moore et al. (2011) surmised that at any given time there are $\sim$ 50 Type II spicules present per supergranule, or $\sim$1 Type II spicule per 2×10^{17} cm^2 of surface area in quiet regions and coronal holes. All given values depend, of course, on the threshold intensity adopted for the spicule visibility and in which height from the solar limb spicules are counted. In some studies, a variation of abundance as a function of solar latitude has been found. More precisely, the number of spicules was found to decrease from poles to equator (Lippincott, 1957; Athay, 1959).

Spicule inclination The inclination of spicules is undoubtedly reflecting the local magnetic field topology. It should be mentioned that what can be measured is their apparent tilt with respect to the local vertical, since what we actually see is the projection of a spicule into the plane normal to the LOS and this leads to an underestimate of its true inclination. Measurements are also biased towards smaller inclination values, since the most inclined spicules are either not raised high enough to be visible or it is difficult to discern the shorter ones due to superposition effects. Old studies, reviewed by Beckers (1968) report a mean variation of $\sim 20^\circ$ of spicules' inclination from the local vertical. Heristchi and Mouradian (1992) measured the apparent tilts to the vertical of 843 spicules and from the distribution of the inclinations they found an average tilt of 29°. It should be noted that their distribution was referred to an axis with a tilt of 14° in the yz plane as they found that spicules tend to lean towards the equator. Recent calculations by Pasachoff et al. (2009) did not find such a large tilt toward the equator. They measured an average absolute inclination to the vertical of 23°. Their statistics, however, contained only 40 spicules. A hint on the inclination of spicules has been achieved recently by the efforts to determine the magnetic field and its inclination

in spicules (see Section 4.1.1). López Ariste and Casini (2005) found a good correlation between the orientation of the magnetic field lines and Hα spicules (see Fig. 12), while Trujillo Bueno et al. (2005) found that the best fit to the observed Stokes profile is obtained for a magnetic field inclination of $\theta = 37°$. Pasachoff et al. (2009) pointed also out that it is possible that spicules' tilt varies with the solar cycle. Since spicules follow the pattern of the magnetic field, such a variation is possible. Considerable differences in the inclinations of spicules at different heliographic latitudes have also been reported. At the polar regions, spicules seem to have less variable inclinations and to be more perpendicular to the surface, whereas they attain more and more larger inclinations towards the equator as the latitude decreases. Bonnet et al. (1980) also found that in Ly–α photographs of the solar limb, spicules appeared to be symmetrically distributed around the polar axis. There are several older studies (van de Hulst, 1953; Lippincott, 1957) that associate spicules' inclination with that of the coronal polar rays, but such detailed correspondence should be re-examined with the current high resolution observations.

Spicule lifetime and birthrate A spicule's lifetime is defined as the average duration of spicule visibility. There is a large dispersion in the reported values of the lifetime of spicules. Most studies agree that the lifetime of spicules is between 2 and 12 min (Roberts, 1945; Rush and Roberts, 1954; Lippincott, 1957; Alissandrakis and Macris, 1971; Cook et al., 1984; Georgakilas et al., 1999) with 5 min considered as a typical mean value. The same range of values has been confirmed for Hα spicules by Pasachoff et al. (2009) who found lifetimes between 3 and 12 min, with a mean value of 7.1±2.3 min. The same authors find shorter lifetimes in TRACE 1600 Å counterparts of Hα spicules pointing out a possible impact of the lower resolution of TRACE observations. The highest resolution available (from SOT/Hinode in the Ca II H passband) have attributed lifetimes around 3 – 7 min for the classical spicules and lifetimes of the order of 10 – 150 s to the extremely short-lived ones termed Type II (De Pontieu et al., 2007b). Beckers (1968) gives as a spicule birthrate the number $330\,\mathrm{s}^{-1}$.

Spicule heights and widths The height of a spicule is conventionally measured from its foot at the photospheric limb up to where the spicule becomes invisible. It should be noted that what is finally measured is the projected height of the structure on the plane of the sky. The height of a spicule is not a well defined quantity, since there is not a sharply defined upper boundary and its foot-point, as well as its location in front or behind the limb cannot be easily established, while its determination depends amongst others on the seeing conditions, line of observation, exposure time, etc. Especially, in the Hα line there is a chromospheric limb, which inhibits the tracing of the spicule to the photosphere. Apart from these difficulties, studies of the distribution of the apparent heights of spicules shows good general agreement. Beckers (1968, 1972) reviewed older studies based on Hα observations, which gave estimates of average heights between 6 500 and 9 500 km. Since then, spicules have been reported to reach up to 15 000 km (Cook et al., 1984) in Hα, but also in He II (Georgakilas et al., 1999). A recent analysis by Pasachoff et al. (2009) based on high resolution Hα observations of the solar North–Western limb combined with co-temporal TRACE images in the 1600 Å channel gives apparent heights in the range 4 200 – 12 200 km with a mean of 7 200±2 000 km and

agree very well with the old results given by Lippincott (1957). They also identified spicules common in both Hα and 1600 Å image data sets and found that in 1600 Å images, they were taller (5 600 – 14 700 km) and correlate very well with the height in Hα. They concluded that the heights reached by spicules observed in the TRACE UV continuum are $\sim$ 2 800 km greater than that reached in Hα. Similarly, spicular structure up to $\approx$ 18 Mm has been reported obtained by TRACE in Ly–α an TRACE 1600 Å at the north solar limb (Alissandrakis et al., 2005). According to De Pontieu et al. (2007b), the maximum lengths of spicules observed in Ca II by Hinode vary from a few hundred kilometers to 10 000 kmwith most below 5 000 km. Type II spicules attain heights between 1 000 and 7 000 km and they are tallest in coronal holes.

The diameter of spicules is probably the property most influenced by observing conditions, such as atmospheric seeing and the diffraction limit of the instrument, as well as overlapping effects that make it difficult to separate individual spicules. Older studies based on Hα and Ca II H and K lines estimate the spicules' diameters to range between 400 and 2 500 km (Beckers, 1968, 1972), with most spicules having diameters between 400 and 1 500 km (Dunn et al., 1960; Lynch et al., 1973) which were characterized, at the time, by Beckers as the "most reliable" values. Recent high resolution Hα observations provide a more strict estimate, in the range 300–1 100 km with a mean diameter of 660 km (Pasachoff et al., 2009) which is in very good agreement with results by Nishikawa (1988) who found an average diameter 615$\pm$250 km. Pasachoff et al. (2009) also found that the width in the 1600 Å TRACE channel is greater than the width measured with the Swedish 1-meter Solar Telescope (SST) at Hα by a factor of over 1.5, ranging between 700 and 2 500 km. They argued that TRACE widths are impacted by the telescope's broad point-broad point-spread function, while the resolution of SST is approximately four times higher that that of TRACE. With the advent of high resolution instruments, thinner structures are being observed ($<$ 200 km) and some have been attributed to Type II spicules. They have also revealed that some Ca II spicules consist of finer threads (double thread structure) (Suematsu et al., 2008). Tavabi et al. (2011) give an extensive Table together with references (see their Table 1) of the various values obtained so far for the diameters of spicules. Furthermore, these authors based on Ca II H SOT/Hinode observations at the northern solar limb found that spicule diameters show a whole range of widths from 200 to more than 1 000 km, with distributions at four distinct diameters.

Spicule temperatures and electron densities Spicule temperatures and densities can be estimated spectroscopically by using spectra taken simultaneously in several different lines. It should be noted that temperature (and electron density) diagnostics of spicules from line intensities rely on data from constituents that are especially difficult to model. In order to interpret line profiles, non-LTE calculations have to be used which is not an easy task. Due to the difficulty of such calculations there are very few reports on temperature and density determinations in spicules and very large discrepancies on the reported values. Unfortunately, recent theoretical results do not exist. Compilation of older theoretical results is given by Beckers (1972). Beckers derived these parameters by assuming that a spicule is a cylinder situated vertically on the Sun and irradiated by the solar radiation having a diameter of 815 km. From the intensity of a spectral line he obtained a T_e–N_e curve. He then compared the observed line intensities with the predictions of theoretical

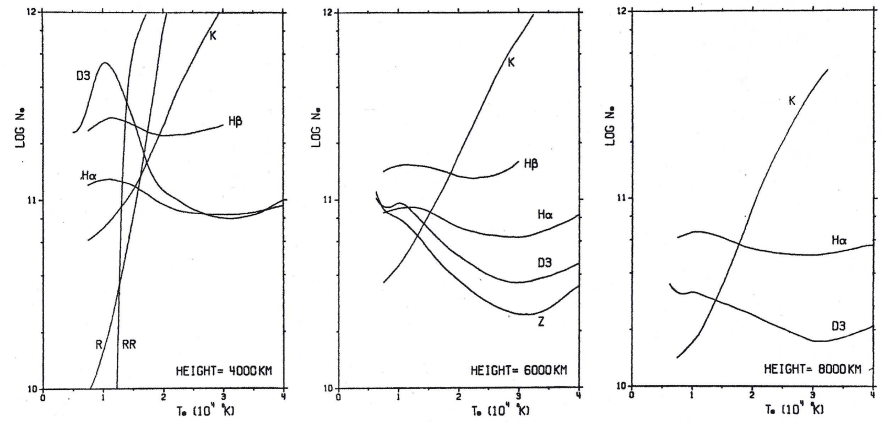

Fig. 5 Relation between spicule temperature and electron density at different heights as derived for different lines. Z stands for the He 10830 line, R, for the ratio of 3888 Å helium to hydrogen line intensity, RR for the ratio of Ca II and He–D_3 line as derived from eclipse spectra (from Beckers (1972))

models. Curves obtained by this way from different lines will intersect, giving a set of temperature and density that is consistent with all observations (Fig. 5). Beckers (1972) derived the temperature from the observed intensities of Hα, He II, and Ca II lines from simple non-LTE calculations. He reports a temperature of 9 000 K and an electron density of $1.6\times10^{11}\mathrm{cm}^{-3}$ at a height of 2 000 km and a temperature of $\sim$ 16 000 K at 4 000 – 8 000 km, while for the electron densities he derived values $1.5\times10^{11}\mathrm{cm}^{-3}$ at 4 000 km and $4.3\times10^{10}\mathrm{cm}^{-3}$ at 8 000 km.

Krat and Krat (1971) obtained simultaneous spectrograms of spicules in the lines Hα, Hβ, D3 and Ca II H and K at heights varying from 5 000 km to 9 000 km above the limb, the slit being set parallel to the limb. They concluded that the emission in the different lines originates in different parts of spicules with different radial and turbulent velocities and that the electron density varies from $10^{11}\mathrm{cm}^{-3}$ to $10^{12}\mathrm{cm}^{-3}$.

Alissandrakis (1973) analyzed simultaneous spectra of spicules at a height of 5 400 km above the limb in the Hα, Hβ and Ca II lines. Since the intensity of the Balmer lines is a very good indicator of the electron density, as they are almost insensitive to temperature, while the K line is sensitive to both the N_e and T_e, he combined the observations to obtain the temperature and density of spicules. He found that the values of the electron density for 36 spicules at a height of 5 400 km range between $6\times10^{10}\mathrm{cm}^{-3}$ and $1.2\times10^{11}\mathrm{cm}^{-3}$, with an average value of $6\times10^{10}\mathrm{cm}^{-3}$, while the range of the electron temperature was between 12 000 K and 15 000 K with an average of 13 000 K.

Krall et al. (1976) analyzed time sequences of simultaneous spectra of limb spicules in the Hα and Ca II H and K lines. Using the measured intensities in these lines they derived electron densities averaged over the entire visible lifetime of spicules of $\sim 6\times10^{10}\mathrm{cm}^{-3}$ at the height of 5 000 km and minimum and maximum values of $\sim 1.1\times10^{11}\mathrm{cm}^{-3}$ at 6 000 km and $2.\times10^{10}\mathrm{cm}^{-3}$ at 10 000 km, respectively. They also found electron temperatures ranging between 12 000 K and 16 000 K,

while from profile half-widths, they concluded that turbulent velocities should be in the range between 12 and 22 km s^{-1}.

Braun and Lindsey (1987) used brightness limb observations at 100 and 200 μm and 2.6 mm. Use of far-infrared continuum observations are useful because the continuum emission is formed in LTE and the source function is just the Planck function, which in the Rayleigh–Jeans limit is proportional to the electron temperature. They calculated limb intensity profiles for a variety of spicule models and found that limb profiles are well fitted by spicules with an electron temperature of the order of 7 000 K up to heights of at least 7 000 km above the photosphere. Particularly the 2.6 mm observations exclude spicule temperatures of 16 000 K below 7 000 km, because this temperature should create a substantial limb brightening, which is not observed.

Matsuno and Hirayama (1988) determined the height distribution of the kinetic temperature of Hα spicules. The temperature was found to decrease from 9 000 K at 2 200 km to 5 000 K at 3 250 km and to increase up to 8 200 K at 6 000 km. They suggested that the decreasing temperature with height might be related to the lateral expansion of rising spicular material along the expanding magnetic field lines, while the increasing temperature above 3 250 km may be due to heating by the penetrating radiation in the Lyman continuum originating in the EUV emission of the transition region–corona.

Socas-Navarro and Elmore (2005) used multiline limb observations of spicules from different elements and, specifically, in the Ca II 8498 Å and 8542 Å lines using the Advanced Stokes Polarimeter (ASP) at the Dunn Solar Telescope (DST) and the He I multiplet at 10830 Å recorded with the Spectro-Polarimeter from INfrared and Optical Regions (SPINOR), to derive some spicule properties. They found that the Doppler widths of the observed spectral lines are similar. Since the Ca atom is ten times heavier than the He atom, if the lines were broadened by microscopic thermal velocities, one would expect the He line to be more than three times broader than the Ca lines, which is not the case. Assuming non-thermal broadening they concluded that the electron temperature of the spicule should be lower than 13 000 K to account for the observed line broadening.

Evolution and velocities of limb structures For limb spicules, different and sometimes contradictory results on the velocities and their variations have been reported. One of the reasons is due to the different types of observations that have been used. Apparent velocities correspond to motions in the plane perpendicular to the LOS and could equally well result from the temporal variation of the excitation or ionization of the spicular material, or the propagation of a shock front. The general description based on measurements of apparent velocities is consistent with a spicule which rapidly elongates upwards with an average velocity of $\sim$ 25 km s^{-1} and reaches its maximum height within a minute or two after its initial appearance. The upward motion is usually fairly regular and continuous, the spicule rising and stopping abruptly at its maximum height. Subsequently, the spicule may either fade from visibility or else descend back to the low chromosphere with a velocity comparable to that of its initial ascent. Measurements of vertical proper motions were made in the 1950's and 1960's by Rush and Roberts (1954) and Lippincott (1957), and have been reviewed by Beckers (1968, 1972) and Bray and Loughhead (1974). In an old work, Lippincott (1957), after studying the apparent motions of spicules, reported that in half of them the ascending phase is followed by a

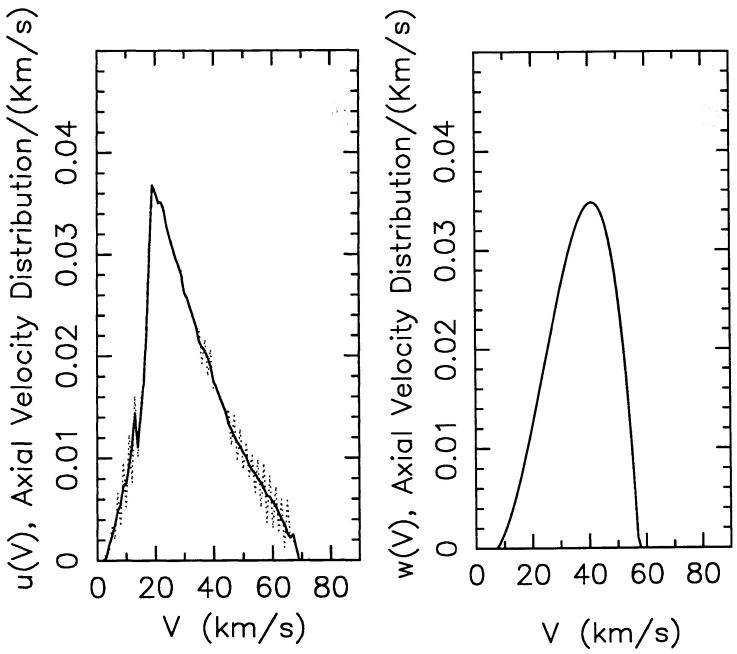

Fig. 6 *Left.* The apparent axial velocity distribution in spicules measured from the time variation of their heights. *Right.* The axial mass velocity distribution obtained from the Doppler velocities (from Heristchi and Mouradian (1992))

descending one, while the other half is fading away; she was also the first to report that some spicules appear to rise from the same source several times. The majority of descending spicules appear to retrace their original paths, but according to Beckers (1972) there are many which fall back along different paths, often forming an arch. Heristchi and Mouradian (1992) combining the observations of Rush and Roberts (1954) and Lippincott (1957), which gave the variation of height with time of spicules, constructed the observed distribution of apparent velocities relating them to the angular distribution of spicules obtained from their axial velocity distribution (Fig. 6, left). They give as the most probable velocity $20\,\mathrm{km\,s^{-1}}$ and a range between $0\,\mathrm{km\,s^{-1}}$ and $60\,\mathrm{km\,s^{-1}}$. De Pontieu et al. (2007b) from the analysis of chromospheric Ca II H observations taken with the broadband filter on board the Hinode mission found that spicules shoot upward at speeds between 20 and $150\,\mathrm{km\,s^{-1}}$. Recently, Pasachoff et al. (2009) reported that in the majority of the 40 spicules examined, they found only ascending velocities because most of the spicules seemed to disappear at their maximum heights. They measured ascending velocities with a mean of $27.0\pm18.1\,\mathrm{km\,s^{-1}}$, a median of $25\,\mathrm{km\,s^{-1}}$ and a range of 3.0 to $75\,\mathrm{km\,s^{-1}}$ (Fig. 7, left).

Apart from the velocities deduced from direct observations of the changes of the height of spicules with time, velocities can also be inferred from spectroscopic observations which give information on Doppler shifts. The Doppler shifts of the emission features can be interpreted as LOS mass motions of the spicular material. It should be noted that for a spicule inclined to the plane of observation, the

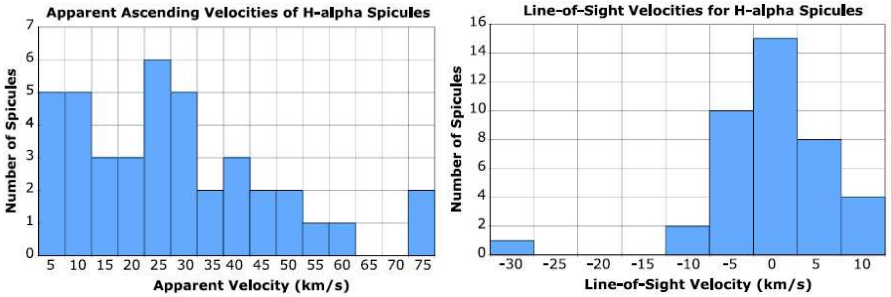

Fig. 7 *Left.* Histogram showing the distribution of apparent ascending velocities. *Right.* Histogram showing the distribution of the LOS velocities of the tops of the spicules when they were at their maximum heights (from Pasachoff et al. (2009))

component of the rise velocity corresponding to the sine of the angle of inclination would be observed.

Alissandrakis (1973) using simultaneous spectra in Hα, Hβ and Ca II K at a height of 5 400 km above the limb obtained the LOS velocity distribution of 50 spicules, as inferred from the position of the maximum of the line profile in the three lines. Thus he found an absolute average value of the LOS velocity of 6.4 km s^{-1} for Hα, 5.6 km s^{-1} for Hβ and 4.9 km s^{-1} for Ca II K. Using this technique Heristchi and Mouradian (1992) measured the LOS velocity component of 90 well–isolated spicules at 5 000–6 000 km above the limb. To improve the statistics they have also added some other available distributions (see their Table I). Relating the measured Doppler velocity distribution (which was approximately symmetric ranging between -30 to 30 km s^{-1}) with the angular distribution of inclinations they obtained as a most probable axial velocity 40 km s^{-1} (Fig. 6, right), i.e. about 20 km s^{-1} larger than the most probable apparent upward velocity. Recently Pasachoff et al. (2009) measured LOS velocities from Doppler shifts of the tops of spicules found at their maximum heights (Fig. 7, right). The Doppler shifts were calculated by fitting Gaussians to 5–wavelength Hα spectra. They reported a mean absolute value of 5.1$\pm$5.1 km s^{-1}, a median of 3.8 km s^{-1} and a range of 0.3 to 30.2 km s^{-1}. This value agrees with the mean value of 6 km s^{-1} quoted by Beckers (1972). They also found that the distribution of the LOS velocities at the bases of the 40 spicules measured (where the base is defined as the location of the apparent limb) has a mean of 3.1$\pm$11.9 km s^{-1} and a range of -17.8 to 51.2 km s^{-1}. As noted from their Doppler measurements, they regularly found oppositely directed motions, i.e. bi–directional, which could be an indication of magnetic reconnection. One has to bear in mind, however, that whereas photographic observations give the vertical velocity of the spicules in the plane of the limb, spectroscopic observations give the velocity component along the LOS and, hence, in the direction normal to the plane of the limb. This fact can explain the discrepancy between the average apparent vertical velocity value of 25 km s^{-1} and an average value of $\sim$ 6 km s^{-1} obtained for the LOS velocity of spicules. Following Athay and Bessey (1964), one can show that the magnitude of the average Doppler velocity of spicules lying in a cone whose axis is normal to the LOS and whose apex angle is 2θ (see Fig. 8) is given by the formula:

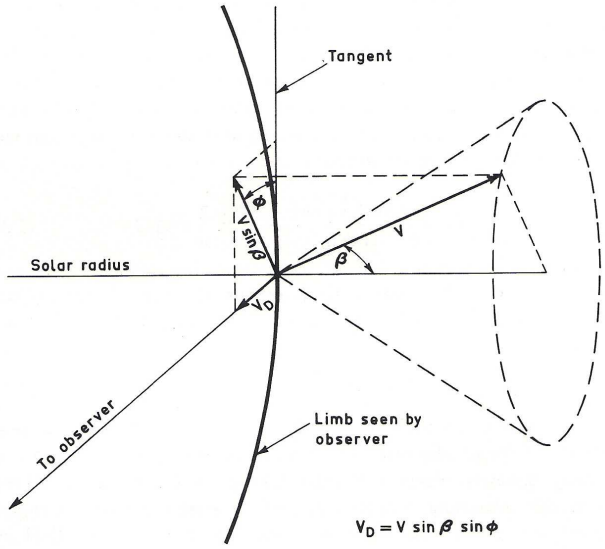

Fig. 8 Resolution of the velocity V of a spicule along the LOS. V_D is the LOS component, β is the angle made by the spicule with the solar radius, and ϕ is the azimuthal angle of the projection of the spicule velocity vector onto a plane tangent to the limb (from Bray and Loughhead (1974))

$$\bar{V}_D = \frac{V \sin\theta \int_0^{\pi/2} \sin\phi d\phi}{\int_0^{\pi/2} d\phi} = \frac{2}{\pi} V \sin\theta \tag{1}$$

where ϕ is the azimuthal angle of the projection of the spicule velocity vector onto a plane tangent to the limb. At greater heights, the observed Doppler shifts will be positive or negative depending on whether the spicule is inclined away from or towards the observer. Thus for V=25 km s^{-1} and θ=30° we get 8 km s^{-1} for the average LOS velocity of spicules, which is close to the value reported from observations.

Heristchi and Mouradian (1992), as stated above, found a large difference ($\sim$ 20 km s^{-1}) between the maxima of the distributions of the axial velocities deduced from the measurements of the apparent and Doppler velocities of spicules. As they anticipated this difference is presumably due to the ionization of the hydrogen atoms, when the spicules, penetrating the corona, are heated. Thus if a partially ionized plasma parcel is moving along the axis of a spicule with a velocity of $\sim$ 40 km s^{-1} and at the same time its front is being ionized and an ionization wave is moving backwards with a velocity of $\sim$ 20 km s^{-1} then the apparent velocity would be equal to 20 km s^{-1}. They also noted, however, that the differences in the obtained values may also be due to the fact that the data they used for their calculations were taken at different periods of the solar cycle, at different locations on the Sun, with different instruments and with different techniques.

The height dependence of the LOS velocity in spicules has also been investigated by several authors. The results obtained differ significantly from each other. For instance, Mouradian (1965) has found that the Doppler shift decreases along

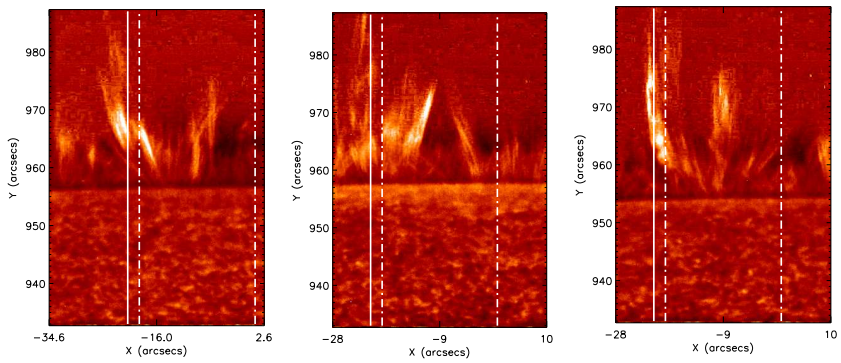

Fig. 9 SOT/Hinode Ca II H images showing spicules taken from left to right, on 2009, April 28 at 16:24 UT, on April 29 at 02:24 UT and 03:28 UT. The over-plotted solid line indicates the position of the SUMER slit, while the dashed-dotted lines indicate the EIS raster field-of-view (FOV) (from Madjarska et al. (2011))

the spicule, Beckers et al. (1966) found an increase of the Doppler shift with height, while Pasachoff et al. (1968) reported a weak or even no observable change of the shift with height. The main reason for these discrepancies are due to the fact that observations of spicules at various heights simultaneously are related to instrumental difficulties. Kulidzanishvili (1980) studied almost simultaneously height sequences of 69 spicules in the Hα line. He claimed that absolute values of LOS velocities increase linearly with height and that no variation of the sign of the LOS velocity along individual spicules is observed.

It is quite evident that spicule motions and their time variations are essential in clarifying the mechanism responsible for their formation. However, reported time variations of Doppler shifts are contradictory. Mouradian (1965) reported that the Doppler shift of spicules increases progressively with time, goes through a maximum and then decreases, but it does not change sign, being always upwards. Pasachoff et al. (1968) found that Doppler velocities of a certain number of spicules do undergo quasi-periodic reversals. Recently, Wilhelm (2000), in a study of spicules observed in several EUV lines by SUMER on SOHO, reported strong red and blue shifts within a feature, which, furthermore, reverse sign. Madjarska et al. (2011) have recently analysed three large spicules (Fig. 9) and found them to be comprised of numerous thin spicules which rise, rotate and descend simultaneously forming a bush-like feature. Their rotation resembles the untwisting of a large flux rope. They show velocities ranging from 50 to 250 km s^{-1}. These data will be further discussed in Part II of these review series.

Nishikawa (1988) studied the proper motion of polar limb spicules using time sequence filtergrams of single wavelength bands centered on Hα–0.9 Å or Hα+0.9 Å (the passband was 0.5 Å) obtained with the Domeless Solar Telescope at the Hida Observatory. After following successively from frame to frame four individual spicules he examined whether spicule motions can be interpreted as representing ballistic or constant velocity. By fitting the height variation with a quadratic function of time (a constant acceleration model) he found large initial velocities of 80 – 100 km s^{-1} and large acceleration of 0.45 – 0.65 km s^{-2}. No disk features that can provide such initial velocities have been observed. He pointed out, however,

the possibility that such a source could be small enough that it is not observed with the current resolution and concluded that the ballistic model of spicule motions cannot be rejected from the observational point of view. He also pointed out the possibility that a rising and a falling motion can be separately fitted with a constant velocity model. In this case, the constant velocities ranged from 30 to 50 $\mathrm{km\,s^{-1}}$.

Christopoulou et al. (2001) applied an image processing technique to high-resolution observations obtained with the DST of the Sacramento Peak Observatory. They estimated the proper motions of the apparent tops of several spicules, by performing a least-square fit to the height measurements as a function of time assuming a ballistic motion, i.e. that the plasma is subject only to gravitational forces. They obtained initial velocities larger than $40\,\mathrm{km\,s^{-1}}$ in all cases examined, suggesting that the magnetic field or other forces should play an important role in the generation of spicules. It is clear from the above that the behaviour of the flow along spicules remains an open question.

Apart from the flows along spicules, motions of spicules themselves parallel to the limb have been reported. From sequences of Hα spectra taken with the slit tangential to the limb, Pasachoff et al. (1968), Nikolsky (1970), Weart (1970), Nikolsky and Platova (1971) found evidence that some spicules change their position along the slit relative to the average positions of other features thus apparently showing a real horizontal component of velocity. Nikolsky and Platova have concluded that the spicules execute quasi–periodic oscillations parallel to the limb with a period of $\sim 1\,\mathrm{min}$, characteristic amplitude of $1''$ and velocities about $10 - 15\,\mathrm{km\,s^{-1}}$. Kukhianidze et al. (2006) performed observations of solar limb spicules at 8 different heights, i.e. $\sim 3\,800 - 8\,700\,\mathrm{km}$ above the photosphere was covered. They found that $\sim 20\%$ of the measured height series showed a periodic spatial distributions in the Doppler velocities with a wavelength of 3.5 Mm and periods in the range of $35 - 70\,\mathrm{s}$. They suggested that the spatial distribution was caused by transverse kink waves. Observations of such lateral or swaying motions have again been revealed recently from the unprecedented high spatial and temporal resolution images obtained with the SOT on-board the Hinode spacecraft. De Pontieu et al. (2007c) analyzed time series of Ca II H images taken with a SOT broadband filter. They reported that many of the short-lived spicules undergo substantial transverse displacements of the order of 500 to 1000 km during their short lifetimes of 10 to 300 s, while some longer-lived spicules undergo a transverse motion with the displacement varying sinusoidally in time (Fig. 10). They suggested that this behavior is strongly indicative of Alfvén waves, where the term Alfvén waves is used to describe incompressible transverse MHD waves that propagate along the magnetic field in an inhomogeneous medium. They pointed out, however, that the observed waves could also be interpreted as MHD kink-mode waves, should a stable waveguide exist in the chromosphere. The fine structure and lateral motion of spicules has also been observed and reported by Suematsu et al. (2008). These authors suggested that spicules can be driven by magnetic reconnection in unresolved spatial scale taking place at their foot-points. They also suggested that since most spicules emanate from a seemingly uni-polar magnetic region the relevant magnetic reconnection must take place in unresolved spatial scale contrary to the larger-scale jets associated with an emergence of a small bipole.

Another unexplained feature that has been reported is that sometimes a "tilt" of the spectral line is observed in spectrograms, i.e., an inclination at a small angle

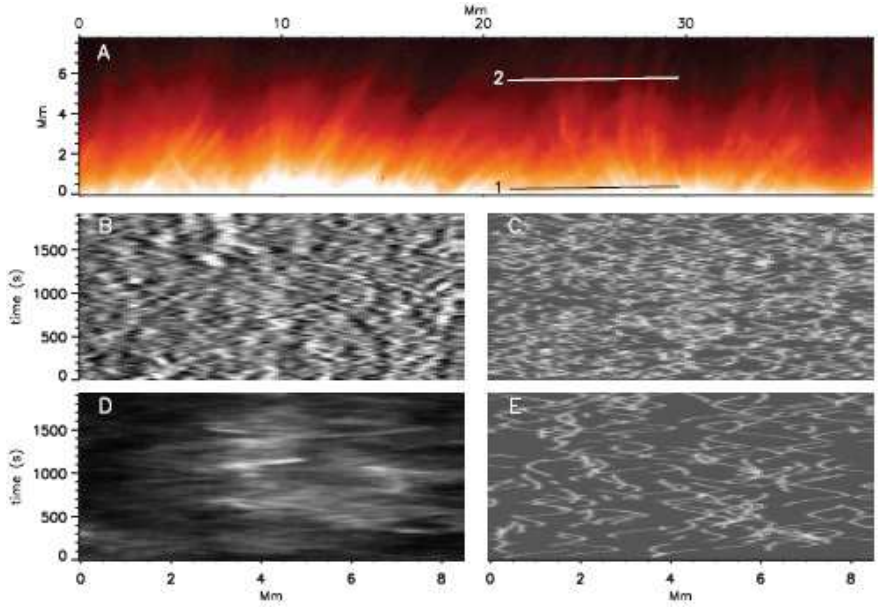

Fig. 10 (A) Spicules observed at the solar limb with SOT/Hinode in Ca II H. (B) A space-time plot (along the cut labeled 1 in (A)) of the Ca II H intensity. (D) A similar cut for the line labeled 2 in (A). The plot is dominated by a multitude of criss-crossed short linear tracks caused by spicular motion transverse to the magnetic field direction. Similar linear tracks are visible, as well as swings. The general characteristics (linear tracks and swings) of (B) and (D) are well reproduced by cuts that are generated from Monte Carlo simulations shown in (C) and (E) (from de De Pontieu et al. (2007c))

of the line profile of some spicules to the direction of the spectrograph's dispersion (Beckers, 1968; Pasachoff et al., 1968; Weart, 1970). Such inclinations have been observed in the Hα and Ca H and K spectra of spicules and could be attributed to an actual difference in the LOS velocities between the two sides of the spicule. One obvious explanation would be that in these cases there is actually not one but two separate unresolved spicules with different Doppler velocities which are seen as one because of the low spatial resolution. Another explanation which was given is that this inclination may be interpreted as resulting from the rotation of the spicule about its axis which would produce differential mass motions. If, for example, the slit of the spectrograph is oriented across the width of a rotating spicule, with the side rotating towards the observer (towards the top of the slit) and the side rotating away (towards the bottom of the slit), then the spectral line will be inclined from the shorter wavelengths to longer wavelengths going from top to bottom along the spectral line. Pasachoff et al. (1968) gave an upper velocity limit for this spicule rotation at about $30\,\mathrm{km\,s^{-1}}$. By considering a simplified model of a spicule as a column of gas 1000 km in diameter rotating with this peripheral speed they pointed out that it would have a velocity gradient of $60\,\mathrm{m\,s^{-1}}$ per km across it which would produce a spectral tilt of about 1°.9 in K and 2°.6 in Hα. As they noticed this peripheral rotation velocity implies a centripetal acceleration of $\sim 1.8\,\mathrm{km\,s^{-1}}$, i.e. about 6 times greater than the value of solar gravity. Alissandrakis (1973), on the other hand, calculated a rotational velocity of $\sim 8\,\mathrm{km\,s^{-1}}$ and concluded that the

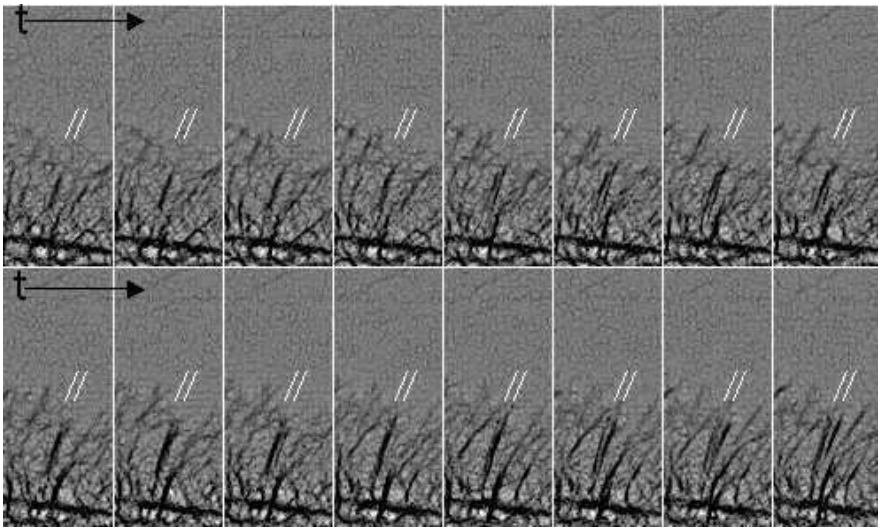

Fig. 11 Time series of sharpened images from Hinode Ca II H filtergrams. The cadence is 5 s. The series shows that the spicule consisting of double thread (indicated by white lines) is spinning as a whole body (from Suematsu et al. (2008))

rotation of spicules is almost negligible. Recently, De Pontieu et al. (2012) using high-quality observations from SST provided evidence that most, if not all, Type II spicules are characterized by the simultaneous action of three different types of motion: (1) field-aligned flows of order 50 – 100 $\mathrm{km\,s^{-1}}$, (2) swaying motions of order 15 – 20 $\mathrm{km\,s^{-1}}$, and torsional motions of order 25 – 30 $\mathrm{km\,s^{-1}}$. These last motions confirm the existence of twisting spicular motions.

Hinode high resolution observations revealed that most spicules show up a double thread structure during their evolution (Suematsu et al. (2008)). They also revealed that the separation of some of the double thread spicules changes with time, alternating between a single-thread phase and double-thread one (Fig. 11). This change in separation can be interpreted by a spinning of spicules as a whole body (spin period of 1 – 1.5 min and velocity $\sim$15 $\mathrm{km\,s^{-1}}$). Sterling et al. (2010) again from Ca II H SOT/Hinode observations reported that they found many spicules to expand laterally or split into two or more strands after being ejected. A possible explanation could be that many of the splitting or expanding spicules could be small-scale magnetic eruptions, analogous to coronal mass ejections. Consistent with this idea, the motion of the splitting spicules is similar to the spreading of the legs of filament eruptions.

Magnetic fields in spicules The determination of the magnetic field vector in solar spicules is an important step to understand them. This determination can be achieved through specto-polarimetric measurements and theoretical modelling of the Zeeman and Hanle effects in suitably chosen spectral lines. The He I 10830 Å triplet is a powerful diagnostic tool for chromospheric magnetic fields (Trujillo Bueno, 2010), because its spectral signatures are sensitive to scattering polarization, while the Zeeman, Hanle and Paschen–Back effects make it a very useful magnetic indicator within a wide range of field strengths.

The Zeeman effect is the splitting of atomic energy levels (and of the associated spectral line) into several components in the presence of a magnetic field. In the linear regime this splitting is proportional to the magnetic field strength and the Landé factor of the energy level. The longitudinal Zeeman effect produces measurable Stokes–V signals in the presence of weak magnetic fields, while to observe the signature of the transverse Zeeman effect on the Stokes Q and U profiles, field strengths of more than 100 G are needed. The Zeeman effect may produce polarized radiation that can be analyzed to infer the properties of the field. However, when the magnetic field is unresolved within the resolution element or cancels out when mixed polarities are present or too weak or absent then the splitting is negligible, there is no polarization signal. In these cases, the Zeeman effect is of no importance as a diagnostic tool of magnetic fields. There is, however, another physical mechanism, the so called Hanle effect, which allows us to "see" the "Sun's hidden magnetism" that the Zeeman effect is impossible to diagnose. The Hanle effect, contrary to the Zeeman effect, works in any topological complex weak-field scenario (even if the net magnetic flux turns out to be exactly zero). Atomic level polarization signals are produced by population imbalances and quantum coherence among the magnetic sublevels of the atom due to radiative transitions induced by the anisotropic incident radiation. The Hanle effect can be defined as any modification of the linear polarization signals due to the presence of a magnetic field inclined with respect to the axis of symmetry of the radiation field. We should note, however, that for magnetic field strengths greater that ≈ 10 G (i.e. the saturated Hanle effect regime), the Hanle effect is sensitive only to the orientation of the magnetic field vector, but not to its intensity. In this context, the Hanle and Zeeman effects can be suitably complemented for exploring magnetic fields in the solar atmosphere.

The first direct empirical demonstration of the existence of magnetized, spicular material was achieved by Trujillo Bueno et al. (2005). They applied a combined Hanle–Zeeman diagnostic to the He I 10830Å multiplet to spectropolarimetric observations obtained with the Tenerife Infrared Polarimeter (TIP) at the German Vacuum Tower Telescope (VTT) on Tenerife, Spain. The spectrograph slit was placed off–limb parallel to the solar limb at an atmospheric height of $\approx 2\,000$ km. They detected non-zero Stokes U profiles which according to the Hanle effect theory is the observational signature of the presence of a magnetic field inclined with respect to the local vertical. To correctly model the Stokes I profiles, the authors solved the radiative transfer equation assuming an optically thick atmosphere. They found from the analysis of quiet-Sun limb spicules at a height of 2 000 km above the photosphere that the best fit to the observed Stokes profiles is obtained for a magnetic field strength of $B \approx 10\,G$ and an inclination angle $\theta \approx 37^{\circ}$. The authors noted that the observed Stokes profiles are due to an averaging along the LOS and thus the possibility of stronger fields occupying a small fraction of the integration volume along the LOS cannot be excluded.

López Ariste and Casini (2005) used spectropolarimetric observations of spicules in the He I D_3 line done with the ASP at the DST of the Sacramento Peak Observatory. The spectrograph slit was placed parallel to the solar limb at $\sim 3\,500$ km above the Hα limb. The data consisted of full Stokes profiles showing significant broadening due to non–thermal effects. They constructed a database of synthetic profiles with different magnetic field parameters. They then applied the Principal Component Analysis (PCA) inversion to a series of spectropolarimetric profiles

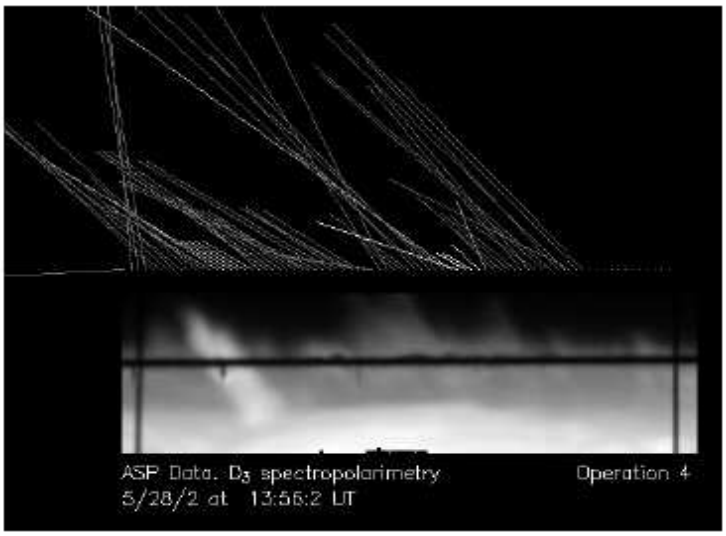

Fig. 12 In the background, is the slitjaw image in Hα showing the position of the slit (horizontal) over the spicules. Superimposed on the same column (with a vertical offset) the inverted solution for the magnetic field vector for each point on the slit is plotted. The direction of the lines is given by the azimuth in the LOS reference frame, and their length by the field strength. The level of gray of each line is scaled according to the intensity of the observed feature in the slit-jaw image (from López Ariste & Casini (2005))

which is performed by searching for the best match of the observed profiles within the precomputed database of profiles. They found a good correlation between the magnetic field orientation and the spicular structures visible in Hα (see Fig. 12). However, due to a 90° ambiguity which they attributed to the small significance of Stokes V in their data, a solution giving a magnetic field approximately perpendicular to the axis of a spicule cannot be excluded a priori. They concluded that weak fields (of the order of 10 G) are more common in spicules, although stronger fields above 30 G should not be excluded in a minority of cases. We must note, however, that these spicules emanated from an active plage.

In the same year, Socas-Navarro and Elmore (2005) obtained off-limb spectropolarimetric observations in the He I 10830 Å triplet using SPINOR in the Ca II 8498Å and 8542Å lines using the ASP at the DST. They found that the ratio of the Q and U signals is different for the Ca and He lines implying a different orientation of the polarization plane. They concluded that this result provides clear evidence of the presence of magnetic fields in spicules by the following reasoning: if there was no magnetic field, one would observe some degree of scattering polarization. The plane of polarization of this signal is given by the geometry of the scattering process and would be the same for all three lines observed. If, however, the scattering atoms are embedded in a magnetic field, then the Hanle effect would rotate the plane of polarization by an amount that depends on some parameters of the transition. In this case, the orientation of the linear polarization would be different in different lines, as was observed.

Recently, Centeno et al. (2010) carried out spectropolarimetric observations of off-limb spicules at various distances from the visible limb in the He I 10830Å

triplet with the TIP at the VTT on Tenerife. With these particular observations, they detected clear Zeeman-induced Stokes V profiles. Such profiles are due to a net LOS component of the magnetic field. They used the inversion code HAZEL (HAnle and ZEeman Light) developed by Asensio Ramos et al. (2008) to invert the Stokes profiles caused by the joint action of atomic level polarization and the Zeeman and Hanle effects in order to infer a number of atmospheric properties together with the magnetic field vector. They inverted the Stokes profiles for all the positions along the slit for two data-sets taken one hour apart from each other. In a small region of the slit they found magnetic field strengths as large as 48 G, where the Zeeman-induced Stokes V signals were particularly large. They also pointed out that the determination of the longitudinal component of the magnetic field depends on the distribution of the orientation of the magnetic fields which may produce a cancellation of the Zeeman-induced Stokes V signal when magnetic field vectors are not aligned, or a significant non-negligible Stokes V signature (and thus a significant B_{LOS} component) when the magnetic field lines team up.

Another method that has been used for the determination of magnetic fields in spicules is based on the *MHD coronal seismology* (Nakariakov and Ofman, 2001). Properties of waves and oscillations (e.g. amplitudes, periods), as well as physical parameters of the medium (e.g. temperature, density) determined from observations can be connected through MHD wave theory to the unknown magnetic field strength and transport coefficients.

Magnetic fields in spicules can also be inferred from observations of waves. Several observations have shown oscillatory transverse displacement of spicule axes. This displacement can be caused by two types of waves: kink or Alfvén waves. In Zaqarashvili and Erdélyi (2009), there is a discussion on difficulties associated with the Alfvén wave scenario. Most authors have interpreted this kind of oscillation in spicules as the observational signature of propagating kink waves. It is well known that transverse kink waves in flux tubes anchored in the photosphere can be generated by buffeting of granular motions (Roberts, 1979; Hasan and Kalkofen, 1999). The propagation of kink waves can be traced either by direct observation of the tube displacement along the limb or spectroscopically by the Doppler shift of spectral lines when the velocity of the kink wave is polarized in the plane of observation. If spicules are considered as flux tubes anchored in the photosphere then the observed transverse displacements of their axes can be interpreted by the propagation of kink waves. Kukhianidze et al. (2006) analyzed Hα spectra of limb spicules obtained at different heights. They found that $\sim$ 20% of the measured heights showed a periodic spatial distribution in the Doppler velocities which they attributed to kink wave propagation. Wave periods were estimated as 35 – 70 s based on the expected kink speed in the chromosphere (50–100 km s^{-1}). Estimated wavelengths at the photospheric level are comparable to the spatial dimensions of granular cells, suggesting a granular origin of the waves. Singh and Dwivedi (2007) used these observations and applied the method of MHD seismology including the effects of gravitational stratification. They estimated magnetic fields in spicules in the range 8 – 16 G. Zaqarashvili et al. (2007) analyzed the same observational data, estimating the kink speed in the range 90 – 115 km s^{-1} they obtained magnetic field strengths in the range 12 – 15 G. Kim et al. (2008) used high resolution Ca II H limb observations obtained by the SOT/Hinode instrument to determine oscillation parameters of spicules, such as periods, amplitudes, transverse velocities, wavelengths and wave speeds. They interpreted the observed oscillations as

MHD kink waves and adopting spicule densities in the range 2.2 10^{-11} kg m^{-3} – 4.0 10^{-10} kg m^{-3} they estimated magnetic field strengths in the range 10 – 76 G. Verth et al. (2011) used also SOT/Hinode Ca II H observations and magnetoseismology to determine the vertical gradient in both magnetic field and plasma density in a spicule by studying the change in velocity and phase speed with height. They found that the magnetic field decreases in strength by a factor of 245 between the photosphere and low corona, while the plasma density decreases by a factor of $\sim$ 1000. However, in all of these works, various assumptions have been used.

The measured values for magnetic field and inclination, therefore, are lower than the values needed for efficient p-mode excitation in inclined flux tubes. A closer investigation of the mechanism, the assumptions made in the analysis coupled with a larger number of spicule magnetic field measurements are required in order to resolve this issue.

4.1.2 Oscillations and waves in spicules

Oscillations and waves in spicules have been detected by both imaging and spectroscopic observations. Reported observations on oscillatory and wave phenomena in spicules, as well as views and discussions about their interpretation can be found in the recent review by Zaqarashvili and Erdélyi (2009).

4.2 On-disk chromospheric structures

The chromosphere is the layer where the plasma-β, changes from above to below unity, signaling a shift from hydrodynamic to magnetic forces as the dominant agent in the structuring of the atmosphere. Due to the combined effects of the pivotal role played by the magnetic field and the small–scale gas thermodynamics, this part of the atmosphere is characterized by an impressive amount of fine-scale structures. In active regions, long and relatively stable fibrils are observed, together with shorter dynamic fibrils, while in quiet Sun regions dark mottles emanate from the magnetic network. Whether or not these structures are similar and are driven by the same mechanism, as well as their relationship to the limb spicules, has been the subject of long-standing discussions for several years.

The line which has been widely used for chromospheric observations, especially following the development of the Lyot filter, is the Balmer Hα line. Thus despite the complicated formation mechanism of this line and the difficulties in the interpretation of Hα observations, much of what we know about the fine-scale on-disk structures (e.g. mottles, fibrils) has been obtained from observations in this line. Substantial work has also been done by using the unique capabilities of the Multichannel Subtractive Double Pass (MSDP) spectrograph which can acquire spectra over an extended FOV (Mein, 2002). The Ca II H and K resonance lines, as well as the Ca II infrared triplet (IR) (8498 Å, 8542 Å and 8662 Å), have also been used for the solar chromosphere diagnostics. The former are the broadest lines in the visible spectrum and sample a wide height of the solar atmosphere. On-disk filtergrams in the Ca II H and K line are usually obtained with broad-band filters and differ significantly in appearance from those obtained in Hα. Rutten (2007) has remarked that dark structures in Ca II H and K filtergrams are barely visible. Observations

in these lines close to the limb show long thin emission features called "straws". Reardon et al. (2009), however, have shown that the lack of well defined chromospheric features in the Ca II K filtergrams, such as fibrils and mottles, is essentially due to observational limitations. Pietarila et al. (2009) found that bright fibrils are ubiquitous in the Ca II K line provided the spatial resolution is sufficiently high and the wavelength band is sufficiently narrow to avoid contamination by photospheric radiation. The Ca II IR and Hα lines differ substantially in their sensitivity to the temperature. The former are, like Hα, subordinate, but whereas the lower level of Hα is coupled to the hydrogen ground level via the extremely strong Ly-α radiative transition, the lower level of the Ca II IR lines is metastable and only coupled to the Ca II ground level via electronic collisions. For more extensive discussion on the formation characteristics of these important chromospheric lines see Cauzzi et al. (2008), Cauzzi et al. (2009) and Leenaarts et al. (2012). High resolution imaging spectroscopy at fast cadence in Ca II IR was initiated by Vecchio et al. (2007) with the Interferometric BIdimensional Spectrometer (IBIS) installed at the DST of the National Solar Observatory (NSO). Cauzzi et al. (2008) using the same instrument obtained monochromatic images at several wavelengths within the Ca II IR line, analyzing several structures. They found that the appearance of the structures in this line is strongly reminiscent of the structures seen in Hα. As in Hα, the structures observed in Ca II IR lines differ noticeably between active regions and the quiet Sun.

4.2.1 Mottles

The traditional term mottles refers to rapidly changing hair-like jets observed in quiet Sun regions on the solar disc, usually in the Hα or the Ca II lines. They have long been recognized to be one of the basic elements that constitute the inhomogeneous chromosphere. Several authors tend to refer to these features as spicules, although spicules do not always necessarily represent only quiet Sun structures seen at the limb. Mottles are organized in a complex geometric pattern over the solar disk outlining the boundaries of the chromospheric network which is more prominent in the Ca lines. They cluster into: a) either small groups called chains, consisting of almost parallel structures emanating along the common boundary of two supergranular cells or b) in larger groups called rosettes, consisting of usually radially expanding structures around the common boundary area of three or more supergranular cells. Tanaka (1974) found about 30% of all the dark mottles are double or can be resolved into double structures when viewed with high resolution Hα wing observations.

Mottles appear as dark (absorbing) against the disk when observed in the wings of Hα and especially enhanced in contrast at H$\alpha\pm0.5$ Å. Near the centre of the Hα line they are much less distinct. Very often in the past it has been reported that at the same locations dark as well as bright mottles are observed. However, even such basic considerations as whether dark and bright mottles are the same feature seen at different heights or not, remains unanswered. Some authors suggested that a bright mottle is the base of a dark elongated one (Banos and Macris, 1970), whereas others claimed that bright and dark mottles are distinctly different phenomena (Alissandrakis and Macris, 1971). Today with the achievement of higher resolution observations one has the impression that what was called bright mottles is simply the bright background below the dark mottles. It is very important to

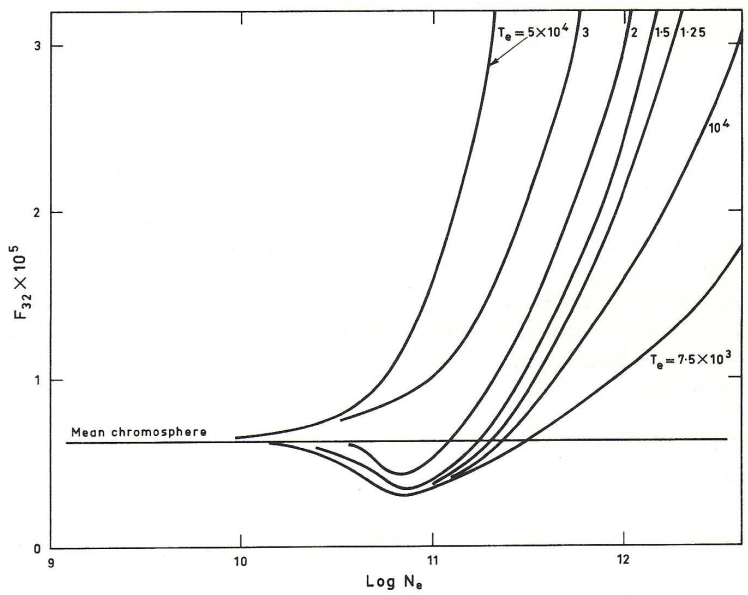

Fig. 13 Hα intensities of the mottles vs the logarithm of the electron density N_e as computed by Giovanelli (1967b) (in cgs units). Different curves correspond to different temperatures. Geometrical thickness of a mottle is $D = 2\,\mathrm{Mm}$

note that the resolution of observations affect drastically the observed morphology of the chromospheric fine structures. Since mottles are usually grouped in rosettes or chains one will fail to discriminate between different structures when using low resolution observations, since each thread and its separation are a few tenths of arcsec wide. With the increasing capability of instruments such as SOUP, CRISP, IBIS or ROSA, we are able to detect fine structure with dimensions at the limit of the resolution.

Lengths and widths of mottles Bray and Loughhead (1974) in their monograph, summarize their properties. Their horizontal dimension ranges between 725 – 10 000 km and they exhibit a variety of shapes. Sawyer (1972) categorized the shapes of mottles into oval, round, filament, arch and lumpy and gave horizontal dimensions between $3''$–$10.6''$ (2 000 – 7 500 km). Although generally elongated, the larger mottles tend to have more irregular shapes. Observations taken towards the limb, at large heliographic latitudes show mottles reduced in size, with widths of the order of $1''$ and dominantly oriented towards the limb.

Lifetime of mottles The lifetime of mottles is difficult to determine. Although the general configuration of mottles around bright points may be preserved for more than 15 min, features change within minutes. Old studies give values ranging between 3 and 15 min, but differences in resolution may affect the measurements. A more recent analysis by Bratsolis et al. (1993) determines the mean lifetime of mottles between 13-14 min.

Spectroscopic properties of mottles Giovanelli (1967a,b) did pioneering extensive NLTE computations of the Hα line contrast profiles relevant to chromospheric fine-scale modelling. In his computations he assumed 1D slabs illuminated by the surrounding atmosphere, having a geometrical thickness 2 000 km and uniform T_e and N_e. For mottles' diagnostics, an important figure is Fig. 13 given by Giovanelli (1967b). In this figure, individual curves represent the Hα line-center intensities as a function of electron density for different temperatures. From this figure one can conclude that portions of the curves below the horizontal line correspond to dark mottles, while those above the line are structures considered as bright mottles. An important ambiguity one can notice is that for each negative contrast, for a given temperature, two values of electron density are obtained. Using the observed contrast measurements, Giovanelli (1967b) has concluded that: a) for dark mottles $T < 10\,000\,\mathrm{K}$, $N_e \simeq 2{\times}10^{11}\mathrm{cm}^{-3}$, b) for less opaque mottles $T > 20\,000\,\mathrm{K}$, $N_e \simeq 10^{11}\mathrm{cm}^{-3}$ and c) for bright mottles $T < 25\,000\,\mathrm{K}$, $N_e > 5{\times}10^{10}{-}10^{11}\mathrm{cm}^{-3}$.

Heinzel and Schmieder (1994) used Hα line profile observations of bright and dark mottles together with a grid of prominence-like NLTE models of Gouttebroze et al. (1993) to derive the physical conditions in these structures. In these models, the structures are considered as vertically–standing 1D slabs irradiated from both sides by an isotropic incident radiation. They have shown that higher-pressure models ($p_g \approx 0.5\,\mathrm{dyn\,cm}^{-2}$) with temperatures around $10^4\,\mathrm{K}$ can explain the profiles of both dark and bright structures. However, it should be pointed out that the NLTE models they used are more suited for prominences located at a height of 10 000 km.

Alissandrakis et al. (1990), Tsiropoula et al. (1993), and Tziotziou et al. (2003) used Hα time series observations of mottles obtained by the MSDP and the cloud model (see Section 8.1). They derived four adjustable parameters of the model, i.e. the source function, the Doppler width $\Delta\lambda_\mathrm{D}$, the optical thickness τ_0, and the LOS cloud velocity v. Although the Hα observations were obtained in different times and regions the results they quoted are very similar. According to the last paper these structures are mostly optically thin with an optical thickness peaking at ~ 0.9. This is reflected on the source function distribution which peaks at ~ 0.156 (the line center quiet-Sun Hα intensity relative to the continuum being 0.169), since optically thin structures allow more of the background radiation to be transmitted through them. Their Doppler width distribution shows a peak around 0.43 Å and has a mean value of 0.35 Å. The corresponding histograms of the four cloud parameters (including the LOS velocity which is described in the following sub-section) are given in Fig. 14.

Tsiropoula and Schmieder (1997) proposed a method which allows the estimation of several physical parameters of dark structures once the four parameters described above have been derived through the cloud model for Hα observations. These parameters are: the population densities at levels 1, 2, 3 (N_1, N_2, N_3) of the hydrogen atom, the total particle density of hydrogen N_H, electron density N_e, electron temperature T_e, gas pressure p, total column mass M, mass density ρ, and degree of hydrogen ionization χ_H. Mean values of these parameters, as well as their standard deviations, estimated from a set of several mottles are given in Table 2. The temperature has been calculated from the Doppler width obtained by the cloud model. They have assumed two different values for the microturbulent velocity, ξ_t (i.e. $10\,\mathrm{km\,s}^{-1}$ and $15\,\mathrm{km\,s}^{-1}$), showing its effect on the values of the temperature and pressure. An assumed value of ξ_t equal to $10\,\mathrm{km\,s}^{-1}$ lead to $\sim$

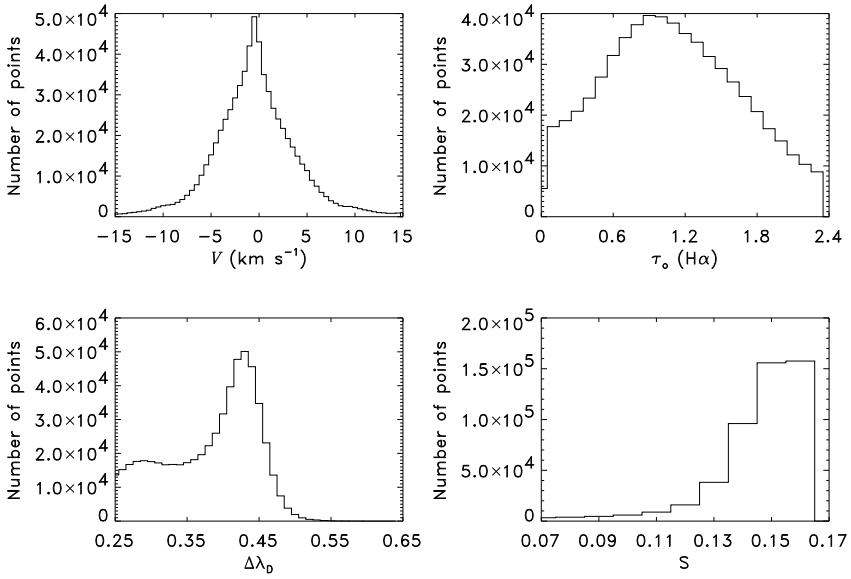

Fig. 14 Histograms of velocity v, optical thickness τ_0, Doppler width $\Delta\lambda_{\rm D}$ and source function S derived from the cloud model for mottles (from Tziotziou et al. (2003))

Table 1 Physical parameters of dark mottles from Tsiropoula and Schmieder (1997)

Parameter	Average value	Standard deviation
N_1, cm^{-3}	1.6 10^{10}	8.3 10^{9}
N_2, cm^{-3}	1.4 10^{4}	1.1 10^{4}
N_3, cm^{-3}	1.6 10^{2}	1.3 10^{2}
N_H cm^{-3}	5.1 10^{10}	2.1 10^{10}
N_e cm^{-3}	3.4 10^{10}	1.5 10^{10}
M, g cm^{-2}	2.2 10^{-5}	9.4 10^{-6}
ρ, g cm^{-3}	1.1 10^{-13}	4.7 10^{-14}
T, K (for $\xi_t = 10$ km s^{-1})	1.4 10^{4}	9.2 10^{3}
T, K (for $\xi_t = 15$ km s^{-1})	1.0 10^{4}	7.7 10^{3}
p, dyn cm^{-2} (for $\xi_t = 10$ km s^{-1})	0.20	0.1
p, dyn cm^{-2} (for $\xi_t = 15$ km s^{-1})	0.14	0.1
χ_H	0.65	0.1

1.7 times greater values of temperature and pressure than the values obtained by assuming ξ_t equal to 15 km s^{-1}.

Spatial and temporal evolution and velocities of dark mottles Among other physical conditions, the study of the flows along these structures is essential because it can add to the understanding of the mechanism driving them. However, the problem is difficult and the present situation is rather confusing because to determine a mottle's motion and its variation with time is a very delicate and difficult matter.

This is not surprising in view of the difficulties of recovering information on the velocities from line profile observations formed from moving material embedded in an absorbing medium at rest. Stable and good seeing conditions are required, while wide wavelength coverage is necessary in order to follow the changes of the LOS velocity. Furthermore, careful co-alignment of images from different times, but also of different wavelengths is required.

Another problem is that the apparent shape of mottles is not simple and is changing with time. Some are very straight, while others are curved. Some mottles are very thin and others are very thick. Some are tapered and others are not. In high resolution Hα line wing filtergrams, as described by Tanaka (1974) and Dara et al. (1998), they show a twined or multiple appearance. It is worth noting that Suematsu et al. (2008) found the similar twined structure for limb spicules (see Fig. 11). Furthermore, the mottles in the Hα blue-wing are thinner and closer to the network boundaries than those observed in the Hα red-wing (Suematsu et al., 1995).

A common practice to infer LOS velocities is to measure Doppler velocities by determining the wavelength of a point midway between two positions of equal intensity in the absorption line profile. In this technique the moving structure is assumed to produce its own profile which is simply shifted with respect to the background profile by an amount $\Delta\lambda_I = \lambda_0 v/c$, where v is the LOS velocity. The determination of the velocities by this technique usually yields inconsistent results due to the lack of knowledge of the effective height of formation of the lines considered. Another technique used for the determination of LOS velocities, when intensities on either side of a line profile are known, is based on the red-blue wing subtraction

$$DS = \frac{I(+\Delta\lambda) - I(-\Delta\lambda)}{I(+\Delta\lambda) + I(-\Delta\lambda)} \tag{2}$$

This technique gives the so-called "Doppler signal". According to this formula, positive Doppler signal denotes upward motion of absorbing material. Of course, one must be aware that the derived values give only a parametric description of the actual velocity field, they can give, however, a qualitative picture of upward and downward moving material (Tsiropoula, 2000).

Although mottles show different appearance and are sometimes displaced laterally among filtergrams of different wavelengths in the Hα line (Suematsu et al., 1995), we should note that no one has analyzed their horizontal motions. Beckers (1963) reported that dark mottles, after disappearing in the Hα-0.5 Å image, often became visible in the Hα+0.5 Å, consistent with up-flows followed by down-flows. Bhavilai (1965) has shown that some mottles are visible in the blue wing, while others appear only in the red wing. Upward and downward velocities, as inferred from Hα spectra, have been reported by Suematsu et al. (1995). These authors after careful co-alignment and examination of a time series of high resolution images at Hα-0.65 Å, Hα line center, and Hα+0.65 Å and Doppler signals proposed the following description for the evolution of disk mottles: at first they appear as faint dark features at the Hα blue-wing filtergrams, elongate and increase in contrast, and then fade out as a whole in this wing. A few minutes later, they appear again as dark features at the Hα line center, and show increased contrast and length. Finally, they appear at the Hα red-wing as faint, but long dark features, and shrink towards the footpoint, increasing their contrast and then fading out. They

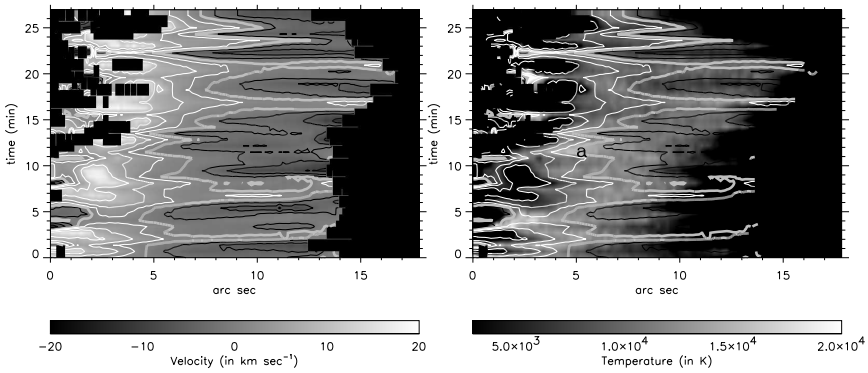

Fig. 15 Time slice images of cloud velocity v (left) and temperature (right) along a dark mottle. On the velocity images the black contours denote upward velocities, white contours downward velocities, while the thick gray line represents the zero velocity contour (from Tziotziou et al. (2003))

concluded that Doppler signals confirm this pattern, i.e. upward radial velocity during the extending phase of the structure and downward during the receding phase or of an up–and–down moving jet as a whole. They also found that in some cases, the red-wing mottles appear near the foot-points of the blue-wing mottles in their extending phase. Cauzzi et al. (2009), on the other hand, compared profile minimum intensities and Doppler shifts of the minimum intensities of Hα profile observed with IBIS. Although there are large scale spatial similarities between the Hα profile-minimum map and the corresponding Doppler shift map, they found two dissimilarities: a) there is a lack of pixel-by-pixel similarity between the two maps and b) mottles in Doppler-shift maps tend to be shorter and are dark or bright (moving upward or downward) without obvious relation to the contrast in the profile-minimum image, except for the brightest and darkest features whose co-spatiality indicates exceptional motions in their lower ends. In the corresponding Ca II infrared line observations of intensities and Doppler shifts, they found slightly higher coherence but with negative correlation, i.e. higher intensity values at locations with larger blue-shifts (dark in the maps).

Suematsu et al. (1995) examined also the proper motion of the apparent top of mottles. They showed that the tops of some mottles approximately follow a parabolic trajectory, when they are traced through the three wavelengths along the Hα line profile. Fitting the trajectory with a quadratic function, they derived an initial velocity and a deceleration of proper motion. Furthermore, they gave a method to derive a tilt angle from the vertical, assuming that mottles move on inclined straight flux tubes and are decelerated only by solar gravity. They found initial velocities ranging from 10 to 50 km s^{-1} with a mean of 28 km s^{-1} and decelerations ranging from -0.2 to -0.02 km s^{-2} with a mean of -0.07 km s^{-2}, which are much smaller than the solar gravitational acceleration of 0.274 km s^{-2} (Suematsu, 1998).

If mottles follow a ballistic trajectory (material motion under a constant gravitational field), we can expect to find some relationship between their lengths and

lifetimes. For example, if the mottle moves along a rigid magnetic flux tube of a given inclination angle, with an initial velocity along the flux tube of v_0, decelerated by solar gravity g, we have a relation between the maximum length L projected on a horizontal plane and a half-lifetime T of

$$L = \frac{v_0}{2}\sqrt{T^2 - T_0^2} \tag{3}$$

where $T_0 = v_0/g$ is the lifetime of a vertical mottle whose apparent length is zero. This equation implies that longer lived mottles have larger apparent lengths, if every mottle has a similar initial velocity. Suematsu et al. (1995) studied this relation and found that longer lived mottles are physically longer and that the relation is consistent with the ballistic hypothesis. They noted, however, that although some mottles are represented by ballistic motions, a pure ballistic trajectory is unrealistic, because the observed values of initial velocity and lifetime are too small to fit the data, while the small decelerations would require the mottles to be tilted typically 60° – 70° from the LOS. Christopoulou et al. (2001), from light curves of mottles, studied their proper motions performing a least–square fit of the ballistic motion to the height measurements as a function of time. Their best fit was for an inclination angle from the local vertical of $\sim 53^\circ$ and an initial velocity of $\sim 56\,\mathrm{km\,s^{-1}}$. Rouppe van der Voort et al. (2007) used high spatial and temporal resolution observations of a quiet Sun region obtained with SST on La Palma. They reported that it was very difficult to track individual dark mottles during their lifetime for several reasons among which: a) many mottles lack a sharp top end, b) they display significant fading which appears to be induced by opacity changes with time and c) many mottles undergo not only up and down motions, but also significant motion transverse to the magnetic field. These factors contribute to LOS superposition and render the identification and follow-up of mottles throughout their lifetime quite problematic. They were able, however, to follow some mottles and found that their tops undergo a parabolic path. In addition, they found that the deceleration and maximum velocity are linearly correlated and they suggested that leakage of global oscillations from the photosphere (with dominant periods around 5 min) plays an important role in the formation and dynamics of at least a subset of quiet Sun mottles. This finding further suggests that the driving mechanism for at least some of the mottles is similar to the driving mechanism of DFs.

Another technique to infer velocities of structures seen in absorption on the solar disk has been introduced by Beckers (1964). It is based on the contrast profile and is called the "cloud" model (see Section 8.1). It has been used extensively in the analysis of observations of identifiable fine structures in absorption on the solar disk (Grossmann-Doerth and von Uexküll, 1971, 1973, 1977; Bray, 1973; Loughhead, 1973; Bray, 1974; Bray and Loughhead, 1983; Tsiropoula et al., 1994; Tziotziou et al., 2003). Grossmann-Doerth and von Uexküll (1971), as well as Bray (1973), applied this model to chromospheric mottles observed at disk centre and derived values for the 4 parameters from the observed contrast profiles. Loughhead (1973), however, showed that this model failed to explain contrast profiles near the limb, also Bray (1974) could not reproduce some contrast profiles of sunspot fibrils. Alissandrakis et al. (1990) have described the range of circumstances under which this model is applicable and were able to map the 2D spatial variation of the obtained parameters. In subsequent work, Tsiropoula et al. (1994) using the "cloud model" showed that the predominant pattern of bulk motion in

dark mottles is that of down-flows at their foot-points and alternating up-flows and down-flows at their tops. This result was re-confirmed by Tziotziou et al. (2003) who used another set of Hα observations obtained by a different instrument. In these works the bi-directional, as well as the recurrent character of the velocities was revealed. This bi-directional flow followed by down-flowing material along the whole structure is shown in Fig. 15. As can be revealed from this figure, the upper parts of the mottles show flows in both directions, while the bottom parts show flows in the downward direction only and the whole process is repeated with a period of ~ 5 minutes. In order to explain this kind of flow pattern they suggested that magnetic reconnection might be the mechanism responsible for the formation and dynamics of these structures. This suggestion is reasonable, since this process seems to be the most suitable physical mechanism that can explain the observed flow of material towards and away from the solar surface. Furthermore, this process can occur at the network boundaries where neighboring pairs of flux tubes of opposite polarity are driven together by external plasma flows and reconnect. Based on these observational findings, they proposed a simple reconnection model. Such a model was also proposed by Pikel'ner (1969). A schematic representation of this model is given in Fig. 16 (of course, unipolar as well as bipolar fields of appropriate polarity could be involved, see Figure 8 of Wilhelm (2000)). According to this model, the squeezing of opposite polarity field lines at the chromospheric level leads to cooling by radiation of the compressed gas, which is trapped between them and consequently to a downflow due to gravity (left part of Fig. 16). When opposite field lines come close, reconnection occurs, then part of the material is carried upward by the reconnected field lines, while the material below the reconnection region moves downwards under the action of both gravity and magnetic forces (middle and right part of Fig. 16). This cycle is repeated until the field is annihilated. Analyzing the same set of data, Tziotziou et al. (2004) showed that sometimes there is a temperature excess at the location where reconnection seems to be occurring, indicating the presence of local heating (Fig. 15, right). Their study of the intensity and Doppler velocity time sequence indicated also that individual mottles appear in bursts, lasting typically for about 5 min and usually reappear several times at the same location. Murawski and Zaqarashvili (2010) developed a 2D rebound shock model in which a velocity pulse is steepened into shocks which produce mottles/spicules and reported quasi-periodic behaviour of the rising material due to consecutive shocks, as well as bi-directional flows due to the superposition of falling off and rising plasma portions.

Contarino et al. (2009) analyzed data acquired along the Ca II 8542 Å line with the IBIS instrument at the DST. They applied the cloud model to four mottles and obtained values for the four parameters given by this model. They found an almost symmetric velocity distribution between -10 and $+10\,\mathrm{km\,s^{-1}}$, which, they suggested, is an indication of the presence of both upward and downward velocities inside the mottles. As they reported, however, the LOS velocities they found did not show a regular behavior. In one of the mottles examined, they obtained alternating upward and downward motion occurring in phase in all the examined segments. In another mottle, they obtained up-flows in one endpoint and down-flows in the other which reverse with a ~ 4 min period. Finally, in the other two mottles, they found both positive and negative velocities which change with an apparent irregularity.

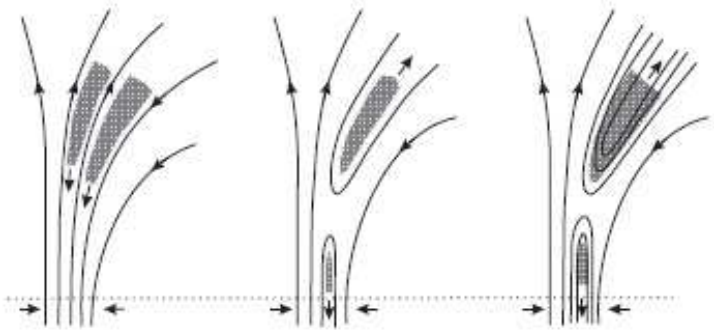

Fig. 16 A simple reconnection model (see text) explaining the observed velocity behaviour in mottles, see Tziotziou et al. (2003)

Oscillations in dark mottles Different physical but mainly magnetic conditions in the internetwork (IN) and network boundaries (NB) are clearly reflected in the oscillatory behaviour of both regions,as well as in dark mottles emanating from the network boundaries. Several issues concerning the dynamics of network and internetwork have been already addressed in the review by Rutten (1999), while intensity and velocity oscillations at both IN and NB have been extensively investigated by several other authors.

Nowadays, the general belief is that NB regions show no power of particular significance below 5 min, in contrast to IN regions that display a dominant period of 3 min, especially in Doppler shifts (Damé et al., 1984; Deubner and Fleck, 1990; Lites et al., 1993; von Uexküll and Kneer, 1995; Cauzzi et al., 2000; Krijger et al., 2001). However, different results have also been reported (see the Introduction of Tsiropoula et al. (2009)), stemming mostly from the use of different methods or from observations in different lines formed at different atmospheric layers. Hansteen et al. (2000) and Banerjee et al. (2001) for example, have reported network oscillations probably attributed to waves, which are produced in bursts with coherence time of about 10 – 20 min. Jess et al. (2009) used observations obtained by SST investigated a group of network bright points. They reported full-width half-maximum (FWHM) oscillations with periodicities ranging from 126 to 700 s originating above a bright point. They also reported a lack of cospatial intensity oscillations and transversal displacements which, as they stated, rules out the presence of magnetic-acoustic waves. They suggested that the FWHM oscillations could be produced by a torsional Alfvén perturbation.

The linkage between NB oscillations and mottles has been extensively addressed by Tziotziou et al. (2004) in a study concerning periodicities of fine structures in a quiet Sun network region where a chain of mottles was observed. Concerning quiet Sun mottles, although differences do exist in the periodicities of intensity and velocity variations, which are often bursty and intermittent, with velocity variations resulting in a large range of periods from 100 to 500 s, individual mottles or regions of mottles do exhibit a most prominent period in the 5 min range (see Fig.17). They also show a 3 min signature which, however, is never the dominant one. Furthermore, an intermittent signature of 100 s (10 mHz), reported also by Hansteen et al. (2000), seems to exist; it is, however, unclear whether this

short period could be associated with the dynamics of recently reported Type II spicules.

More recently, Tsiropoula et al. (2009) in a multi-wavelength analysis of a solar network region showed that both mottles and NB show a periodicity of ~ 5 min in all considered lines. Phase differences in the network boundary region indicated an upward propagation of waves, while in the region of mottles the phase difference was mainly negative for periods of 250 – 400 s suggesting a downward propagation due probably to refraction of waves from the inclined magnetic field of mottles. A dominant peak around 1000 s has also been reported which is, however, unclear if it is related to the presumed in literature lifetime of mottles. The relationship between the oscillatory properties of a network region and the magnetic configuration of the chromosphere has been the subject of study by Kontogiannis et al. (2010b). Based on a previous paper (Kontogiannis et al., 2010a), they showed the existence of power enhancement and suppression (power halos and magnetic shadows respectively) in 3, 5 and 7 min Hα oscillations and they concluded that p-mode leakage, mode conversion, as well as reflection and refraction of waves on the magnetic canopy (see Section 6 for further details) can play an important role to the observed properties of network oscillations.

The dominant 5-min periodicity present in both NB and dark mottles is compatible with the idea of the leakage of photospheric 5-min acoustic oscillations, which are the well-known p-modes, to higher layers. Commonly, it was accepted that only waves with periods above the acoustic cut–off period (which at the chromospheric level is of the order of 3 min) could travel freely in the solar atmosphere, whereas waves with higher periods were considered as evanescent. However, several theoretical studies (Michalitsanos, 1973; Bel and Leroy, 1977; Suematsu, 1990) have shown that the acoustic cut-off period is increased when waves are propagating along inclined flux tubes allowing the leakage of p-modes to higher layers. For the first time p-mode leakage has been suggested by De Pontieu et al. (2004) to be related to the formation of active region fibrils. p-mode leakage, however, seems to be present also in quiet Sun mottles which are also inclined flux tubes (Suematsu, 1990; Tsiropoula et al., 2009; Kontogiannis et al., 2010a,b). It should also be stressed that measured periods of the order of 5 min in IN regions close to NB could well be attributed to the presence of inclined mottles that cover these regions. Recent results reported by Jefferies et al. (2006) show that a sizable fraction of the photospheric acoustic power at periods above the acoustic cut–off might propagate to higher layers within and around the magnetic NBPs. They referred to these regions as "magneto-acoustic portals" and showed that through these regions a significant portion of energy is provided for heating the solar chromosphere. Khomenko et al. (2008a) has also suggested that propagation of longer-period waves (i.e. equal or greater than 5 min) is even possible in vertical magnetic flux tubes, resulting from radiative losses in NBPs that may lead to the lowering of the acoustic cut-off frequency. Recently, Murawski and Zaqarashvili (2010) developed a 2D rebound shock model which predicts quasi-periodic raising of chromospheric jet-like structures with a period of ~ 5 min. In their simulations this periodicity results from a non-linear wake that is formed behind a leading pulse rather than from p-mode leakage. They found that the periodicity strongly depends on the amplitude of the initial pulse and can be longer for stronger pulses.

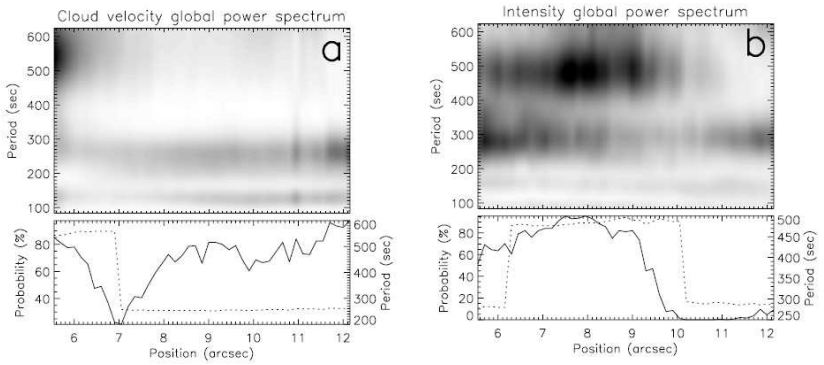

Fig. 17 Wavelet analysis results for a) the velocity and b) the Hα line-center intensity variations along the axis of a mottle, showing a dominant period close to 5 min. Top panels show the global power spectrum as a function of period and position along the length of the mottle while bottom panels show the variations of the global probability (solid line) obtained with a randomization method and the period (dotted line) of the maximum global power peak corresponding to this probability (from Tziotziou et al. (2004))

4.2.2 Fibrils

The term fibrils refers to mottle-like, dark (absorbing), highly dynamic, jet-like, on-disc structures which are observed above or in the direct vicinity of active region plages. The term fibrils refers also to dark structures which are observed in the penumbra of sunspots (penumbral fibrils) radially expanding around the umbra and creating a filamentary structure and to structures in active region plages which do not show jet-like behaviour; both are probably associated with low-lying loop-like structures that connect regions with opposite polarity magnetic flux. Jet–like fibrils related to active region plages are relatively shorter than penumbral fibrils or non jet-like fibrils or mottles and probably constitute also a fraction of the observed on-limb spicules.

A close inspection of Hα filtergrams of plages reveals several marked resemblances to the quiet Sun regions. In particular, the basic components of the rosette structure, i.e. NBPs and dark mottles are similar in several respects to the fine structure of plages, i.e. facular granules and dark fibrils. The principal differences of the two regions are: a) the number of facular granules in a plage is much larger than the number of NBPs in the centre of a rosette and b) the fibrils around a plage are generally much more elongated than the mottles around a rosette. Foukal (1971) proposed a continuous relationship between the basic constituents of the quiet and active chromosphere. According to this author there is a gradual progression between the mottles oriented more close to the vertical and the fibrils which are rather horizontally deflected because of the stronger field which constrains the plasma to follow low-lying field lines. Foukal (1971) gives some observed parameters of fibrils, e.g. length, lifetime, density, temperature, velocity and magnetic field and compared them to the corresponding parameters of spicules. He concluded that the corresponding parameters are rather similar except from the length (fibrils are longer) and the magnetic field strength which is higher in fibrils. March (1976) performed a systematic study of the lifetimes, lengths and evolution of fibrils in an active region. He reported that all fibrils he examined

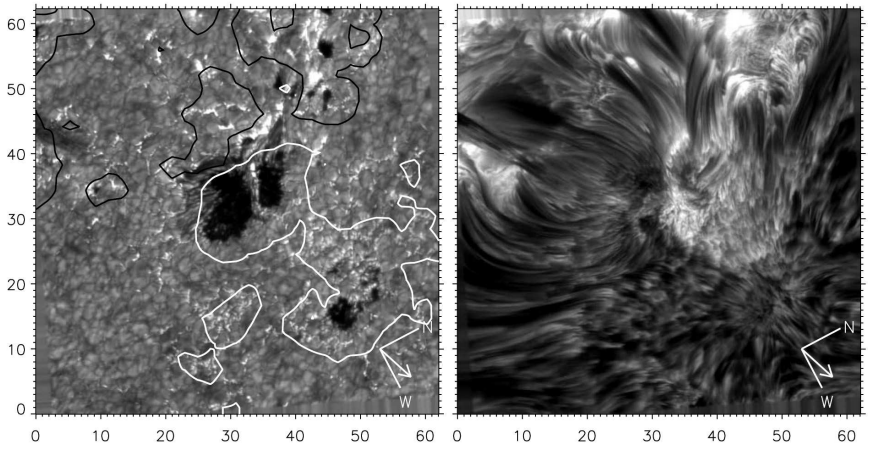

Fig. 18 Hα wideband (*left panel*) and Hα line center (*right panel*) images of NOAA AR 10813 taken by SST. The white and black contours in the left image outline the positive and negative magnetic flux, respectively. The DFs are predominantly observed in the mostly unipolar plage region between the two sunspots. The arrow indicates the direction of the disk center (from De Pontieu et al. (2007a))

evolved by an upward extension followed by a downward retraction. He also found that the lifetime of a fibril is a monotonically increasing function of its maximum apparent length. Based on this relationship, together with the variation of fibril lengths with time he suggested that fibrils result from material being impulsively injected into magnetic field lines at $\approx 30\,\mathrm{km\,s^{-1}}$, and returning back under gravity.

Pietarila et al. (2009) presented high-resolution observations of an active region in the Ca II K line obtained from the SST on La Palma. They found that very thin, bright fibrils are a prevailing feature over large portions of the observed field. Fibrils have not been observed with such detail in this line before for several reasons. One of them is that observations in this line are, usually, obtained with broad-band filters. However, only the Ca II K line core is purely chromospheric, while the wings are formed in the photosphere. With filters having a large passband, the intensity is summed over a significant portion of the line profile and thus the intensity of the line core originating from the chromosphere is rather small relative to the intensity of the line wings originating from the photosphere. If, however, observations are performed in a sufficiently narrow wavelength band to avoid contamination by photospheric radiation then fibrils can be observed. Another reason is that these structures are very thin and thus very high-resolution observations are required. The fibrils are structured by the underlying magnetic field and the bright endpoints are clearly co-spatial with the magnetic concentrations in the photosphere. This is not as obvious in the strong plage where the density of the fibrils is high enough to make identifying the endpoints difficult. They reported that in a strong plage, where there is more magnetic flux and due to unipolar crowding the field is more vertical, and so are the fibrils, which are also short, and form a thick carpet covering the underlying photosphere. At the plage edges, on the other hand, the fibrils become longer and more organized, they extend radially away from the

magnetic concentrations, are nearly parallel to one another, more inclined and extend over multiple granules towards the quiet Sun.

While mottles have been the major constituent of the quiet solar chromosphere, recent high resolution observations revealed that in active regions there exist mottle–like structures called dynamic fibrils (DF) which appear to form a subset of what have traditionally been called active region fibrils. Another subset is constituted from fibrils that do not show jet-like behaviour and which are apparently low-lying, heavily inclined structures connecting opposite polarity magnetic flux. This subset of much longer fibrils is more stable in time than the DFs.

Lengths, widths and lifetimes of DFs DFs were extensively studied by Hansteen et al. (2006) and De Pontieu et al. (2007a) who have measured their morphological properties and described their dynamic behavior using very high spatial (120 km) and temporal resolution (1 s) Hα observations obtained with the SST on La Palma. They found DFs are shorter than mottles; their mean length is 1 250 km with values ranging between 400–5 200 km. Their average width, which does not vary much with time and height, is ∼340 km with most of them being 120–380 km wide, although much wider structures can be found (∼ 1 100 km). The lifetime of DFs is shorter than that of mottles and lies between 120 s and 650 s, with an average of 290 s. These properties are subject to regional differences, i.e. they vary significantly with position in the FOV. De Pontieu et al. (2007a) found that DFs (see Fig. 18) were shorter in length and lifetime in the denser plage. Pietarila et al. (2009) applied a method to isolate individual fibrils and measured their widths and lengths. They found that most fibrils have widths between 80 km and 100 km, while widths of fibrils in a strong plage have a wide distribution with a max over 150 km. Anan et al. (2010) using SOT/Hinode Ca II H observations of an active plage identified 169 fibrils. They found that 80% were "parabolic" showing a cycle of rise and retreat and 10% "faded out", i.e. did not show a complete retreat cycle. It should be pointed out that these authors use the term "parabolic" (or "ballistic") motion in the context of constant deceleration during the downward phase which is not necessarily a free-fall dominated by gravity. The mean heights of the "parabolic" and the "fade out" fibrils were 1 300 km and 820 km, while their lifetimes were 179 s and 197 s respectively. It has not been examined yet which is the exact relationship between the DFs observed in Hα with the SST and those observed in Ca II H with the SOT/Hinode broadband filter which for on-disk observations gives a predominantly photospheric signal.

Evolution and velocities of DFs De Pontieu et al. (2007a) studied the evolution of these structures using very high spatial and temporal resolution Hα observations. In order to find the temporal behavior of individual DFs they constructed $x - t$ plots showing the evolution of the extent of a DF as a function of time. They analyzed 257 DFs and concluded that the length of the DFs as a function of time is well described by a parabola (see, e.g. Fig. 19). Fitting the time evolution of the length of the DFs with a parabola they derived the maximum velocity (on ascent or descent), maximum extent, deceleration and duration. The parabolic paths are characterized by a large initial velocity, usually of order of $15 - 20\,\mathrm{km\,s^{-1}}$, that decrease linearly with time. The deceleration is, usually, between 120 and $280\,\mathrm{m\,s^{-2}}$. The deceleration is typically only a fraction of the solar gravity and incompatible with a ballistic path at solar gravity. For the particular DF shown in Fig. 19 they

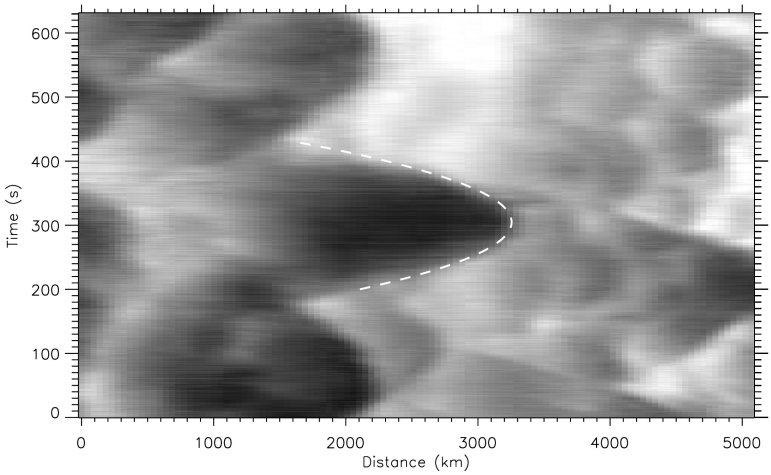

Fig. 19 An $x - t$ plot of the evolution of a DF (along the projected path). It follows a near perfect parabolic path in its rise and descent. The white dashed line indicates the best fit used to derive deceleration, maximum velocity, duration and maximum length (from De Pontieu et al., 2007a)
.

found a deceleration of $216\,\mathrm{m\,s^{-2}}$, a maximum velocity of $27\,\mathrm{km\,s^{-1}}$, a maximum extent of 1 800 km, and a lifetime of 240 s. They also found that DFs exhibit lower velocities and higher deceleration in the denser plage and that these differences cannot be attributed to projection effects. They also constructed scatter plots of various DF properties found in two different regions within the FOV. One of the regions contained a dense plage, i.e. strong magnetic field concentrations in which the magnetic field is generally more vertical, while the other was located at the edge of the plage region containing more inclined magnetic fields. They reported significant differences of fibril properties between those occurring above the dense plage and those occurring at the edge of the plage. From the scatter plots they derived some intriguing correlations. One interesting correlation is that between the deceleration and the maximum velocity of the DFs which shows a clear linear relationship (Fig. 20, *top left*). Another interesting correlation is that between the maximum length and the duration of the DFs (Fig. 20, *top right*). The longer DFs tend to have longer lifetimes. They also found that the maximum velocity and maximum length of DFs are well correlated: DFs with higher maximum velocity tend to be longer (Fig. 20, *bottom right*). The deceleration of DFs shows a somewhat less clear correlation with the DF duration (Fig. 20, *bottom left*). Although it seems that longer lived DFs typically experience lower decelerations, there is a large spread in the values. There are clear differences between the two regions, while the correlations are not quite linear. Anan et al. (2010) found that the DFs they examined follow a ballistic motion with constant deceleration. They found mean maximum velocities of the parabolic and fade out fibrils of $34\,\mathrm{km\,s^{-1}}$ and $16\,\mathrm{km\,s^{-1}}$, respectively, and mean accelerations of $-510\,\mathrm{m\,s^{-2}}$ and $-130\,\mathrm{m\,s^{-2}}$, respectively. They also found that the deceleration was proportional to the maximum velocity, i.e. the initial velocity of the ejection. The range of the maximum

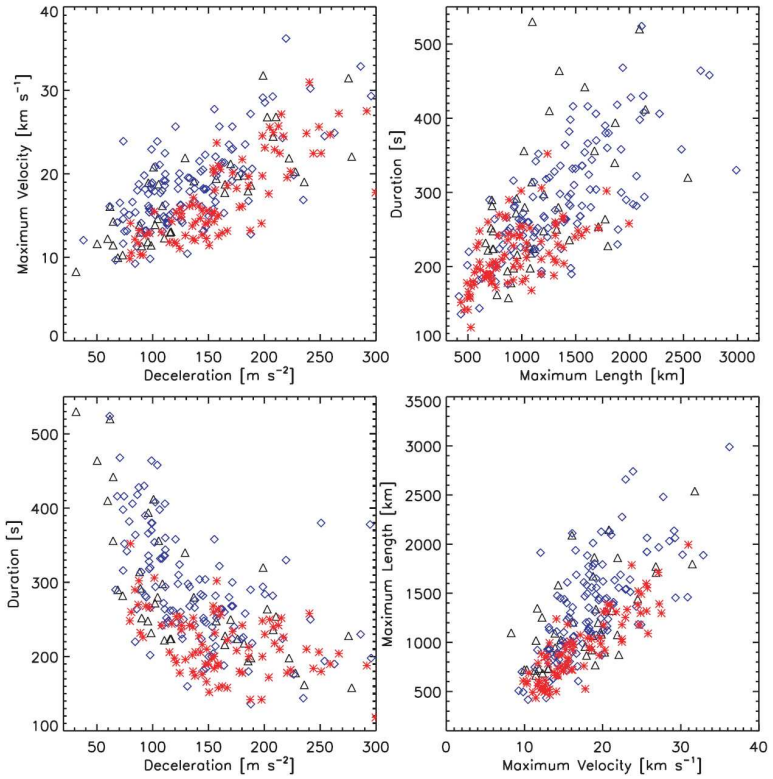

Fig. 20 Scatter plots of deceleration vs maximum velocity (*top left*), maximum length vs duration (*top right*), deceleration vs duration (*bottom left*), and maximum velocity vs maximum length (*bottom right*). DFs in two different regions were considered: one region contained dense plage (*red asterisks*) and the other was found at the edge of the plage (*blue diamonds*). The scatter plots for the two regions often seem to have different slopes (from De Pontieu et al. (2007a))

velocity was between $6\,\mathrm{km\,s^{-1}}$– $110\,\mathrm{km\,s^{-1}}$for the parabolic fibrils, whereas it was between $5\,\mathrm{km\,s^{-1}}$ – $40\,\mathrm{km\,s^{-1}}$ for the fade out spicules.

Apart from the above mentioned analyses of fibrils based on filtergrams, only a few quantitative spectroscopic studies have been undertaken. Langangen et al. (2008a) obtained spectrograms in the Ca II 8662 Å line using the SST spectrograph. They identified 26 DFs and infer Doppler shifts from the spectra. They also derived mean values $\sim 89\,\mathrm{m\,s^{-2}}$ for the deceleration, $11.3\,\mathrm{km\,s^{-1}}$ for the maximum velocity and 217 s for the lifetimes. These values are lower than those obtained by De Pontieu et al. (2007a) who measured proper motions in narrow-band images. Langangen et al. (2008a) performed also numerical simulations and explained the discrepancies in the lower maximal velocities derived from Doppler measurements compared to the proper-motion velocities as due to both the low formation height and the extensive width of the contribution function of the Ca II 8662 Å line. They also concluded that their observations support the result that DFs are driven by magnetoacoustic shocks excited by convective flows and p–modes.

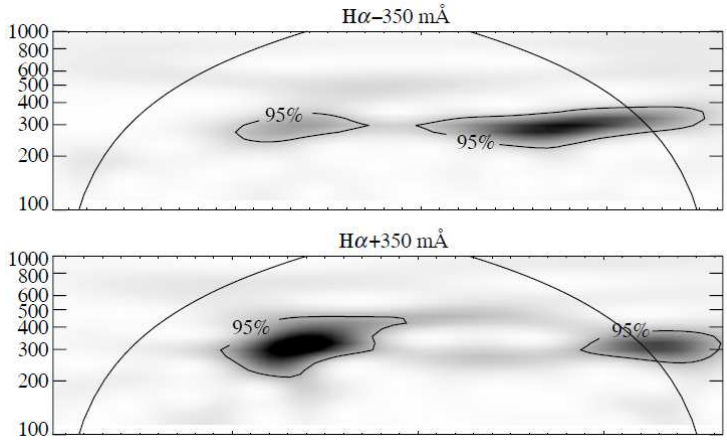

Fig. 21 Wavelet power spectra for Hα-350 mÅ and Hα+350 mÅ chromospheric oscillations in fibrils showing intermittent 5-min periods (from De Pontieu and Erdélyi (2006))

Langangen et al. (2008b) used a time series of filtergrams obtained in the red and blue wings of the Hα line near the solar disk center and measured proper motions and Doppler signals in 124 DFs. They obtained mean lifetimes of ~ 258 s. Again they found Doppler velocities to be a factor of $2 - 3$ smaller than velocities derived from proper motions in the image plane and the corresponding decelerations to have a difference of a factor of 5. They attributed the difference to the radiative processes involved, since the Doppler velocity originates from a wide range of heights in the atmosphere, in contrast to the proper-motion velocity, which is a very local quantity, because it is measured from the sharply defined bright tops of the DFs.

A combination of high-resolution observations and advanced numerical simulations have shown that DFs are most likely driven by magneto-acoustic shocks that form when photospheric oscillations leak into the chromosphere along inclined flux tubes (Hansteen et al. (2006); De Pontieu et al. (2007a)). The inclination of the magnetic field lowers the acoustic cut-off frequency sufficiently to allow p-modes with the dominant low frequency to propagate along flux tubes (Michalitsanos, 1973; Bel and Leroy, 1977; Suematsu, 1990). The results of the simulations spanning from the upper convection zone to the corona, lead to the conclusion that DFs are formed by chromospheric shocks driven by global p-modes and convective flows.

Oscillations in fibrils Although quiet and active regions are considered to be made up by the same elementary magnetic flux tubes, there are important differences in the observed magnetic flux densities mainly due to the different filling factors, which are manifested also in the respective oscillatory behavior. However, far less work exists in the literature for oscillations in plages and fibrils compared to work for oscillations in IN, NB and mottles.

Bhatnagar and Tanaka (1972) examining Hα filtergrams have reported 5 min oscillations in plages, while Muglach (2003) using UV observations from the Transition Region and Coronal Explorer (TRACE) found 5 min oscillations in both

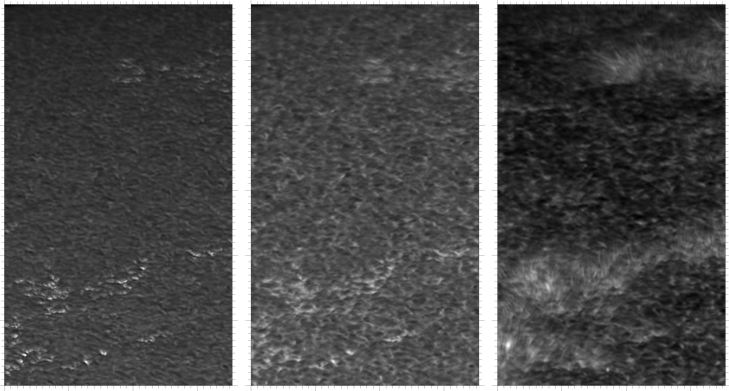

Fig. 22 DOT picture of the sun taken on June 18, 2003 in the G band, the Ca II H wing, and the Ca II H core. The region is close to the solar limb. Scale: the tick marks are separated by $1''$. The magnetic network, shows up as bright patches in the Ca II H wing and the G band. The long thin structures in the Ca II H core sticking out of the network are termed "straws" (from Rutten (2006))

plage and network regions and 3 min oscillations in IN regions. De Pontieu et al. (2003) examining high-resolution SST observations of dynamic fibrils in a plage region reported the presence of significant oscillatory power, although only a small fraction of dynamic fibrils showed oscillations or recurrence. Oscillatory periods in dynamic fibrils range between 4 and 6 min, similarly to dark mottles in quiet Sun regions, and seem to be concentrated mostly in the more inclined structures (De Pontieu et al., 2004; De Pontieu and Erdélyi, 2006). This similarity in the oscillatory behavior of fibrils and dark mottles has been clearly shown by Tziotziou et al. (2004), who analyzed a plage region containing almost vertical fibrils, named as dark grains, which exhibited a unique, high-probability period of ~ 5 min. This period has been explained as the period signature of either flows along vertical structures anchored in the photosphere or as a possible signature of a maximum amplitude p-mode interference wavetrain, compatible with the idea of p-mode leakage reported by De Pontieu et al. (2004) or as due to consecutive shocks as predicted by the 2D rebound shock of Murawski and Zaqarashvili (2010). Furthermore, Tziotziou et al. (2004) showed that the fibril-free area, although in close spatial proximity to the fibril area, had IN-like characteristics with periods closer to 3 min in contrast to the 5-min period of fibrils which is similar to the period obtained for dark mottles.

The oscillatory characteristics of DFs, as De Pontieu et al. (2004) have shown, exhibit similarities to photospheric p-mode oscillations, such as variable periods between 200 – 600 s and intermittency (existence of wave packets). Moreover, observations have indicated that DFs tend to occur near the peripheries of plages where magnetic field lines are often more inclined. This has led De Pontieu et al. (2004) to suggest that DFs are driven by leakage of normally evanescent p-modes in inclined magnetic fields, as Suematsu (1990) had also previously suggested, something that can explain the observed 5-min periodicities.

4.2.3 Straws

Rutten (2006, 2007) using high-resolution ground-based observations obtained with DOT in the wide-passband (of 1.4 Å) Ca II H filter observed some new features, which are finer than the traditional mottles and were termed "straws" (Fig. 22). These structures are long, highly dynamic, bright against dark internetwork background, extend radially outward from network bright points, and occur in "hedge rows". The hedge rows of upright straws are bright and thin in Ca II H, bright, optically thick, twice as high and much thicker than in Ca II H in Ly-α, much less distinct and dark in Hα line center, and more prominent, but less upright and very dark in the Hα wings. Rutten (2006) concluded that straws reflect transition region conditions and the differences in the different lines are due to radiative transfer effects. Such features were also recently observed with the Solar Optical Telescope at the solar limb in Ca II H images. De Pontieu et al. (2007b) refers to these straw-like features as "Type II" spicules.

4.2.4 Rapid blueshifted excursions (RBEs)

A class of short-lived events observed on the solar disk with IBIS/DST and characterized by large Doppler shifts that appear only in the blue wing of the Ca II IR line have been recently reported by Langangen et al. (2008c). They were found at the edges of the rosettes as sudden broadening of the line profile on the blue side of the line without an associated redshift and were denoted as rapid blue-shifted excursions (RBEs) by the same authors. For the measured RBEs they derived an average length of 1.2 Mm, an average width of 0.5 Mm, a mean lifetime of 45±13 s, and velocities of the order of 15 – 20 km s^{-1}. Using Monte Carlo simulations, they showed that the observed blue-shifts can be explained by a wide range of spicule orientations combined with a lack of opacity in the upper chromosphere. Similar events, but longer lived and spatially more extended, have been reported earlier (Wang et al., 1998). These events were also revealed using spectral imaging data in the Ca II 854.2 nm and Hα lines obtained with the CRisP Imaging Spectropolarimeter at the 1-m aperture SST on La Palma (Rouppe van der Voort et al., 2009). These authors used a manual detection scheme together with an automated algorithm to detect RBEs. They identified 413 features in the Ca II 8542 Å data set and 608 in the Hα data set and claimed that the number of RBEs if they were observed at the limb would be 1.9 per linear arcsec. Judge et al. (2011) exrapolating the number of RBE detections of Rouppe van der Voort et al. (2009) estimated that there should be $\sim 10^5$ RBEs on the Sun at any given moment. They found rapid blue-ward excursions in the line profiles of both chromospheric lines (Fig. 23) and suggested that these structures may be the on-disk counterparts of Type II spicules. They measured lengths, Doppler velocities and widths of RBEs and found that the values of these quantities are consistently higher for the Hα RBEs compared to the Ca II RBEs. Thus Hα RBEs are on average longer (of order 3 Mm vs 2 Mm), higher widths (13 km s^{-1} vs 7 km s^{-1}) and have higher average Doppler shifts toward the blue (35 km s^{-1} vs 15 km s^{-1}).

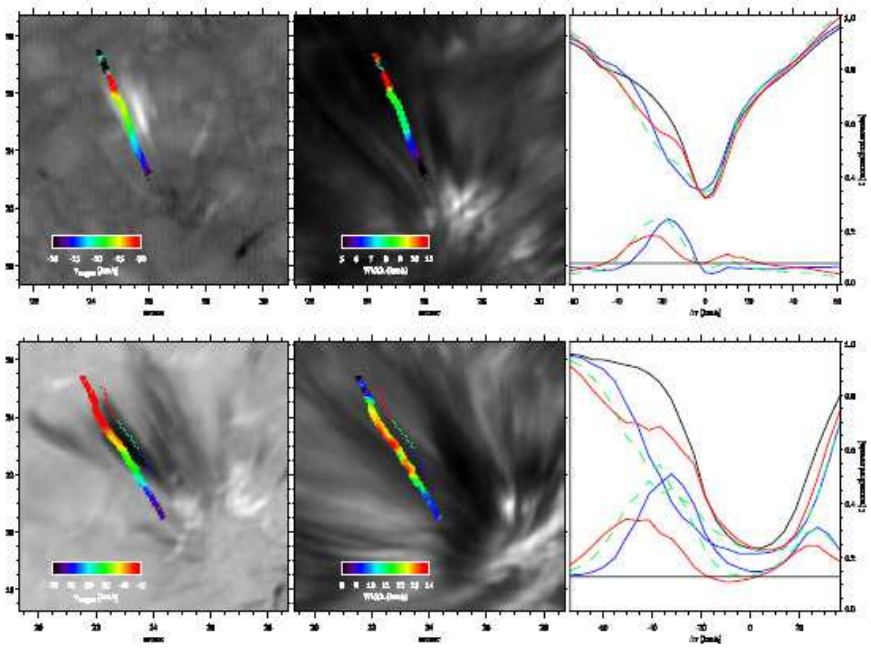

Fig. 23 Properties as a function of position of an RBE in the Ca II 8542 Å data set (top panels) and the Hα data set (bottom panels). Color-coded-measured Doppler velocity (left panels), width (middle panels), and mean spectra over three portions of the RBE (right panels: closest to foot-point in blue, middle part as dashed green, part furthest away in red and mean spectrum in black. Upper curves show the spectral profile, the lower curves show the subtraction of the average spectrum and the spectral profile). The extracted RBE is shown with a thin colored line in the left and middle panels with blue for the third of the length closest to the foot-point, green for the middle part, and red for the part furthest away from the foot-point. The measured parameter is shown displaced to the left of the RBE. The background image is at line center (middle panels), at a blue position of 36 km s^{-1} (bottom left panel), and a Dopplergram at 30 km s^{-1} (top left panel). At both the bottom and top end of the RBEs the amount of blue-ward absorption drops significantly. When this happens, the Doppler velocity and width is set to zero. This is why the black color coding at both ends of the RBEs is not indicative of lower velocities or widths, but rather signifies the spatial extent of the blue absorbing feature. From Rouppe van der Voort et al. (2009)

5 Relation between mottles/fibrils and photospheric bright points

Multi-wavelength photospheric and chromospheric observations of quiet solar regions, such as the ones presented in Fig. 2, show a clear spatial relationship between the dark elongated structures, called mottles, emanating from the network boundaries and the photospheric bright points. Hence, it is quite natural to think that these structures are somehow related. Bright points, which can be regarded as proxies of small-scale magnetic elements in the photosphere, are prominent at network boundaries in the Hα line-wing images at high spatial resolution (e.g. Dunn and Zirker, 1973; Suematsu et al., 1995; Leenaarts et al., 2006). As Suematsu et al. (1995) showed, by comparing Hα–0.65 Å and Hα+0.65 Å filtergrams, bright points are very prominent at network boundaries in the blue-wing, while only a few appear in the red-wing or line center. Recently, Leenaarts et al.

(2006) concluded that in the blue Hα wing bright points represent a promising proxy magnetometer to locate isolated magnetic elements.

It is of great interest to investigate whether the appearance of bright points, which represent intense magnetic concentrations, is related to fine structure formation at the network boundaries. However, it is extremely difficult to directly associate bright points to specific dark mottles. Dunn et al. (1974), used their excellent Hα filtergrams, but they were not able to find a definite relationship between them. Suematsu et al. (1995), using time series of Hα observations were able to connect a bright point with a mottle through its whole life. They reported, however, that there were many mottles which were not associated with bright points. They also noted that bright points often appear at the foot-points of mottles at Hα–0.65 Å, but during their peak extension or falling phase rather than at their beginning. In Hα+0.65 Å bright points seem to be obscured by falling material. In the blue wing, however, and in the falling phase of mottles one can see a much deeper layer due to an effective red shift of the line. Enhancement of the brightness in -0.65 Å could occur due to compression of the atmosphere by in-falling spicule material that penetrates deeper the solar atmosphere, delivering its potential energy. The infalling material may even distort and kink the flux tube inward; this is inferred from the inward offset of the spicule base in the red-wing compared to its blue-wing position (see Suematsu, 1998; Dara et al., 1998). Cauzzi et al. (2009), in simultaneous Hα and Ca II infrared observations obtained from IBIS noticed that in Hα at minimum intensity dark structures show sometimes marked brightenings towards one end. Comparison with magnetograms showed that these bright endings correspond to the stronger magnetic concentrations, although the magnetic network, which is easier to see in the respective Ca II infrared images, is not easily recognized in this line. Sterling et al. (2010) used Ca II H observations of a north pole coronal hole obtained with SOT/Hinode and investigated the roots of some spicule-like features seen on the disk near the limb. They found that these features seem to emanate from fast moving Ca II brightenings. Frequently the ejected spicules, which have speeds $\sim 100\,\mathrm{km\,s^{-1}}$, seem to occur when these brightenings, which have horizontal velocities of a few $10\,\mathrm{km\,s^{-1}}$ appear to collide and disappear. These spicules could be associated to the so-called Type II spicules. Based on their findings, they suggested that Ca II brightenings could represent acoustic shocks or fast-moving interacting magnetic elements. As they stated it is hard to understand how the energy from acoustic shocks could be converted to spicules of such high velocities. If, on the other hand, Ca II brightenings represent different magnetic elements, their merging could lead to magnetic cancellation and reconnection, resulting to the deposition of thermal energy in the low atmosphere.

The existence of a relationship between bright points and the corresponding structures found in active regions, called fibrils, has been examined by Pietarila et al. (2009) in Ca II K line observations. They reported that bright foot-points of fibrils are clearly co-spatial with the photospheric magnetic concentrations. As they noticed, however, in a strong plage it is not easy to identify such a correlation, because the density of the fibrils is very high, the fibrils are more vertical and form a carpet covering the surface.

6 Mottles and fibrils and the formation of the magnetic canopy

The highly ordered photospheric magnetic fields of the plages and magnetic network spread out and occupy the whole atmosphere as they extend upwards. Thus, instead of the bright points that constitute the network and the facular granules that constitute the plages, which more or less represent the cross-sections of rather vertical flux tubes, thin, elongated, and usually inclined structures dominate in the chromosphere and provide evidence of its complex structure. Gabriel (1976) proposed that the magnetic field of the upper solar atmosphere has a wine glass geometry as a result of magnetic field lines fanning out of the network. Such a general configuration of the chromospheric magnetic field was already assumed before (see e.g. Kopp and Kuperus, 1968) and is physically anticipated. Due to the almost exponential decrease of the gas pressure with height, the magnetic flux tubes expand and form a funnel-like magnetic geometry with almost horizontal fields. One interesting quantity describing the relative importance of gas and magnetic field is the plasma β parameter (where $\beta = 8\pi\, p/B^2$). The $\beta = 1$ layer, i.e. the layer where the gas and magnetic pressures are equal (or, equivalently, the sound speed equals the Alfvén speed) is called *magnetic canopy*. This layer is of critical importance because it partitions the atmosphere into contiguous volumes of gas pressure (high-β) and magnetic pressure (low-β) dominated plasma. The location of the magnetic canopy depends on the photospheric magnetic flux and on the pressure profile of the atmosphere in which the flux tubes are embedded. Therefore, in principle, one may expect that it should be lower near active regions and higher around the chromospheric network in quiet Sun. In the quiet Sun the canopy is situated somewhere between ~ 1 and 2 Mm above $\tau_{5000} = 1$ (Solanki and Steiner, 1990). Thus it is within the chromosphere that β falls below 1 and magnetic forces start to gain control on the dynamics of the solar plasma. This results not only in mode conversion, refraction and reflection of waves, but also, together with the local thermodynamic properties, in the plethora of fine structures that characterize this part of the atmosphere.

Concerning wave propagation, it has been shown by numerical simulations and theoretical studies that the canopy acts as a boundary. Waves that propagate from the photosphere into the chromosphere, undergo mode conversion, refraction and reflection when they reach the canopy (see e.g. Rosenthal et al., 2002; Bogdan et al., 2003; Schunker and Cally, 2006; Cally, 2007; Khomenko et al., 2008b; Kuridze et al., 2009; Nutto et al., 2012). Through the interaction between the various MHD modes at the canopy, energy is transferred at higher atmospheric layers. This interaction has also been revealed by observational studies which show the distribution of the oscillatory power on the FOV. It was found that high frequency oscillatory power at the photosphere is increased around intense magnetic concentrations, in active regions, forming the so-called *power halos* (Braun et al., 1992; Brown et al., 1992; Hindman and Brown, 1998; Thomas and Stanchfield, 2000; Jain and Haber, 2002; Muglach, 2003). It was also noted that the power is reduced above strong magnetic concentrations at the chromospheric level. Muglach et al. (2005) combined power maps and magnetic field extrapolation in an active region and showed that closed lines are associated with a further increase in power, due to reflection of acoustic waves. The same areas of enhanced power were less extended around nearly vertical open field lines. It is, generally, accepted that this enhancement is due to the interaction of acoustic waves with the canopy. On the

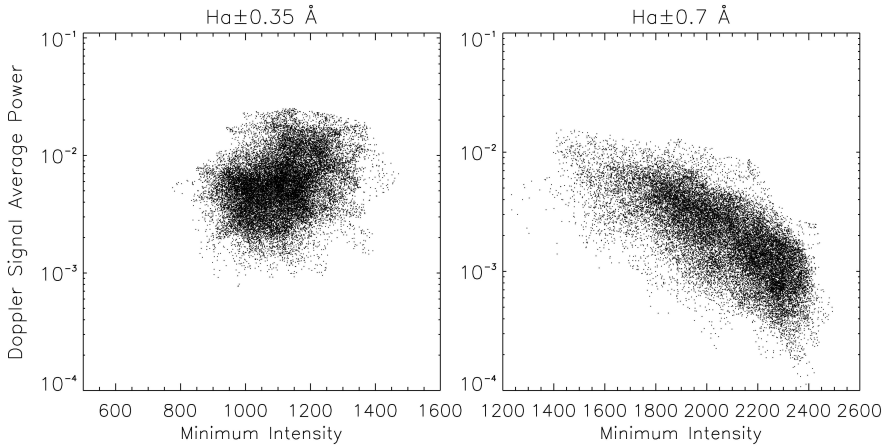

Fig. 24 Scatter plots of the average power of Doppler signal variations in a logarithmic scale vs the H$\alpha\pm$0.35 Å minimum intensity (*left column*) and of the H$\alpha\pm$0.7 Å minimum intensity (*right column*) in a rosette region consisting of mottles from Kontogiannis et al. (2010a))

other hand, over the network regions the presence of reduced power has been revealed by Judge et al. (2001) through TRACE and SUMER observations. These authors used the term *magnetic shadow* to describe this power deficit observed in areas adjacent to the NBPs and not only above them. Magnetic shadows were also detected in chromospheric lines, such as Ca II IR or Hα (Vecchio et al., 2007; Kontogiannis et al., 2010a). It was explained that the interaction of waves with the magnetic canopy is also responsible for the formation of the magnetic shadows (McIntosh et al., 2003). In Kontogiannis et al. (2010a) it was further found that around NBPs and over rosettes magnetic shadows were detected at H$\alpha\pm$0.35 Å, while at H$\alpha\pm$0.7 Å acoustic halos were detected at the same positions. They also noticed that, interestingly, the power maps show a fibrilar structure which correlated very well with the positions of dark mottles.

The different types of fibrilar structures seen in chromospheric lines (especially in the Hα line) chart inclined magnetic flux tubes. These flux tubes contain more atoms and ions in the right state for absorption (or emission) in the corresponding lines than their surroundings. It is reasonable to assume that the chromospheric structures are somehow connected with the formation of the magnetic canopy and should play an important role in wave propagation. Kontogiannis et al. (2010a) examined the relation between power enhancement or suppression within a rosette region and the positions of dark mottles. They gave scatter plots (shown in Fig. 24) between the average power of the oscillations of the Doppler signal and the minimum intensity in H$\alpha\pm$0.35 Å and H$\alpha\pm$0.7 Å (which are obviously related to dark structures). In the left scatter plot lower power values correspond to lower minimum H$\alpha\pm$0.35 Å intensity values. The inverse is observed for the H$\alpha\pm$0.7 Å intensities (right scatter plot). The authors arrived to the conclusion that power enhancement/suppression is directly related to mottles. Potential magnetic field extrapolation using photospheric magnetograms has shown that mottles follow, in most cases, the magnetic field lines of the chromospheric field (see 25), (Kontogiannis et al., 2010b).

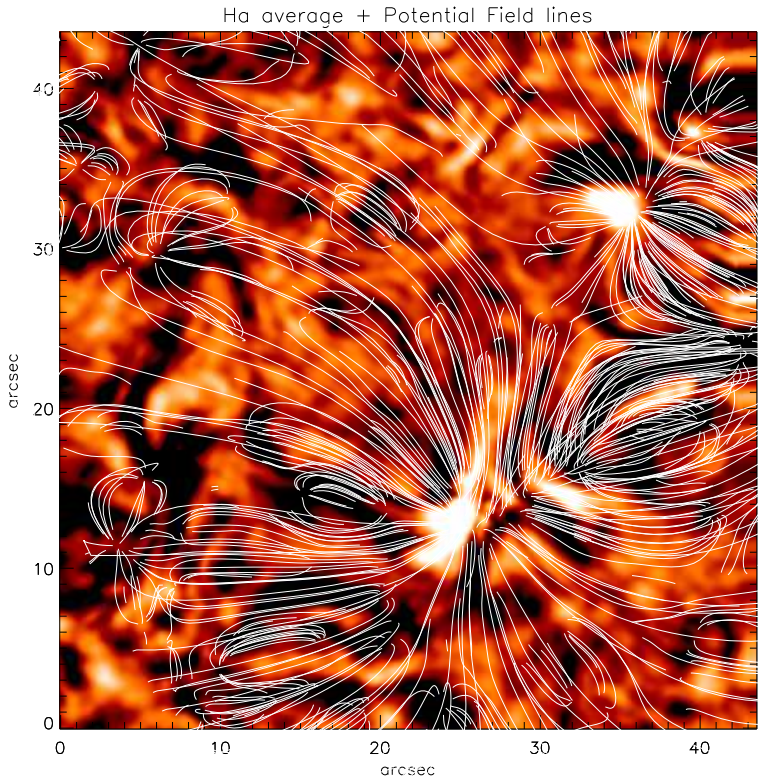

Fig. 25 Hα line centre 30-minute average intensity image. Overlayed are the field lines of the extrapolated magnetic field using the potential field approximation (from Kontogiannis et al. (2010b))

In this same study the authors have assumed a VAL 3C model for the solar atmosphere and used SOT/SP magnetograms. They obtained the LOS and transversal components of the magnetic field, its inclination to the vertical, as well as the plasma-β. From these parameters they calculated the height of formation of the magnetic canopy. They showed that the magnetic canopy is directly related to the dark mottles, which seem to provide the loci where wave mode conversion, refraction and reflection occur. They also showed that the modulation of the oscillatory power is defined by the inclination of the magnetic field and the relative positions of the magnetic canopy and the height-of-formation of the line used for the observations. In a subsequent paper Kontogiannis et al. (2011) used high-precision measurements of the magnetic field in a network region provided by SOT/SP on-board the Hinode mission and MDI/SoHO measurements together with potential magnetic field extrapolation. They showed that the data of the latter instrument lead to higher formed and less horizontally extended canopies. The authors concluded that the sensitivity of the instrument used to measure the photospheric magnetic field is very important in the derivation of the height of formation of the magnetic canopy.

7 Trends in observation

The study of the fine and highly dynamic solar structures requires high angular, temporal and spectral resolution observations. Solar observations are moving into a new era of high-resolution observations. Ground-based observations, traditionally restricted by seeing conditions, are now profiting from adaptive optics and post-detection image restoration techniques to achieve a much better angular resolution than was possible before, while new large-aperture telescope projects have already been initiated. Space-based observations are providing large volumes of data in the visible, ultraviolet and X-ray wavelengths, covering extended temporal durations, and have revolutionized solar science during the past years with successful missions such as YOHKOH, SoHO, TRACE, STEREO, HINODE and more recently SDO, while new exciting projects are under way.

Ground-based solar telescopes are equipped with state-of-the art instruments and CCD cameras. The Télescope Héliographique pour l'Étude du Magnétisme et des Instabilités Solaires (THEMIS), the 90-cm aperture French-Italian solar physics facility in Tenerife, is equipped with a Fabry-Pérot filter magnetograph (MTR) and a large double-pass spectrograph (MSDP) for multi-line spectropolarimetry and 2-D spectrometry. The 45-cm Dutch Open Telescope (DOT) provides solar images at nearly $0.2''$ resolution while the SST has been recently operating a new CRisp Imaging SpectroPolarimeter (CRISP). The Interferometric BIdimensional Spectrometer (IBIS), a bi-dimensional spectrometry instrument based on a dual Fabry-Pérot interferometric system, plus ROSA (Rapid Oscillations in the Solar Atmosphere camera) are already operating at Dunn Solar Telescope of the Sacramento Peak Observatory. The German VTT telescope operates with spectropolarimeter instruments such as POLIS (for the iron line pair at 630.2 nm) and TIP (for the near infrared) and TESOS which is a 2D spectrometer. The 1.6-meter New Solar Telescope (NST) at Big Bear Solar Observatory (BBSO), uses a large set of new instruments such as broad-band filter imagers (e.g. a TiO filter centered at a wavelength of 705.7 nm, with a bandpass of 1 nm) to deliver high resolution images of small-scale photospheric features with high cadence exposures. Knowledge acquired from past and present instrumentation will be used in new solar telescopes like the 1.5-meter German Gregory Coudé Telescope in Tenerife and future large-telescopes like the US Advanced Technology Solar Telescope (ATST) and the European Solar Telescope (EST). Post-detection image restoration, although it requires a large amount of processing, enhances the spatial resolution close to the theoretical telescope diffraction limit through techniques, such as the phase-diverse image registration (e.g., Loefdahl et al., 1998) which is used in SST and speckle image reconstruction (e.g., Sütterlin et al., 2001). An extension of the first image restoration technique called Multi-Object Multi-Frame Blind Deconvolution (MOMFBD, van Noort et al., 2005) operates now at SST. Speckle image reconstruction works by dividing the observed field in isoplanatic subfields which are reconstructed independently by describing a seeing-sampling sequence of perturbed images called "speckle burst" with a model of atmospheric turbulence, and finally rejoining them in one single image. This technique has been extensively used for post-restoring of images from several telescopes, such as the DOT, VTT, DST and SST. However, although these techniques produce high resolution solar images, usage of such images for the quantitative determination of different physical parameters with inversion techniques (e.g. cloud modelling) can sometimes lead

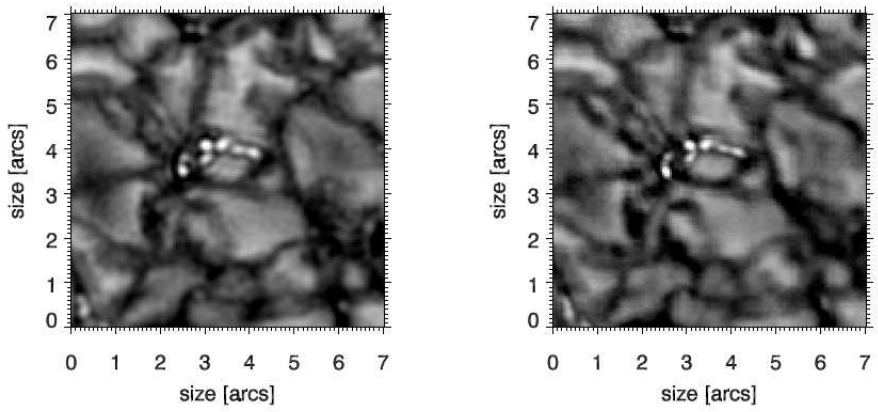

Fig. 26 *Left*: Deconvolved Hinode SOT image, *Right*: Reconstructed DST image (Wöger et al. (2008))

to spurious results and hence possible effects and artifacts of image restoration on the data should always be examined before such a scientific analysis.

Real-time image correction in ground-observations is nowadays achieved with adaptive optics. Adaptive optics try to correct the incoming wavefront, similarly to the speckle reconstruction principles, by dividing the aperture plane into sub-apertures (ideally smaller than the seeing) and applying a wavefront correction to compensate for deformations caused by seeing conditions and imperfections in the optical system. Adaptive optics makes it feasible to build very large meter(s)-class innovative solar telescopes such as the NST at Big Bear Solar Observatory and the GREGOR in Tenerife and the even larger future telescopes like ATST and EST.

Adaptive optics systems are now commonly used on several advanced solar telescopes to enhance the spatial resolution of the recorded data. Post image reconstruction techniques such as speckle interferometry can be used to achieve near-diffraction limited resolution over a large FOV rather than the limited area where the wavefront sensor of the adaptive optics system measures the wavefront distortions. Wöger et al. (2008) investigated the reconstruction properties of the Kiepenheuer-Institut Speckle Interferometry Package (KISIP) code. Comparisons were made between simultaneous observations of the Sun using the ground-based Dunn Solar Telescope and the space-based SOT/Hinode telescope. The analysis showed that near real-time image reconstruction with high photometric accuracy of ground-based solar observations is possible, even for observations in which an adaptive optics system was utilized to obtain the speckle data (Fig. 26).

8 Trends in interpretation of line profiles

The on-disk solar chromosphere can be observed in the cores of strong absorption lines at visible or near-UV wavelengths, while many of the emission lines in the EUV part of the spectrum arise in the upper chromosphere. Fine-scale chromospheric features are usually observed in the Hα Lyα, Ca II H & K and the Ca II infrared triplet. In principle the solar chromosphere is optically thick at these wave-

lengths and, consequently, their computation from a model atmosphere requires solving the well known radiative transfer equation together with the statistical equilibrium equations self-consistently, a problem which is both highly non-linear and non-local. However, a simple method called the cloud model, which does not involve such elaborate computations and assumes optically thin structures and a constant source function along the observed structure has been successfully applied over the years for several chromospheric structures observed in Hα (see review by Tziotziou, 2007) for the determination of physical parameters. Below we discuss in more detail the cloud model, other radiative transfer techniques and recent and future trends in interpretation of line profiles.

8.1 The cloud model

For the deduction of different physical parameters of chromospheric structures from observations in the Hα line a method is used which is based in the so called "cloud" model, introduced by Beckers (1964), (see also Alissandrakis et al., 1990). The model is valid for optically thin structures located well above the background. It considers for an observed intensity profile $I(\Delta\lambda)$ the contrast profile:

$$C(\Delta\lambda) = \frac{I(\Delta\lambda) - I_0(\Delta\lambda)}{I_0(\Delta\lambda)} = \left(\frac{S}{I_0(\Delta\lambda)} - 1\right)(1 - e^{-\tau(\Delta\lambda)}) \tag{4}$$

with a Gaussian wavelength dependence for the optical thickness:

$$\tau(\Delta\lambda) = \tau_0\, e^{-\left(\frac{\Delta\lambda - \Delta\lambda_{\rm I}}{\Delta\lambda_{\rm D}}\right)^2} \tag{5}$$

where $I_0(\Delta\lambda)$ is the reference profile emitted by the background and $\Delta\lambda_{\rm I} = \lambda_0 v/c$ is the Doppler shift with λ_0 being the line center wavelength and c the speed of light. The four adjustable parameters of the model are the source function S, the Doppler width $\Delta\lambda_{\rm D}$, the optical depth τ_0 and the line-of-sight (LOS) velocity v. All these parameters are assumed to be constant through the structure.

Once the four parameters are determined from the cloud model, the estimation of several other parameters can be made. From the calculated Doppler width values and if we assume a value for the micro-turbulent velocity, ξ_t, we can deduce the temperature, T_e. From the optical depth at line center, which may be written as:

$$\tau_0 = \frac{\pi^{\frac{1}{2}} e^2}{m_e c}\,\frac{f\lambda^2}{c}\,\frac{N_2}{\Delta\lambda_D} d \tag{6}$$

and $\Delta\lambda_D$, N_2, e.g. the number density in the second hydrogen level, can be obtained. Then the electron density, N_e, the total particle density of hydrogen (i.e., neutral plus ionized), N_H, the gas pressure, p, the total column mass, m, the mass density, ρ, can be determined from the following relations:

$$N_e = 3.2\,10^8\,\sqrt{N_2}\,cm^{-3} \tag{7}$$

$$N_H = 5\,10^8\,10^{0.5\log N_2} \tag{8}$$

$$p = k(N_e + 1.0851 N_H) T_e \tag{9}$$

$$m = (N_H m_H + 0.0851 N_H \times 3.97 m_H)\, d \tag{10}$$

$$\rho = \frac{m}{d} \tag{11}$$

where d is the path length along the LOS (for details about the derivation of these parameters Tsiropoula and Schmieder (1997)).

8.1.1 Optically thick radiative transfer

For any given species the radiation field is determined from the source function. The source function is derived from the atomic level populations that are in turn determined by the local radiation field. This inter-dependence defines the highly non-linear and non-local aspect of optically thick radiative transfer.

As already mentioned (see Section 4.2.1) Giovanelli (1967a,b) did pioneering extensive NLTE computations of the Hα line contrast profiles relevant to chromospheric fine-scale modelling assuming 1D slabs illuminated by the surrounding atmosphere. Heinzel and Schmieder (1994) used Hα line profile observations of bright and dark mottles together with a grid of NLTE models of prominence-like structures considered as vertically-standing 1D slabs irradiated from both sides by an isotropic incident radiation and derived the physical conditions in these structures.

In general, most radiative transfer codes used so far for the diagnostics of isolated solar structures, combine the accelerated (or approximate) Lambda iteration (ALI) or multilevel ALI (MALI) schemes (e.g. Cannon, 1973; Scharmer and Carlsson, 1985; Rybicki and Hummer, 1991, 1992; Olson et al., 1986) with efficient algorithms for computing the radiation field (Feautrier's method, Feautrier, 1964; Auer, 1967) and direct integration techniques (e.g. Mihalas et al., 1978; Olson and Kunasz, 1987) in order to solve the intricate radiative transfer problem.

There already exist several 1D-geometry radiative codes, such as MULTI (Carlsson, 1986), MALI (Heinzel, 1995) and RH (Uitenbroek, 2001, the 1D version) that compute the radiative transfer problem in plane parallel atmospheres, using atoms containing several or even hundreds of levels and/or thousands of lines. However, the solar chromosphere has a complex 3D structure which should be taken into account when evaluating the radiation field with non-Local Thermodynamic Equilibrium (NLTE) codes. Such codes are usually required to use local ALI operator, since any non-local operator would require computationally expensive inversions of very large sparse matrices. Since the typical size of 3D radiative transfer problems is quite large, some form of parallelization (either over frequency and angle, or using domain decomposition, or a not-yet implemented hybrid parallelization strategy) is required to speed up convergence to a physical solution. Nowadays, there exist three 3D NLTE radiative transfer codes, the MUGA code (see, e.g Fabiani Bendicho et al., 1997; Botnen and Carlsson, 1999) the RH code by Uitenbroek (2001) and the Multi3D (Fabiani Bendicho and Trujillo Bueno, 1999; Leenaarts et al., 2009) code, for calculating chromospheric models.

The situation that prevails in the atmosphere of the Sun poses several different, problems in the computation of the radiation field with NLTE codes. For example, the hydrogen line radiative transfer problem, requires to take into account non-equilibrium hydrogen ionization in the chromosphere and hydrogen level

populations out of statistical equilibrium. This stems from the fact that the assumption of statistical equilibrium for hydrogen fails in the chromosphere, because the timescale of hydrogen ionization and recombination is of the same order as the hydrodynamic timescale. The existing codes fail to reproduce the Hα line center intensity, as well as the fibrilar structure of the chromosphere. This is because apart from taking into account non-equilibrium ionization processes, 3D NLTE time-dependent radiative transfer codes are required in order to compute the detailed hydrogen line profiles and get reasonably realistic electron density and temperature which are very important parameters for the modelling of the chromospheric structures. On the other hand, the Ca II lines suffer less than Hα from non-equilibrium ionization processes and thus can be modeled assuming statistical equilibrium. The cores of Ca II H & K, however, form in partial redistribution, which is computationally far less trivial than complete redistribution and still has not been fully implemented in 3D. To make the problem of simulating these lines even worse we mention that the Ca II H & K lines are usually observed with wide filters which deliver intensity contributions from a wide range of formation heights. Partial redistribution effects are less important for the Ca II infrared triplet and, moreover, these lines can be computed in 3D. Current state-of-the-art instruments have delivered many high-quality chromospheric observations in the Ca II 8542 Å line, in particular, although this line has a lower line-core opacity than Hα and Ca II H & K. The NLTE Ca II 8542 Å computation using a 3D simulation (Leenaarts et al., 2009; Leenaarts and Carlsson, 2009), does not show, however, the fibrilar elongated structures delineating magnetic field lines around the network. This lack may be do to several reasons, such as the low resolution of the grid used for the simulation, need for larger scale magnetic field configuration, etc. Another possibility is that Ca II 8542 Å opacity in the fibrils is caused by physical processes currently included in the existing simulation codes. On the other hand, quite recently Leenaarts et al. (2012) using 3D NLTE radiative transfer computations and MHD simulations investigated the Hα line formation in the solar chromosphere. They were able to reproduce the fibril-like dark structures seen in Hα line-core observations. Furthermore, their simulations support the commonly held notion that fibril-like structures indeed trace the magnetic field.

Knowledge of the physical conditions in isolated structures is very important in order to elucidate the physical processes which are occurring in them. A state-of-the-art method to improve this knowledge is the forward modelling by which data from a combination of radiation-MHD simulation codes with 3D NLTE radiative transfer codes are converted into observed quantities and after being compared with observations can give more reliable initial values for the codes. Although existing codes still suffer from severe limitations, they are producing promising results, e.g. the computation of the emerging Ca II 8542 Å and Hα line profiles with a 3D NLTE model using an RMHD simulation (Leenaarts et al., 2009, 2012), the spectral line response to reconnection events in the photosphere and transition region (Heggland et al., 2009), Monte-Carlo simulations of the line profile response to upward propagating material, such as in the case of rapid blue-shifted events, (Langangen et al., 2008c), and toy models of the solar atmosphere to qualitatively explain the appearance of the solar limb in the Hinode Ca II H passband caused by large line-of-sight velocities or wide spicule line profiles (Judge and Carlsson, 2010).

9 Inter-relations between the different fine-scale chromospheric structures seen on the disk and at the limb

One of the outstanding questions in spicule research concerns the relationship between spicules at the limb and structures observed on the disk. Although spicules, mottles and fibrils are all nowadays treated as jet-like features of the solar chromosphere and the similarity of many of their properties strongly suggests that some of these phenomena are related, if not the same, there has been a strong debate in the solar community about the exact relationship between them. In particular, it has long been suspected and even assumed that the *dark mottles* are the direct manifestations of *spicules*, and considerable effort has been expended to prove this relationship. The mass velocity is one of the properties that could help establishing a kinship between mottles and spicules. Grossmann-Doerth and Schmidt (1992) have examined two distributions of axial velocities, one based on limb the other on disk observations. They arrived to the conclusion that the two distributions disagree, that the velocity in spicules is significantly greater than in mottles and thus that mottles are not the disk counterparts of spicules. They discussed several possibilities for this discrepancy, but the most important we think – not discussed in that paper – is that the velocities from which these distributions were derived have been obtained by different methods: for the limb velocities distribution the Doppler shift method was used, while for the disk velocities distribution they used the "cloud" model. These two techniques yield very different results, as it is stated by Tsiropoula et al. (1994). The discrepancies on the velocities between structures seen on the disk and at the limb, apart from the problem in associating with spicules some easily identified class of disk structures, must, furthermore, be sought as due to several other reasons. These include various selection effects arising from different visibilities of the features, different wavelengths used for their observations, different phases in their evolution and also eventual bias in the data arising from the methods of analysis. They are also arising from the fact that the structures are observed under very different conditions: in one case (limb) at great heights and along the horizontal LOS; in the other case (disk) at low heights and along the vertical. Direct observational evidence for the identification of fine dark mottles with spicules would be that of a dark mottle crossing the solar limb. Christopoulou et al. (2001) found several examples of individual mottles crossing the solar limb and provide further support to the association between spicules and mottles. On the other hand, some authors suggested that similarities in dimensions, lifetime, and physical conditions, such as density and temperature, provide indirect evidence to the identity of spicules and dark mottles (Tsiropoula and Schmieder, 1997).

It is also not clear which the relationship is between quiet Sun *dark mottles* and active region *long fibrils* and *short dynamic fibrils* (DFs). Long fibrils are found at the edges of plages, are longer, more stable, longer lived and more horizontally oriented than the most dynamic DFs, which are found towards the center of the plages, are more vertically oriented and have shorter lifetimes (although their lifetime depends on their inclination being longer for the more inclined ones). The more complex topology of the quiet Sun with its mixed polarity magnetic fields are to be opposed to plage regions which are considered as unipolar with magnetic flux tubes packed close together. Due to these differences the conditions between quiet Sun and plage regions should differ considerably and this must be reflected in the dynamics, as

well as the mechanisms responsible for the formation of mottles and fibrils. Thus for mottles magnetic reconnection has been suggested as the more likely formation mechanism (Tsiropoula et al., 1994; Tziotziou et al., 2003), while for fibrils magnetoacoustic shock waves driven by leakage of convective motions and oscillations from the photosphere into the chromosphere along magnetic fields have been suggested as the formation mechanism. Tsiropoula et al. (1994), and Tziotziou et al. (2003) derived LOS velocities along mottles using the cloud model. Examining the temporal evolution of the LOS velocity they found that the predominant motion is downward at their foot-points and alternatively upward and downward at their tops. Mottles are found at the network boundaries where bipolar elements are swept by the supergranular flow. Interactions of the magnetic fields have as a result the enhancement of the flux concentration in the case of same polarities or its cancellation in the case of opposite polarities. The bipolar nature of the flux cancellation process most likely involves magnetic reconnection and thus it is reasonable to consider this process as the driver of mottles. Murawski and Zaqarashvili (2010) studying the formation of chromospheric jet-like structures in the framework of the rebound shock model which was based on a localized velocity pulse launched from the lower atmosphere which quickly steepens into shocks. They were able to explain the observed speed, width, heights and periods of type I spicules, as well as the observed multi-structural and bidirectional flows. Fibrils, on the other hand, are found at active region plages which are considered as unipolar, with high filling factor of the magnetic field, while the field lines are only moderately inclined and the spatial distribution of magnetic flux in their core evolves slowly. It is possible that different mechanisms have to be considered as their driver. For dynamic fibrils examination of their proper motions have shown that their tops follow parabolic paths. Recent observations, as well as several new, usually 2D, simulations have suggested that dynamic fibrils are driven by magnetoacoustic shock waves, which originate in the convection zone and photosphere. It has long been recognized that along inclined magnetic flux tubes p-modes leak sufficient energy from the gloabal resonant cavity into the chromosphere (Hansteen et al., 2006; De Pontieu et al., 2007a; Heggland et al., 2007). Heggland et al. (2009) performed 2D simulations that included the effects of radiation and heat conduction and that involved reconnection events induced by waves propagating upward from the photosphere/convection zone and were able to produce a number of jet phenomena among them spicules. Martínez-Sykora et al. (2009) performed 3D simulations and showed that some structures having the properties of mottles and DFs can be formed by upwardly propagating chromospheric waves through several driving mechanisms: collapsing granules, magnetic energy release in the photosphere or low chromosphere, p-modes, etc. They suggested that magnetic energy release events might be related to magnetic field line reconnection and thus both mechanisms, i.e. magnetic reconnection and shock waves could co-exist in the jets. Their simulations, however, do not reproduce the observed values for the duration and maximum height of the jets. Thus, they found durations of $2 - 3$ min (instead of $5 - 10$ min) and maximum heights less than 2 Mm (instead of ~ 10 Mm). There is a bias also towards rather vertical structures which cannot account for the heavily inclined structures that, as it is known, are responsible for the formation of the magnetic canopy. Their simulations, on the other hand, showed that half of the events they found were driven by magnetic energy release, most likely related to the emergence of new field into a pre-existing ambient field. Such conditions, how-

ever, do not prevail in plage regions and thus these simulations are still far from what works in the real Sun. From the above it seems more plausible to consider that both drivers, i.e. waves and magnetic reconnection should be considered as responsible for the formation of both mottles and fibrils.

It is also unclear what the relationship is between the recently named *Type I* and *Type II spicules* and the *traditional spicules*. Traditional spicules show mean velocities of order $20 - 30\,\mathrm{km\,s^{-1}}$, lifetimes of order $5 - 10\,\mathrm{min}$, and heights of $5\,000 - 10\,000\,\mathrm{km}$. Type I spicules appear to rise up from the limb and fall back again and show similar dynamical evolution as active region DFs (Hansteen et al., 2006; De Pontieu et al., 2007a), as well as a subset of quiet–Sun mottles (Rouppe van der Voort et al., 2007). For these structures magnetoacoustic shocks have also been suggested as their driven mechanism ((Hansteen et al., 2006; De Pontieu et al., 2007b; Heggland et al., 2007; Martínez-Sykora et al., 2009)). The so-called Type II spicules, on the other hand, appear to exhibit upward motion followed by rapid fading without a downward moving phase. They have shorter lifetimes ($10 - 100\,\mathrm{s}$), high apparent velocities ($50 - 150\,\mathrm{km\,s^{-1}}$), and lower widths (150 and 700 km). They undergo a swaying motion which has been suggested to be caused by the upward propagation of Alfvén waves (De Pontieu et al., 2007c). Thus it seems that Type I and Type II spicules, as seen by SOT on Hinode, look totally different from what are considered as traditional spicules described in the literature. It has to be noticed, however, that the properties of the newly discovered Type I and Type II spicules have been derived from observations in the Ca II H intensity images obtained with the broad-band filter onboard the Hinode spacecraft, while most of the earlier works were based on filtergrams and/or spectra obtained in the Hα line. Furthermore, since spicules are so dynamic and many undergo transverse motions during their lifetime, in order to infer a reliable measure of their properties if a fixed cut almost perpendicular to the limb is used then one has to rely only on spicules that did not move transversely so that their full lifetime can be covered. In a recent work Zhang et al. (2012) re-analyzing the same data sets used by De Pontieu et al. (2007b) traced the intensity along individual structures in quiet Sun and CH. They claimed that they could not find a single convincing example of Type II spicules. Furthermore, they claimed that more than 60% of the identified spicules in each region showed a complete cycle, i.e., the majority are Type I spicules. Due to these discrepancies, it cannot be clear how the traditional spicules are related to the Type I and Type II SOT/Hinode spicules. Furthermore, what is measured in Ca II H images is apparent motions and it is unclear whether they are associated with bulk mass motions derived sometimes in the Hα line. The differences in the heights, lifetimes, velocities and driving mechanisms that pointed that there are two types of spicules should also be questioned. Are there really two different distributions of the different parameters or one broad distribution with a wide range of values? Bray and Loughhead (1974) gave histograms of upward and downward velocities in traditional spicules in the range $\pm 60 - 70\,\mathrm{km\,s^{-1}}$, lifetimes in the range $2 - 10\,\mathrm{min}$, heights in the range $6 - 16\,\mathrm{Mm}$. Heristchi and Mouradian (1992) give also a distribution of the apparent velocities in the so-called traditional spicules from which it can be seen that they are in the range $0 - 70\,\mathrm{km\,s^{-1}}$ (see Fig.6, left). Regarding the formation mechanisms, Shibata et al. (1982a) found that: if the explosion (reconnection) occurs below the middle chromosphere, the jets are formed as a result of shocks; if the explosion (reconnection) occurs above the middle chromosphere the jets are directly driven

by reconnection. Shibata and Suematsu (1982b) using the shock model explained why spicules are taller in coronal holes and shorter in active regions. Thus in our opinion the question whether there really exist two types of spicules or one type of spicules with very broad distributions of heights, lifetimes and velocities, remains open.

Recently an important effort has been undertaken to establish a relationship between *Type I* or *Type II spicules* and *structures on the disk*, such as straws and RBEs. It is suggested that straws seen in DOT Ca II H near-limb images appearing bright against the very dark background and fast-waving might be identical to the fast-waving Type II spicules. Langangen et al. (2008c), suggested that Ca II 8542 Å RBEs might be the on-disk counterparts of type II spicules observed at the limb by the Hinode Ca II H broad filter. This suggestion was based on the similarity in evolution, lifetime, spatial extent and location. RBEs, however, show low blue-shifts of $15 - 20\,\mathrm{km\,s^{-1}}$, as opposed to the high apparent velocities reported for Type II spicules. In order to explain this discrepancy they used Monte Carlo simulations and showed that the low observed blue-shifts can be explained by a wide range of spicule orientations combined with a lack of opacity (Langangen et al., 2008c). Of course, type II spicules have very short lifetimes, small spatial dimensions and change very fast and thus they are on the limit of what can be resolved with present-day telescopes. Rouppe van der Voort et al. (2009) from spectral observations in the Hα and Ca II H 8542 Å lines reported also that the disk counterparts of Type II spicules might be the RBEs based on the similarities on their appearance, lifetimes, longitudinal and transverse velocities and occurrence rate. Recently, De Pontieu et al. (2011) used on-disk Hα observations of RBEs obtained with SOT/Hinode and reported that they found direct evidence of a strong correlation between the RBEs and short-lived brightenings in a wide range of transition region (TR) and coronal passbands observed with the Atmospheric Imaging Assembly (AIA) on-board the Solar Dynamics Observatory (SDO) space mission. They, also, found evidence that chromospheric spicules observed in Ca II H with SOT/Hinode at the limb in coronal holes are intimately linked to the formation of features at (TR) and coronal temperatures and concluded that on-disk RBEs and Ca II H limb spicules are connected.

It should also be mentioned that in a recent work, Judge et al. (2011) questioned whether spicules (and fibrils) are straw-like fine structures (as assumed by most authors) or whether they are best described as warps in a sheet. Readron (2012, private comm.) suggests that some features may appear within ≈2 sec, clearly questioning the plasma ejection flux-tube model as this implies Mach speeds well in excess of 100. Higher cadence data from present-day imaging spectrometers will allow us to access whether (or what fraction) of these features are jet/tube features or as suggested by Judge et al. (2011) as current sheets. Spicules produced by these current sheets could also be a natural explanation for the Ca II H Type II spicules which are very fast and seem to disappear rather than falling back to the lower atmosphere.

Furthermore, it is not known if spicule-like structures seen in UV and EUV are some aspects of traditional spicules or totally independent features. Several authors suggest that UV spicules may be the result of heating of chromospheric spicules to UV temperatures. This would provide an explanation for the reports that spicules often "fade from view" when being observed in chromospheric spectral lines (e.g.,

Beckers (1968). Another possibility is that UV spicules are a transition region "sheath" that surrounds the chromospheric spicules.

10 Summary

In this review we present observations and physical parameters of fine-scale structures observed in the solar chromosphere. The solar chromosphere is dominated by a variety of thin, jet-like features omnipresent in quiet, as well as in active regions, and on the disk, as well as at the limb. Because of their small size and the limitations of ground-based observations, for many decades it was difficult to characterize completely their properties, and much less to determine with confidence their interrelationship and the mechanism(s) responsible for their generation. In recent years because of the improved quality of observations acquired by ground and space-based instrumentation and, especially, with the current ability to observe the chromosphere with high resolution and high time cadence exciting jet-like features have been detected that were not recognized earlier. Their properties are not yet fully unraveled, while new names have been attributed to distinguish them from those previously observed. The nomenclature is nowadays rather confusing, but there are strong indications that, at least some if not all of the several observed fine-scale structures, are physically closely related, if not the same.

It seems also that all these small-scale structures are related to the fine-scale structure of the magnetic field and its evolution. Magnetic field lines are the most likely channels for transporting convective energy to the solar upper atmospheric layers. Detailed spatial and temporal high-resolution observations of the magnetic fields are crucial for understanding the small-scale structures and investigating their role in powering the Sun's outer atmosphere. Magnetic field extrapolations are also very important tools in reconstructing the 3-D topology of the upper solar layers. Different methods have been proposed so far based on different assumptions. Of particular interest is the reconstruction of the 3-D magnetic topology in inclined fine-scale structures, such as e.g. spicules. These structures, being magnetic flux tubes following the local inclination of the magnetic field lines, define the layer of the magnetic canopy, i.e. the layer where the plasma β (ratio of the gas to the magnetic pressure) is equal to 1. This layer is very important, since acoustic waves generated by the convective motions upon meeting this layer undergo mode conversion, refraction, reflection and transmission with important effects to the upper solar atmosphere.

The state-of-the-art in the understanding of small-scale events and their interrelationship requires simultaneous, co-spatial, multi-wavelength, high spatial and temporal resolution ground-based observations combined with observations from forefront observing space facilities of the same solar region. Such observations will permit their follow-up from the photospheric to the lower coronal level of the solar atmosphere. They will also permit a better correlation between manifestations of the same phenomenon in different atmospheric heights and, hence, are a powerful tool for understanding the physics that governs the generation and dynamics of fine-scale structures.

Apart from different types of studies based on analyses of observations, there is an on-going development and refinement of non-LTE and cloud model inversion codes of spectral line profiles based on better understood physics of spectral line

formation and radiation transfer. These codes together with advances in theory are an indispensable tool for a more accurate determination of several physical parameters that describe the observed fine structures. Quantitative determinations of such parameters is an essential ingredient not only for their modelling, but also for the modelling of the solar atmosphere as a whole. By their accurate determination it will also be possible to define the basic physics of, at least, some of the coronal heating processes and the origin and generation of the solar wind.

These developments go hand in hand with improvements in numerical simulations and improvement of observational technology. Numerical simulations, using 3D MHD codes together with forward modelling that produce precise synthetic data which are able to mimic accurately improved observations are important to correctly interpret them. It is hoped that, in the near future, the combination of state-of-the art multi-wavelength observations, along with improved NLTE codes, realistic MHD simulations and forward modelling, will provide a breakthrough in our understanding of the fine-scale chromospheric structures.

Acknowledgements The authors would like to thank the International Space Science Institute (ISSI) in Bern, Switzerland, for the hospitality provided to the members of the team on "Solar small-scale transient phenomena and their role in coronal heating", as well as the members of the team for fruitful discussions. We also acknowledge the remarks and suggestions made by the two referees which helped to improve the paper.

References

C.E. Alissandrakis, A Spectroscopic Study of Solar Spicules in Hα, Hβ and K. Solar Phys. **32**, 345–359 (1973)

C.E. Alissandrakis, C.J. Macris, A Study of the Fine Structure of the Solar Chromosphere at the Limb. Solar Phys. **20**, 47–56 (1971)

C.E. Alissandrakis, G. Tsiropoula, P. Mein, Physical parameters of solar H-alpha absorption features derived with the cloud model. Astron. Astrophys. **230**, 200–212 (1990)

C.E. Alissandrakis, T. Zachariadis, C. Gontikakis, Trace Observations of Solar Spicules Beyond the Limb in Ly-a and CIV, in *The Dynamic Sun: Challenges for Theory and Observations*. ESA Special Publication, vol. 600, 2005

T. Anan, R. Kitai, T. Kawate, T. Matsumoto, K. Ichimoto, K. Shibata, A. Hillier, K. Otsuji, H. Watanabe, S. Ueno, S. Nagata, T.T. Ishii, H. Komori, K. Nishida, T. Nakamura, H. Isobe, M. Hagino, Spicule Dynamics over a Plage Region. Pub. Astron. Soc. Japan **62**, 871 (2010)

A. Asensio Ramos, J. Trujillo Bueno, E. Landi Degl'Innocenti, Advanced Forward Modeling and Inversion of Stokes Profiles Resulting from the Joint Action of the Hanle and Zeeman Effects. Astrophys. J. **683**, 542–565 (2008)

R.G. Athay, The Number of Spicules in the Middle Chromosphere. Astrophys. J. **129**, 164 (1959)

R.G. Athay (ed.), The solar chromosphere and corona: Quiet sun, in *Astrophysics and Space Science Library*, Astrophysics and Space Science Library, vol. 53 1976

R.G. Athay, R.J. Bessey, Doppler Shifts and Line Broadening in Spicules. Astrophys. J. **140**, 1174 (1964)

L. Auer, Improved Boundary Conditions for the Feautrier Method. Astrophys. J. Lett. **150**, 53 (1967)

D. Banerjee, E. O'Shea, J.G. Doyle, M. Goossens, The nature of network oscillations. Astron. Astrophys. **371**, 1137–1149 (2001)
G.J. Banos, C.J. Macris, New Observational Results for the Solar Chromosphere. Solar Phys. **12**, 106–114 (1970)
J.M. Beckers, Study of the Undisturbed Chromosphere from Ha-disk Filtergrams, with Particular Reference to the Indentification of Spicules. Astrophys. J. **138**, 648 (1963)
J.M. Beckers, A study of the fine structures in the solar chromosphere, PhD thesis, University of Utrecht (AFCRL-Environmental Research Paper, No.49), (1964), 1964
J.M. Beckers, Solar Spicules (Invited Review Paper). Solar Phys. **3**, 367–433 (1968)
J.M. Beckers, Solar Spicules. An. Rev. Astron. Astroph. **10**, 73 (1972)
J.M. Beckers, E.H. Schröter, The Intensity, Velocity and Magnetic Structure of a Sunspot Region. I: Observational Technique; Properties of Magnetic Knots. Solar Phys. **4**, 142–164 (1968)
J.M. Beckers, R.W. Noyes, J.M. Pasachoff, New Observations of Solar Chromospheric Spicules. Astron. Journal **71**, 155–156 (1966)
N. Bel, B. Leroy, Analytical Study of Magnetoacoustic Gravity Waves. Astron. Astrophys. **55**, 239 (1977)
T.E. Berger, A.M. Title, On the Dynamics of Small-Scale Solar Magnetic Elements. Astrophys. J. **463**, 365 (1996)
T.E. Berger, A.M. Title, On the Relation of G-Band Bright Points to the Photospheric Magnetic Field. Astrophys. J. **553**, 449–469 (2001)
T.E. Berger, L.H.M. Rouppe van der Voort, M.G. Löfdahl, M. Carlsson, A. Fossum, V.H. Hansteen, E. Marthinussen, A. Title, G. Scharmer, Solar magnetic elements at 0.1 arcsec resolution. General appearance and magnetic structure. Astron. Astrophys. **428**, 613–628 (2004)
A. Bhatnagar, K. Tanaka, Intensity Oscillation in Hα-Fine Structure. Solar Phys. **24**, 87–97 (1972)
R. Bhavilai, The structure of the solar chromosphere, I: Identification of spicules on the disk. Month. Not. Roy. Astr. Soc. **130**, 411 (1965)
T.J. Bogdan, M. Carlsson, V.H. Hansteen, A. McMurry, C.S. Rosenthal, M. Johnson, S. Petty-Powell, E.J. Zita, R.F. Stein, S.W. McIntosh, Å. Nordlund, Waves in the Magnetized Solar Atmosphere. II. Waves from Localized Sources in Magnetic Flux Concentrations. Astrophys. J. **599**, 626–660 (2003)
R.M. Bonnet, M. Decaudin, E.C. Bruner Jr., L.W. Acton, W.A. Brown, High-resolution Lyman-alpha filtergrams of the sun. Astrophys. J. Lett. **237**, 47–50 (1980)
A. Botnen, M. Carlsson, Multi3D, 3D Non-LTE Radiative Transfer, in *Numerical Astrophysics*, ed. by S. M. Miyama, K. Tomisaka, & T. Hanawa. Astrophysics and Space Science Library, vol. 240, 1999, p. 379
E. Bratsolis, D. Dialetis, C.E. Alissandrakis, A new determination of the mean lifetime of bright and dark chromospheric mottles. Astron. Astrophys. **274**, 940 (1993)
D. Braun, C. Lindsey, A solar chromosphere and spicule model based on far-infrared limb observations. Astrophys. J. **320**, 898–903 (1987)
D.C. Braun, T.L. Duvall Jr., B.J. Labonte, S.M. Jefferies, J.W. Harvey, M.A. Pomerantz, Scattering of p-modes by a sunspot. Astrophys. J. Lett. **391**, 113–

116 (1992)
R.J. Bray, High-Resolution Photography of the Solar Chromosphere. X: Physical Parameters of Hα Mottles. Solar Phys. **29**, 317–325 (1973)
R.J. Bray, High-resolution photography of the solar chromosphere. XIII - Hα contrast profiles of sunspot fibrils. Solar Phys. **38**, 377–388 (1974)
R.J. Bray, R.E. Loughhead, *The solar chromosphere* 1974
R.J. Bray, R.E. Loughhead, High-resolution photography of the solar chromosphere. XVI Hα contrast profiles of active region loops. Solar Phys. **85**, 131–140 (1983)
T.M. Brown, T.J. Bogdan, B.W. Lites, J.H. Thomas, Localized sources of propagating acoustic waves in the solar photosphere. Astrophys. J. Lett. **394**, 65–68 (1992)
P.S. Cally, What to look for in the seismology of solar active regions. Astronomische Nachrichten **328**, 286 (2007). doi:10.1002/asna.200610731
C.J. Cannon, Frequency-Quadrature Perturbations in Radiative-Transfer Theory. Astrophys. J. **185**, 621–630 (1973)
M. Carlsson, A computer program for solving multi-level non-LTE radiative transferproblems in moving or static atmospheres. Uppsala Astronomical Observatory Reports **33** (1986)
G. Cauzzi, A. Falchi, R. Falciani, Network and internetwork: a compared multi-wavelength analysis. Astron. Astrophys. **357**, 1093–1104 (2000)
G. Cauzzi, K.P. Reardon, H. Uitenbroek, F. Cavallini, A. Falchi, R. Falciani, K. Janssen, T. Rimmele, A. Vecchio, F. Wöger, The solar chromosphere at high resolution with IBIS. I. New insights from the Ca II 854.2 nm line. Astron. Astrophys. **480**, 515–526 (2008)
G. Cauzzi, K. Reardon, R.J. Rutten, A. Tritschler, H. Uitenbroek, The solar chromosphere at high resolution with IBIS. IV. Dual-line evidence of heating in chromospheric network. Astron. Astrophys. **503**, 577–587 (2009)
R. Centeno, J. Trujillo Bueno, A. Asensio Ramos, On the Magnetic Field of Off-limb Spicules. Astrophys. J. **708**, 1579–1584 (2010)
R. Centeno, H. Socas-Navarro, B. Lites, M. Kubo, Z. Frank, R. Shine, T. Tarbell, A. Title, K. Ichimoto, S. Tsuneta, Y. Katsukawa, Y. Suematsu, T. Shimizu, S. Nagata, Emergence of Small-Scale Magnetic Loops in the Quiet-Sun Internetwork. Astrophys. J. Lett. **666**, 137–140 (2007). doi:10.1086/521726
E.B. Christopoulou, A.A. Georgakilas, S. Koutchmy, Fine Structure of the Magnetic Chromosphere: Near-Limb Imaging, Data Processing and Analysis of Spicules and Mottles. Solar Phys. **199**, 61–80 (2001)
L. Contarino, F. Zuccarello, P. Romano, D. Spadaro, I. Ermolli, Morphological and dynamical properties of small-scale chromospheric features deduced from IBIS observations. Astron. Astrophys. **507**, 1625–1633 (2009)
J.W. Cook, G.E. Brueckner, J. Bartoe, D.G. Socker, HRTS observations of spicular emission at transition region temperatures above the solar limb. Advances in Space Research **4**, 59–62 (1984)
L. Damé, P. Gouttebroze, J.M. Malherbe, Observation and analysis of intensity oscillations in the solar K-line. Astron. Astrophys. **130**, 331–340 (1984)
H.C. Dara, S. Koutchmy, Y. Suematsu, Properties of Hα spicules from disk and limb high-resolution observations, in *Solar Jets and Coronal Plumes*, ed. by T.-D. Guyenne. ESA Special Publication, vol. 421, 1998, p. 255
B. De Pontieu, R. Erdélyi, The nature of moss and lower atmospheric seismol-

ogy. Royal Society of London Philosophical Transactions Series A **364**, 383–394 (2006)
B. De Pontieu, R. Erdélyi, A.G. de Wijn, Intensity Oscillations in the Upper Transition Region above Active Region Plage. Astrophys. J. Lett. **595**, 63–66 (2003)
B. De Pontieu, R. Erdélyi, S.P. James, Solar chromospheric spicules from the leakage of photospheric oscillations and flows. Nature **430**, 536–539 (2004)
B. De Pontieu, V.H. Hansteen, L. Rouppe van der Voort, M. van Noort, M. Carlsson, High-Resolution Observations and Modeling of Dynamic Fibrils. Astrophys. J. **655**, 624–641 (2007a)
B. De Pontieu, S. McIntosh, V.H. Hansteen, M. Carlsson, C.J. Schrijver, T.D. Tarbell, A.M. Title, R.A. Shine, Y. Suematsu, S. Tsuneta, Y. Katsukawa, K. Ichimoto, T. Shimizu, S. Nagata, A Tale of Two Spicules: The Impact of Spicules on the Magnetic Chromosphere. Pub. Astron. Soc. Japan **59**, 655 (2007b)
B. De Pontieu, S.W. McIntosh, M. Carlsson, V.H. Hansteen, T.D. Tarbell, C.J. Schrijver, A.M. Title, R.A. Shine, S. Tsuneta, Y. Katsukawa, K. Ichimoto, Y. Suematsu, T. Shimizu, S. Nagata, Chromospheric Alfvénic Waves Strong Enough to Power the Solar Wind. Science **318**, 1574 (2007c)
B. De Pontieu, S.W. McIntosh, M. Carlsson, V.H. Hansteen, T.D. Tarbell, P. Boerner, J. Martinez-Sykora, C.J. Schrijver, A.M. Title, The Origins of Hot Plasma in the Solar Corona. Science **331**, 55 (2011)
B. De Pontieu, M. Carlsson, L.H.M. Rouppe van der Voort, R.J. Rutten, V.H. Hansteen, H. Watanabe, Ubiquitous Torsional Motions in Type II Spicules. Astrophys. J. Lett. **752**, 12 (2012)
A.G. de Wijn, J.O. Stenflo, S.K. Solanki, S. Tsuneta, Small-Scale Solar Magnetic Fields. Space Sci. Rev. **144**, 275–315 (2009). doi:10.1007/s11214-008-9473-6
F.L. Deubner, B. Fleck, Dynamics of the solar atmosphere. III - Cell-network distinctions of chromospheric oscillations. Astron. Astrophys. **228**, 506–512 (1990)
J.G. Doyle, C.J. Butler, Ultraviolet radiation from stellar flares and the coronal X-ray emission for dwarf-Me stars. Nature **313**, 378–380 (1985)
R.B. Dunn, J.B. Zirker, The Solar Filigree. Solar Phys. **33**, 281–304 (1973)
R.B. Dunn, J.T. Jefferies, F.Q. Orrall, The line and continuous emission observed in two limb flares. The Observatory **80**, 31–33 (1960)
R.B. Dunn, J.B. Zirker, J.M. Beckers, Properties of the Solar Filigree Structure, in *Chromospheric Fine Structure*, ed. by R. G. Athay. IAU Symposium, vol. 56, 1974, p. 45
P. Fabiani Bendicho, J. Trujillo Bueno, Three-dimensional radiative transfer with multilevel atoms, in *Polarization*, ed. by K. N. Nagendra & J. O. Stenflo. Astrophysics and Space Science Library, vol. 243, 1999, pp. 219–230
P. Fabiani Bendicho, J. Trujillo Bueno, L. Auer, Multidimensional radiative transfer with multilevel atoms. II. The non-linear multigrid method. Astron. Astrophys. **324**, 161–176 (1997)
P. Feautrier, A Procedure for computing the Mean Intensity and the Flux. SAO Special Report **167**, 80 (1964)
P. Foukal, Hα Fine Structure and the Chromospheric Field. Solar Phys. **20**, 298–309 (1971)
P. Foukal, Morphological Relationships in the Chromospheric Hα Fine Structure. Solar Phys. **19**, 59–71 (1971)
A.H. Gabriel, A magnetic model of the solar transition region. Royal Society of

London Philosophical Transactions Series A **281**, 339–352 (1976)
A.A. Georgakilas, S. Koutchmy, C.E. Alissandrakis, Polar surges and macrospicules: simultaneous Hα and He II 304 Angstroms observations. Astron. Astrophys. **341**, 610–616 (1999)
R.G. Giovanelli, Excitation of hydrogen and CaII under chromospheric conditions. Australian Journal of Physics **20**, 81 (1967a)
R.G. Giovanelli, Structure of the Normal Chromosphere, in *Solar Physics*, ed. by J. N. Xanthakis, 1967b, p. 353
P. Gouttebroze, P. Heinzel, J.C. Vial, The hydrogen spectrum of model prominences. Astron. Astrophys. Suppl. Ser. **99**, 513–543 (1993)
U. Grossmann-Doerth, W. Schmidt, Chromospheric fine structure revisited. Astron. Astrophys. **264**, 236–242 (1992)
U. Grossmann-Doerth, M. von Uexküll, Spectral Investigation of Chromospheric Fine Structure. Solar Phys. **20**, 31–46 (1971)
U. Grossmann-Doerth, M. von Uexküll, Spectral Investigation of the Chromosphere. II. The Nature of the Mottles and a Model of the Overall Structure. Solar Phys. **28**, 319–332 (1973)
U. Grossmann-Doerth, M. von Uexküll, Spectral investigation of the chromosphere. VI - Observations of H-alpha close to the limb. Solar Phys. **55**, 321–333 (1977)
H.J. Hagenaar, Ephemeral Regions on a Sequence of Full-Disk Michelson Doppler Imager Magnetograms. Astrophys. J. **555**, 448 (2001)
H.J. Hagenaar, M.L. DeRosa, C.J. Schrijver, The Dependence of Ephemeral Region Emergence on Local Flux Imbalance. Astrophys. J. **678**, 541 (2008)
H.J. Hagenaar, C.J. Schrijver, A.M. Title, The Distribution of Cell Sizes of the Solar Chromospheric Network. Astrophys. J. **481**, 988 (1997)
V.H. Hansteen, R. Betta, M. Carlsson, Rapid intensity and velocity variations in solar transition region lines. Astron. Astrophys. **360**, 742–760 (2000)
V.H. Hansteen, B. De Pontieu, L. Rouppe van der Voort, M. van Noort, M. Carlsson, Dynamic Fibrils Are Driven by Magnetoacoustic Shocks. Astrophys. J. Lett. **647**, 73–76 (2006)
S.S. Hasan, W. Kalkofen, Excitation of Oscillations in Photospheric Flux Tubes through Buffeting by External Granules. Astrophys. J. **519**, 899–910 (1999)
L. Heggland, B. De Pontieu, V.H. Hansteen, Numerical Simulations of Shock Wave-driven Chromospheric Jets. Astrophys. J. **666**, 1277–1283 (2007)
L. Heggland, B. De Pontieu, V.H. Hansteen, Observational Signatures of Simulated Reconnection Events in the Solar Chromosphere and Transition Region. Astrophys. J. **702**, 1–18 (2009)
P. Heinzel, Multilevel NLTE radiative transfer in isolated atmospheric structures: implementation of the MALI-technique. Astron. Astrophys. **299**, 563 (1995)
P. Heinzel, B. Schmieder, Chromospheric fine structure: Black and white mottles. Astron. Astrophys. **282**, 939–954 (1994)
D. Heristchi, Z. Mouradian, On the inclination and the axial velocity of spicules. Solar Phys. **142**, 21–34 (1992)
B.W. Hindman, T.M. Brown, Acoustic Power Maps of Solar Active Regions. Astrophys. J. **504**, 1029 (1998)
R. Jain, D. Haber, Solar p-modes and surface magnetic fields: Is there an acoustic emission?. MDI/SOHO observations. Astron. Astrophys. **387**, 1092–1099 (2002)
S.M. Jefferies, S.W. McIntosh, J.D. Armstrong, T.J. Bogdan, A. Cacciani, B.

Fleck, Magnetoacoustic Portals and the Basal Heating of the Solar Chromosphere. Astrophys. J. Lett. **648**, 151–155 (2006)
D.B. Jess, M. Mathioudakis, R. Erdélyi, P.J. Crockett, F.P. Keenan, D.J. Christian, Alfvén Waves in the Lower Solar Atmosphere. Science **323**, 1582 (2009)
P.G. Judge, M. Carlsson, On the Solar Chromosphere Observed at the LIMB with Hinode. Astrophys. J. **719**, 469–473 (2010)
P.G. Judge, T.D. Tarbell, K. Wilhelm, A Study of Chromospheric Oscillations Using the SOHO and TRACE Spacecraft. Astrophys. J. **554**, 424–444 (2001)
P.G. Judge, A. Tritschler, B. Chye Low, Thermal Fine Structure and Magnetic Fields in the Solar Atmosphere: Spicules and Fibrils. Astrophys. J. Lett. **730**, 4 (2011)
E. Khomenko, M. Collados, T. Felipe, Nonlinear Numerical Simulations of Magneto-Acoustic Wave Propagation in Small-Scale Flux Tubes. Solar Phys. **251**, 589–611 (2008b)
E. Khomenko, R. Centeno, M. Collados, J. Trujillo Bueno, Channeling 5 Minute Photospheric Oscillations into the Solar Outer Atmosphere through Small-Scale Vertical Magnetic Flux Tubes. Astrophys. J. Lett. **676**, 85–88 (2008a)
Y. Kim, S. Bong, Y. Park, K. Cho, Y. Moon, Y. Suematsu, Estimation of Spicule Magnetic Field Using Observed MHD Waves by the Hinode SOT. Journal of Korean Astronomical Society **41**, 173–180 (2008)
I. Kontogiannis, G. Tsiropoula, K. Tziotziou, Power halo and magnetic shadow in a solar quiet region observed in the Hα line. Astron. Astrophys. **510**, 41 (2010a). doi:10.1051/0004-6361/200912841
I. Kontogiannis, G. Tsiropoula, K. Tziotziou, Hinode SOT/SP and SoHO/MDI quiet Sun magnetic field. Implications of their differences on the extrapolated chromospheric field and the height of the magnetic canopy. Astron. Astrophys. **531**, 66 (2011)
I. Kontogiannis, G. Tsiropoula, K. Tziotziou, M.K. Georgoulis, Oscillations in a network region observed in the Hα line and their relation to the magnetic field. Astron. Astrophys. **524**, 12 (2010b). doi:10.1051/0004-6361/201015066
R.A. Kopp, M. Kuperus, Magnetic Fields and the Temperature Structure of the Chromosphere-Corona Interface. Solar Phys. **4**, 212–223 (1968)
K.R. Krall, R.J. Bessey, J.M. Beckers, A time evolution study of limb spicule spectra. Solar Phys. **46**, 93–114 (1976)
V.A. Krat, T.V. Krat, On Physical Properties of Solar Spicules. Solar Phys. **17**, 355–368 (1971)
J.M. Krijger, R.J. Rutten, B.W. Lites, T. Straus, R.A. Shine, T.D. Tarbell, Dynamics of the solar chromosphere. III. Ultraviolet brightness oscillations from TRACE. Astron. Astrophys. **379**, 1052–1082 (2001)
V. Kukhianidze, T.V. Zaqarashvili, E. Khutsishvili, Observation of kink waves in solar spicules. Astron. Astrophys. **449**, 35–38 (2006)
V.I. Kulidzanishvili, Dynamics of H alpha spicules according to spectral observations at various heights of the solar chromosphere. Solar Phys. **66**, 251–258 (1980)
D. Kuridze, T.V. Zaqarashvili, B.M. Shergelashvili, S. Poedts, Acoustic oscillations in the field-free, gravitationally stratified cavities under solar bipolar magnetic canopies. Astron. Astrophys. **505**, 763–770 (2009). doi:10.1051/0004-6361/200811484
Ø. Langangen, L. Rouppe van der Voort, Y. Lin, Measurements of Plasma Motions

in Dynamic Fibrils. Astrophys. J. **673**, 1201–1208 (2008b)
Ø. Langangen, M. Carlsson, L. Rouppe van der Voort, V. Hansteen, B. De Pontieu, Spectroscopic Measurements of Dynamic Fibrils in the Ca II λ8662 Line. Astrophys. J. **673**, 1194–1200 (2008a)
Ø. Langangen, B. De Pontieu, M. Carlsson, V.H. Hansteen, G. Cauzzi, K. Reardon, Search for High Velocities in the Disk Counterpart of Type II Spicules. Astrophys. J. Lett. **679**, 167–170 (2008c)
J. Leenaarts, M. Carlsson, MULTI3D: A Domain-Decomposed 3D Radiative Transfer Code, in *The Second Hinode Science Meeting: Beyond Discovery-Toward Understanding*, ed. by B. Lites, M. Cheung, T. Magara, J. Mariska, & K. Reeves. Astronomical Society of the Pacific Conference Series, vol. 415, 2009, p. 87
J. Leenaarts, M. Carlsson, L. Rouppe van der Voort, The Formation of the Hα Line in the Solar Chromosphere. Astrophys. J. **749**, 136 (2012)
J. Leenaarts, R.J. Rutten, P. Sütterlin, M. Carlsson, H. Uitenbroek, DOT tomography of the solar atmosphere. VI. Magnetic elements as bright points in the blue wing of Hα. Astron. Astrophys. **449**, 1209–1218 (2006)
J. Leenaarts, M. Carlsson, V. Hansteen, L. Rouppe van der Voort, Three-Dimensional Non-LTE Radiative Transfer Computation of the Ca 8542 Infrared Line From a Radiation-MHD Simulation. Astrophys. J. Lett. **694**, 128–131 (2009)
S.L. Lippincott, Chromospheric Spicules. Smithsonian Contributions to Astrophysics **2**, 15 (1957)
B.W. Lites, R.J. Rutten, T.E. Berger, Dynamics of the Solar Chromosphere. II. Ca II H_2V and K_2V Grains versus Internetwork Fields. Astrophys. J. **517**, 1013–1033 (1999)
B.W. Lites, R.J. Rutten, W. Kalkofen, Dynamics of the solar chromosphere. I - Long-period network oscillations. Astrophys. J. **414**, 345–356 (1993)
B.W. Lites, M. Kubo, H. Socas-Navarro, T. Berger, Z. Frank, R. Shine, T. Tarbell, A. Title, K. Ichimoto, Y. Katsukawa, S. Tsuneta, Y. Suematsu, T. Shimizu, S. Nagata, The Horizontal Magnetic Flux of the Quiet-Sun Internetwork as Observed with the Hinode Spectro-Polarimeter. Astrophys. J. **672**, 1237–1253 (2008)
S.H.B. Livi, J. Wang, S.F. Martin, The cancellation of magnetic flux. I - On the quiet sun. Australian Journal of Physics **38**, 855 (1985)
M.G. Loefdahl, T.E. Berger, R.S. Shine, A.M. Title, Preparation of a Dual Wavelength Sequence of High-Resolution Solar Photospheric Images Using Phase Diversity. Astrophys. J. **495**, 965 (1998)
A. López Ariste, R. Casini, Magnetic Fields Measured in Spicules., in *Chromospheric and Coronal Magnetic Fields*, ed. by D. E. Innes, A. Lagg, & S. A. Solanki. ESA Special Publication, vol. 596, 2005
R.E. Loughhead, High-Resolution Photography of the Solar Chromosphere. XI: Hα Constrast Profiles of Mottles near the Limb. Solar Phys. **29**, 327–332 (1973)
D.K. Lynch, J.M. Beckers, R.B. Dunn, A Morphological Study of Solar Spicules. Solar Phys. **30**, 63–70 (1973)
M.S. Madjarska, K. Vanninathan, J.G. Doyle, Can coronal hole spicules reach coronal temperatures? Astron. Astrophys. **532**, 1 (2011)
S.F. Martin, The identification and interaction of network, intranetwork, and ephemeral-region magnetic fields. Solar Phys. **117**, 243 (1988)
S.F. Martin, Small-Scale Magnetic Features Observed in the Photosphere **138**, 129

(1990)
S.F. Martin, S.H.B. Livi, J. Wang, The cancellation of magnetic flux. II - In a decaying active region. Australian Journal of Physics **38**, 929 (1985)
J. Martínez-Sykora, V. Hansteen, B. De Pontieu, M. Carlsson, Spicule-Like Structures Observed in Three-Dimensional Realistic Magnetohydrodynamic Simulations. Astrophys. J. **701**, 1569–1581 (2009)
K. Matsuno, T. Hirayama, The height distribution of the kinetic temperature and turbulent velocity of solar H-alpha spicules. Solar Phys. **117**, 21–36 (1988)
S.W. McIntosh, B. Fleck, P.G. Judge, Investigating the role of plasma topography on chromospheric oscillations observed by TRACE. Astron. Astrophys. **405**, 769–777 (2003)
J.P. Mehltretter, Observations of photospheric faculae at the center of the solar disk. Solar Phys. **38**, 43–57 (1974)
P. Mein, The MSDP of THEMIS: Capabilities, first results and prospects. Astron. Astrophys. **381**, 271–278 (2002)
A.G. Michalitsanos, The Five Minute Period Oscillation in Magnetically Active Regions. Solar Phys. **30**, 47–61 (1973)
D. Mihalas, L.H. Auer, B.R. Mihalas, Two-dimensional radiative transfer. I - Planar geometry. Astrophys. J. **220**, 1001–1023 (1978)
R.L. Moore, A.C. Sterling, J.W. Cirtain, D.A. Falconer, Solar X-ray Jets, Type-II Spicules, Granule-size Emerging Bipoles, and the Genesis of the Heliosphere. Astrophys. J. Lett. **731**, 18 (2011)
Z. Mouradian, Contribution à l'étude du bord solaire et de la structure chromosphérique. Annales d'Astrophysique **28**, 805 (1965)
K. Muglach, Dynamics of solar active regions. I. Photospheric and chromospheric oscillations observed with TRACE. Astron. Astrophys. **401**, 685–697 (2003)
K. Muglach, A. Hofmann, J. Staude, Dynamics of solar active regions. II. Oscillations observed with MDI and their relation to the magnetic field topology. Astron. Astrophys. **437**, 1055–1060 (2005)
R. Muller, The fine structure of the quiet sun. Solar Phys. **100**, 237–255 (1985)
R. Muller, The Quiet Solar Photosphere: Dynamics and Magnetism, in *Lecture Notes in Physics, Berlin Springer Verlag*, ed. by J.P. Rozelot, C. Neiner. Lecture Notes in Physics, Berlin Springer Verlag, vol. 832, 2011, p. 87
R. Muller, T. Roudier, Variability of the quiet photospheric network. Solar Phys. **94**, 33–47 (1984)
K. Murawski, T.V. Zaqarashvili, Numerical simulations of spicule formation in the solar atmosphere. Astron. Astrophys. **519**, 8 (2010)
V.M. Nakariakov, L. Ofman, Determination of the coronal magnetic field by coronal loop oscillations. Astron. Astrophys. **372**, 53–56 (2001)
G.M. Nikolsky, The Observation of the Chromospheric Fine Structure by the 53-cm Lyot Coronagraph. Solar Phys. **12**, 379–390 (1970)
G.M. Nikolsky, A.G. Platova, Motions of Hα-spicules along the solar limb. Solar Phys. **18**, 403–409 (1971)
T. Nishikawa, Spicule observations with high spatial resolution. Pub. Astron. Soc. Japan **40**, 613–625 (1988)
C. Nutto, O. Steiner, W. Schaffenberger, M. Roth, Modification of wave propagation and wave travel-time by the presence of magnetic fields in the solar network atmosphere. Astron. Astrophys. **538**, 79 (2012)
G.L. Olson, P.B. Kunasz, Short characteristic solution of the non-LTE transfer

problem by operator perturbation. I. The one-dimensional planar slab. Journal Quant. Spectr. Rad. Trans. **38**, 325–336 (1987)
G.L. Olson, L.H. Auer, J.R. Buchler, A rapidly convergent iterative solution of the non-LTE line radiation transfer problem. Journal Quant. Spectr. Rad. Trans. **35**, 431–442 (1986)
E.N. Parker, Nanoflares and the solar X-ray corona. Astrophys. J. **330**, 474–479 (1988)
C.E. Parnell, A model of the Solar Magnetic Carpet. Solar Phys. **200**, 23 (2001)
J.M. Pasachoff, W.A. Jacobson, A.C. Sterling, Limb Spicules from the Ground and from Space. Solar Phys. **260**, 59–82 (2009)
J.M. Pasachoff, R.W. Noyes, J.M. Beckers, Spectral Observations of Spicules at Two Heights in the Solar Chromosphere. Solar Phys. **5**, 131–158 (1968)
A. Pietarila, J. Hirzberger, V. Zakharov, S.K. Solanki, Bright fibrils in Ca II K. Astron. Astrophys. **502**, 647–660 (2009)
S.B. Pikel'ner, A Mechanism for the Formation of Chromospheric Spicules. Astronomicheskij Zhurnal **46**, 328 (1969)
K.P. Reardon, H. Uitenbroek, G. Cauzzi, The solar chromosphere at high resolution with IBIS. III. Comparison of Ca II K and Ca II 854.2 nm imaging. Astron. Astrophys. **500**, 1239–1247 (2009)
B. Roberts, Spicules - The resonant response to granular buffeting. Solar Phys. **61**, 23–34 (1979)
W.O. Roberts, A Preliminary Report on Chromospheric Spicules of Extremely Short Lifetime. Astrophys. J. **101**, 136 (1945)
C.S. Rosenthal, T.J. Bogdan, M. Carlsson, S.B.F. Dorch, V. Hansteen, S.W. McIntosh, A. McMurry, Å. Nordlund, R.F. Stein, Waves in the Magnetized Solar Atmosphere. I. Basic Processes and Internetwork Oscillations. Astrophys. J. **564**, 508–524 (2002)
L.H.M. Rouppe van der Voort, V.H. Hansteen, M. Carlsson, A. Fossum, E. Marthinussen, M.J. van Noort, T.E. Berger, Solar magnetic elements at 0.1 arcsec resolution. II. Dynamical evolution. Astron. Astrophys. **435**, 327–337 (2005)
L.H.M. Rouppe van der Voort, B. De Pontieu, V.H. Hansteen, M. Carlsson, M. van Noort, Magnetoacoustic Shocks as a Driver of Quiet-Sun Mottles. Astrophys. J. Lett. **660**, 169–172 (2007)
L. Rouppe van der Voort, J. Leenaarts, B. de Pontieu, M. Carlsson, G. Vissers, On-disk Counterparts of Type II Spicules in the Ca II 854.2 nm and Hα Lines. Astrophys. J. **705**, 272–284 (2009)
J.H. Rush, W.O. Roberts, Recent Studies of Chromospheric Spicules. Australian Journal of Physics **7**, 230 (1954)
R.J. Rutten, (Inter-),Network Structure and DynamicS, in *Third Advances in Solar Physics Euroconference: Magnetic Fields and Oscillations*, ed. by B. Schmieder, A. Hofmann, & J. Staude. Astronomical Society of the Pacific Conference Series, vol. 184, 1999, pp. 181–200
R.J. Rutten, On the Nature of the Solar Chromosphere, in *Solar MHD Theory and Observations: A High Spatial Resolution Perspective*, ed. by J. Leibacher, R. F. Stein, & H. Uitenbroek. Astronomical Society of the Pacific Conference Series, vol. 354, 2006, p. 276
R.J. Rutten, Observing the Solar Chromosphere, in *The Physics of Chromospheric Plasmas*, ed. by P. Heinzel, I. Dorotovič, & R. J. Rutten. Astronomical Society of the Pacific Conference Series, vol. 368, 2007, p. 27

R.J. Rutten, The quiet chromosphere. Old wisdom, new insights, future needs. Memorie della Societa Astronomica Italiana **81**, 565–576 (2010)
G.B. Rybicki, D.G. Hummer, An accelerated lambda iteration method for multilevel radiative transfer. I - Non-overlapping lines with background continuum. Astron. Astrophys. **245**, 171–181 (1991)
G.B. Rybicki, D.G. Hummer, An accelerated lambda iteration method for multilevel radiative transfer. II - Overlapping transitions with full continuum. Astron. Astrophys. **262**, 209–215 (1992)
C. Sawyer, Hα Mottles. Solar Phys. **24**, 79–86 (1972)
G.B. Scharmer, M. Carlsson, A new approach to multi-level non-LTE radiative transfer problems. Journal of Computational Physics **59**, 56–80 (1985)
C.J. Schrijver, A.M. Title, A.A. van Ballegooijen, H.J. Hagenaar, R.A. Shine, Sustaining the Quiet Photospheric Network: The Balance of Flux Emergence, Fragmentation, Merging, and Cancellation. Astrophys. J. **487**, 424 (1997)
H. Schunker, P.S. Cally, Magnetic field inclination and atmospheric oscillations above solar active regions. Month. Not. Roy. Astr. Soc. **372**, 551–564 (2006)
A. Secchi, *L'astronomia in Roma nel pontificato DI Pio IX*. 1877
D.H. Sekse, L. Rouppe van der Voort, B. De Pontieu, Statistical Properties of the Disk Counterparts of Type II Spicules from Simultaneous Observations of Rapid Blueshifted Excursions in Ca II 8542 and Hα. Astrophys. J. **752**, 108 (2012)
K. Shibata, Y. Suematsu, Why are spicules absent over plages and long under coronal holes. Solar Phys. **78**, 333–345 (1982b)
K. Shibata, T. Nishikawa, R. Kitai, Y. Suematsu, Numerical hydrodynamics of the jet phenomena in the solar atmosphere. II - Surges. Solar Phys. **77**, 121–151 (1982a)
G.W. Simon, R.B. Leighton, Velocity Fields in the Solar Atmosphere. III. Large-Scale Motions, the Chromospheric Network, and Magnetic Fields. Astrophys. J. **140**, 1120 (1964)
K.A.P. Singh, B.N. Dwivedi, Estimation of spicule magnetic field using observed kink waves. New Astron. **12**, 479–482 (2007)
H. Socas-Navarro, D. Elmore, Physical Properties of Spicules from Simultaneous Spectropolarimetric Observations of He I and Ca II Lines. Astrophys. J. Lett. **619**, 195–198 (2005)
S.K. Solanki, O. Steiner, How magnetic is the solar chromosphere? Astron. Astrophys. **234**, 519–529 (1990)
J.O. Stenflo, J.W. Harvey, Dependence of the properties of magnetic fluxtubes on area factor or amount of flux. Solar Phys. **95**, 99–118 (1985)
A.C. Sterling, Solar Spicules: A Review of Recent Models and Targets for Future Observations - (Invited Review). Solar Phys. **196**, 79–111 (2000)
A.C. Sterling, R.L. Moore, C.E. DeForest, Hinode Solar Optical Telescope Observations of the Source Regions and Evolution of "Type II" Spicules at the Solar Polar Limb. Astrophys. J. Lett. **714**, 1–6 (2010)
Y. Suematsu, Influence of Photospheric 5-Minute Oscillations on the Formation of Chromospheric Fine Structures, in *Progress of Seismology of the Sun and Stars*, ed. by Y. Osaki & H. Shibahashi. Lecture Notes in Physics, Berlin Springer Verlag, vol. 367, 1990, p. 211
Y. Suematsu, Solar Spicules: A brief review of recent high-resolution observations, in *Solar Jets and Coronal Plumes*, ed. by T.-D. Guyenne. ESA Special Publication, vol. 421, 1998, p. 19

Y. Suematsu, H. Wang, H. Zirin, High-Resolution Observation of Disk Spicules. I. Evolution and Kinematics of Spicules in the Enhanced Network. Astrophys. J. **450**, 411 (1995)

Y. Suematsu, K. Ichimoto, Y. Katsukawa, T. Shimizu, T. Okamoto, S. Tsuneta, T. Tarbell, R.A. Shine, High Resolution Observations of Spicules with Hinode/SOT, in *First Results From Hinode*, ed. by S. A. Matthews, J. M. Davis, & L. K. Harra. Astronomical Society of the Pacific Conference Series, vol. 397, 2008, p. 27

P. Sütterlin, R.H. Hammerschlag, F.C.M. Bettonvil, R.J. Rutten, V.I. Skomorovsky, G.N. Domyshev, A Multi-Channel Speckle Imaging System for the DOT, in *Advanced Solar Polarimetry – Theory, Observation, and Instrumentation*, ed. by M. Sigwarth. Astronomical Society of the Pacific Conference Series, vol. 236, 2001, p. 431

K. Tanaka, Evolution of Chromospheric Fine Structures on the Disk, in *Chromospheric Fine Structure*, ed. by R. G. Athay. IAU Symposium, vol. 56, 1974, p. 239

E. Tavabi, S. Koutchmy, A. Ajabshirizadeh, A statistical analysis of the SOT-Hinode observations of solar spicules and their wave-like behavior. New Astron. **16**, 296–305 (2011)

J.H. Thomas, D.C.H. Stanchfield II, Fine-Scale Magnetic Effects on P-Modes and Higher Frequency Acoustic Waves in a Solar Active Region. Astrophys. J. **537**, 1086–1093 (2000)

A.M. Title, C.J. Schrijver, The Sun's Magnetic Carpet, in *Cool Stars, Stellar Systems, and the Sun*, ed. by R. A. Donahue & J. A. Bookbinder. Astronomical Society of the Pacific Conference Series, vol. 154, 1998, p. 345

A.M. Title, K.P. Topka, T.D. Tarbell, W. Schmidt, C. Balke, G. Scharmer, On the differences between plage and quiet sun in the solar photosphere. Astrophys. J. **393**, 782–794 (1992)

K.P. Topka, T.D. Tarbell, A.M. Title, Properties of the Smallest Solar Magnetic Elements. II. Observations versus Hot Wall Models of Faculae. Astrophys. J. **484**, 479 (1997)

J. Trujillo Bueno, Spectropolarimetric investigations of the magnetization of the quiet Sun chromosphere. ArXiv e-prints (2010)

J. Trujillo Bueno, L. Merenda, R. Centeno, M. Collados, E. Landi Degl'Innocenti, The Hanle and Zeeman Effects in Solar Spicules: A Novel Diagnostic Window on Chromospheric Magnetism. Astrophys. J. Lett. **619**, 191–194 (2005)

G. Tsiropoula, Physical parameters and flows along chromospheric penumbral fibrils. Astron. Astrophys. **357**, 735–742 (2000)

G. Tsiropoula, B. Schmieder, Determination of physical parameters in dark mottles. Astron. Astrophys. **324**, 1183–1189 (1997)

G. Tsiropoula, K. Tziotziou, The role of chromospheric mottles in the mass balance and heating of the solar atmosphere. Astron. Astrophys. **424**, 279–288 (2004)

G. Tsiropoula, C.E. Alissandrakis, B. Schmieder, The fine structure of a chromospheric rosette. Astron. Astrophys. **271**, 574 (1993)

G. Tsiropoula, C.E. Alissandrakis, B. Schmieder, Time evolution of fine structures in the solar chromosphere. Astron. Astrophys. **290**, 285–294 (1994)

G. Tsiropoula, K. Tziotziou, P. Schwartz, P. Heinzel, Multiwavelength analysis of a solar quiet region. Astron. Astrophys. **493**, 217–225 (2009)

K. Tziotziou, Chromospheric Cloud-Model Inversion Techniques, in *The Physics*

of Chromospheric Plasmas, ed. by P. Heinzel, I. Dorotovič, & R. J. Rutten. Astronomical Society of the Pacific Conference Series, vol. 368, 2007, p. 217

K. Tziotziou, G. Tsiropoula, P. Mein, On the nature of the chromospheric fine structure. I. Dynamics of dark mottles and grains. Astron. Astrophys. **402**, 361–372 (2003)

K. Tziotziou, G. Tsiropoula, P. Mein, On the nature of the chromospheric fine structure. II. Intensity and velocity oscillations of dark mottles and grains. Astron. Astrophys. **423**, 1133–1146 (2004)

K. Tziotziou, G. Tsiropoula, P. Sütterlin, DOT tomography of the solar atmosphere. V. Analysis of a surge from AR10486. Astron. Astrophys. **444**, 265–274 (2005)

H. Uitenbroek, Multilevel Radiative Transfer with Partial Frequency Redistribution. Astrophys. J. **557**, 389–398 (2001)

H.C. van de Hulst, The Chromosphere and the Corona, ed. by Kuiper, G. P. 1953, p. 207

M. van Noort, L. Rouppe van der Voort, M.G. Löfdahl, Solar Image Restoration By Use Of Multi-frame Blind De-convolution With Multiple Objects And Phase Diversity. Solar Phys. **228**, 191–215 (2005)

A. Vecchio, G. Cauzzi, K.P. Reardon, K. Janssen, T. Rimmele, Solar atmospheric oscillations and the chromospheric magnetic topology. Astron. Astrophys. **461**, 1–4 (2007)

G. Verth, M. Goossens, J.S. He, Magnetoseismological Determination of Magnetic Field and Plasma Density Height Variation in a Solar Spicule. Astrophys. J. Lett. **733**, 15 (2011)

M. von Uexküll, F. Kneer, Oscillations of the Sun's chromosphere. VII. K grains revisited. Astron. Astrophys. **294**, 252–259 (1995)

H. Wang, H. Zirin, Study of supergranules. Solar Phys. **120**, 1–17 (1989)

H. Wang, F. Tang, H. Zirin, J. Wang, The Velocities of Intranetwork and Network Magnetic Fields. Solar Phys. **165**, 223–235 (1996)

H. Wang, A. Johannesson, M. Stage, C. Lee, H. Zirin, Study of HA Jets on the Quiet Sun. Solar Phys. **178**, 55–69 (1998)

S.R. Weart, The Horizontal Component of Spicule Motion. Solar Phys. **14**, 310–314 (1970)

S. Wedemeyer-Böhm, A. Lagg, Å. Nordlund, Coupling from the Photosphere to the Chromosphere and the Corona. Space Sci. Rev. **144**, 317–350 (2009)

K. Wilhelm, Solar spicules and macrospicules observed by SUMER. Astron. Astrophys. **360**, 351–362 (2000)

F. Wöger, O. von der Lühe, K. Reardon, Speckle interferometry with adaptive optics corrected solar data. Astron. Astrophys. **488**, 375–381 (2008). doi:10.1051/0004-6361:200809894

T.V. Zaqarashvili, R. Erdélyi, Oscillations and Waves in Solar Spicules. Space Sci. Rev. **149**, 355–388 (2009)

T.V. Zaqarashvili, E. Khutsishvili, V. Kukhianidze, G. Ramishvili, Doppler-shift oscillations in solar spicules. Astron. Astrophys. **474**, 627–632 (2007)

Y.Z. Zhang, K. Shibata, J.X. Wang, X.J. Mao, T. Matsumoto, Y. Liu, J.T. Su, Revision of Solar Spicule Classification. Astrophys. J. **750**, 16 (2012)

H. Zirin, *Astrophysics of the sun* 1988